ABSTRACT

ELMARKABI, ISMAIL MOHAMED. Control and Protection of Distribution Networks with Distributed Generators, under the direction of Dr. Mesut Baran.

The connection of distributed generators to distribution networks greatly influences the performance and stability of such networks. The purpose of the dissertation has been to investigate and attempt to resolve the impacts of connecting distributed generators to distribution networks. Two main problems were defined and studied, which are the effect of distributed generators on the feeder voltage regulation and on the feeder protection schemes.

A central supervisory controller designed to regulate the feeder's voltage is presented, and the architecture of the controller is shown along with test results illustrating the ability of the controller to regulate the voltage along a feeder with distributed generators with minimum cost. In an attempt to regulate the feeder's voltage without the need for the feeder's explicit model, a multi-agent based distributed controller is proposed. The multi-agent system structure and design are illustrated, and test results comparing the performance of the two proposed controllers are shown.

The dissertation then presents an approach to extend conventional fault analysis studies to include inverter interfaced distributed generators. Such an approach is essential for the proper selection and coordination of protective devices for a feeder with distributed generators.

Finally, the dissertation illustrates the extent of deterioration a DG can cause on the overcurrent protective relay performance. An approach to solve this problem and restore the overcurrent relay performance is presented.

CONTROL AND PROTECTION OF DISTRIBUTION NETWORKS WITH DISTRIBUTED GENERATORS

By

ISMAIL MOHAMED ELMARKABI

A dissertation submitted to the Graduate Faculty of
North Carolina State University
in partial fulfillment of the
requirements for the Degree of
Doctor of Philosophy

ELECTRICAL AND COMPUTER ENGINEERING

Raleigh

2004

To my parents, *Mohamed and Zeinab El-Markabi*

To the love and friendship of my wife, *Aleya*

BIOGRAPHY

Ismail Elmarkabi received his Bachelor of Science degree in Electrical Engineering with honors from Cairo University, Cairo, Egypt, in 1997.

By year 2000 he finished his studies for the Masters of Business Administration (MBA) from Maastricht School of Management, Maastricht, Netherlands, through their outreach program in Cairo, Egypt.

Ismail Elmarkabi was admitted to the Masters of Science in electrical engineering program at North Carolina State University, Raleigh, in 2000. After receiving his masters degree in 2001 he was admitted to the Ph.D. program. During his graduate studies at North Carolina State University he worked as a research assistant in the power systems lab. This thesis completes the requirements for his Ph.D. degree.

ACKNOWLEDGMENTS

I wish to express my sincere gratitude to my advisor, Dr. Mesut Baran, for his guidance and mentorship during my graduate studies. His impressive knowledge, technical skills and creative thinking have been source of inspiration throughout the course of this work. Without him this work would not have been completed. I would also like to express my appreciation to Dr. Joel Trussell, Dr. Mo-Yuen Chow and Dr. Michael Young for serving on my Ph.D. committee and for their help.

I am indebted to my beloved wife Aleya for her sacrifices, never-ending support and encouragement during the course of my study. I would like to thank her for being a constant source of inspiration and motivation for me.

My deepest gratitude goes to my mother and father, to whom I am most indebted. I thank them for nurturing and educating me, for their constant love and prayers, and for their patience and support while I was studying abroad. I know I can never come close to returning their favor upon me.

I will always be thankful to my friends and colleagues for their unlimited support, and special thanks to my friend Nedal Safwat who made my stay in the states much smoother. I extend my thanks to all the Egyptian community that gave me a second family away from home.

I would like to thank my colleagues Nikhil Mahajan and Kim Jinsang for the enriching technical and cultural discussions.

Lastly, but certainly not the least, I would like to express my sincere appreciation to my mother and father in law for their prayers and support.

TABLE OF CONTENTS

List of figures

List of tables

CHAPTER ONE

Introduction

1.1 Motivation

The presence of small generating units connected to the power distribution network is greatly increasing. One study [BD00] estimates that by the year 2015, about 20 percent of all new generation going online in the US will be produced by small power generators, also known as distributed generators (DGs). Thus, investments in DG manufacturing and research in DG integration with the distribution network has been increasing exponentially in the last few years.

Unfortunately, the integration of DGs into current power distribution networks is not yet problem free. This is mainly due to the distribution networks being designed based on the assumption that only loads, and not generators, will be connected to it. As shown by [DM02] and [BD00], high penetration levels of DGs in a distribution network will cause an unacceptable deterioration in the network's performance. This greatly affects the network's ability to properly regulate its feeders' voltage level and effectively protect its components. Thus, the need for identifying and solving such problems is essential for seamlessly integrating DGs into distribution networks and for the future growth of the DG industry.

The motivation for this research was two–fold. The first goal has been to develop a better understanding of the impact the DG presence will have on the voltage regulation and protection of distribution networks. The second goal was to design and develop novel voltage control and protection techniques that can well address the two challenges related to DG integration into distribution networks.

1.2 Overview

For the last 10 years, there has been an increasing belief that distributed generation is the new alternative for supplying power to some consumers. Rather than the old-fashioned power generation where few, large, and remotely dispersed power generators were used, distributed generation relies on large numbers of small generators located near the loads. This fundamental change in the power grid structure will result in several serious problems, which have been the focus of many researchers.

To solve the conflicts resulting from connecting DGs to the distribution network, some researchers, [Ghm99] and [dfo01], focused on determining the maximum level of DGs penetration allowable for each distribution network and then prohibiting the connection of any DGs beyond that limit. This solution attempts to avoid deterioration of the network performance. However, this approach has been greatly criticized especially by DG manufacturers. The approach presented in this dissertation is to modify the existing voltage regulation and protection devices in order to seamlessly integrate as many DGs as needed into the distribution network without sacrificing any of the network performance standards.

The dissertation focuses on 1) the design of a supervisory controller capable of regulating the feeder's voltage with the hypothesis that all feeder information is available, 2) the development of a multi-agent system (MAS) capable of regulating the feeder's voltage without the need for a complete view of the feeder, 3) the understanding of DG behavior under fault conditions and how it affects the network's protective devices and developing a DG model that could be used in fault analysis studies, and 4) determining the DG impact on the over-current protective relay performance and developing a method to mitigate that impact.

1.2.1 Supervisory control approach for feeder voltage regulation

A framework for specifying the voltage regulation problem and solving it is proposed. The framework formulates the voltage regulation problem as a minimization problem, where the objective is to minimize the contribution of the DGs while maintaining the voltage level

along the feeder within acceptable voltage limits. The dissertation develops a solution approach for the voltage regulation problem based on a supervisory central controller approach with the hypothesis that the feeder model data is known to the controller. Such a hypothesis means that the central controller can be viewed as an omniscient agent that can sense and control the entire network. Thus, the controller performance is considered ideal and is used later as a reference point to measure the effectiveness of other control strategies.

The supervisory controller is capable of receiving feeder information and sending command signals to different components of the feeder. The design and architecture of the central controller is presented and its effectiveness is evaluated through a test simulation. An IEEE 34 node prototype feeder is simulated, the controller performance is monitored and presented for two cases: a normal steady state operating condition and an event occurrence, such as a sudden disconnection of a DG. The test results indicate that the controller performs perfectly and provides a tight voltage regulation on the feeder under both normal conditions and severe contingencies.

1.2.2 MAS approach for feeder voltage regulation

The major drawback in using the supervisory controller previously presented is the need for an accurate feeder model, such a condition obliterates the notion of making the connection of a DG to the network as easy as connecting a PC to the Internet. In order to achieve such a goal, also known as the *plug-and-play* goal, this dissertation attempts to utilize the strengths of employing the MAS approach for solving the voltage regulation problem. In the proposed MAS, each system component will be equipped with an agent, and all agents will cooperate together to help maintain the feeder voltage level within limits at a minimum cost.

The approach this dissertation employs to solve the complex voltage regulation optimization problem in a distributed manner, which without knowing the explicit system model, is to exploit special features and characteristics in the problem to determine simple relationships between the overall goal and all available actions. These relationships will be used together with the ability of each agent to directly sense and measure its local variables to reformulate the optimization problem in a simpler form. This simple problem will then be solved via MAS using the contract net protocol (CNP).

A test simulation is presented to evaluate the performance of the proposed MAS, with the performance contrasted against that of the omniscient agent. The test shows the MAS's ability to reach the optimum solution previously reached by the central controller, despite the absence of a feeder model.

1.2.3 Fault analysis on distribution systems with DGs

The behavior of conventional types of DGs, such as synchronous and induction generators, during fault conditions has been thoroughly investigated by several researchers [BJ02], but more research and effort is needed to understand the behavior of new evolving DG technologies. This dissertation attempts to analyze and understand the behavior of inverter interfaced DGs, such as fuel cells, photo-voltaic and micro-turbines, under different fault conditions.

Moreover, the dissertation presents an approach to model inverter interfaced DGs under fault conditions and integrate such a model into conventional fault analysis studies, thus taking the DG's fault contribution into account when sizing protective devices.

1.2.4 Adaptive over-current protection for feeders with DGs

Although several papers have mentioned the fact that the presence of DGs affects the performance of the over-current (OC) relay protecting the feeder, none has presented enough data to show how severe the deterioration in the OC relay performance is, and whether it is acceptable to ignore it or if it must be resolved. This dissertation presents an empirical result on how the size and location of a DG along a feeder can affect the OC relay protecting that feeder and shows that the deterioration in the OC relay performance can leave large portions of the feeder unprotected against different types of faults.

Furthermore, the dissertation offers an adaptive technique that can anticipate the impact of the DG on the relay performance and accordingly change the relay pick up current to ensure that the whole feeder is protected at all times, with or without DGs.

1.3 Outline

Chapter 2 introduces a literature review on DGs, distribution networks, and the impact of DGs on the distribution network. Further, it identifies and describes the impact of DGs on the feeder voltage regulation and the impact of DGs on the feeder protection.

Chapter 3 addresses the voltage regulation problem using a supervisory central controller and introduces the problem formulation, controller design approach, and the test results to show the effectiveness of the controller.

Chapter 4 focuses on solving the voltage regulation problem using the MAS approach. It presents the methodology used to approximate the original problem into a simpler problem that the MAS is capable of solving. Further, it shows the test result proving the effectiveness of the MAS approach.

Chapter 5 studies the DG's reaction to a fault in its feeder and proposes an approach to model such behavior and integrate inverter interfaced DGs into conventional fault analysis studies. It also presents a case study showing the effectiveness of the proposed approach in determining the DG's contribution to different types of faults.

Chapter 6 investigates the impact of DGs on the OC relay performance. It shows empirically the severity of the deterioration in the relay's ability to protect the whole feeder. It concludes by presenting a technique to solve such problem by adaptively changing the OC relay setpoint.

Chapter 7 concludes the dissertation, states the dissertation contributions, and indicates possible future research efforts that could improve the findings of the dissertation.

CHAPTER TWO

Distributed Generation and Distribution Networks: Protection and Control Challenges

2.1 Introduction

This chapter presents a literature review on the impacts of DGs on the distribution network performance. The chapter starts with an introduction on the structure of distribution networks and the concept of distributed generation. The chapter then focuses on the impact of DGs on the feeder voltage regulation during different operating conditions. Lastly, a detailed explanation on the impact of DG on the feeder protection is presented.

2.1.1 Electric power grid

Today's power system is a complex interconnected network that can be subdivided into four major parts: generation, transmission, distribution, and loads. In the generation phase, electric power is generated at 11-30 kV via large central generators located in remote areas. The purpose of the overhead transmission network is to transfer electric energy from generating units at various locations to the distribution network.

The distribution network is a medium to low voltage network that is connected to a high voltage transmission network through "step down" transformers. Each transformer feeds power to a number of feeders to which customers are connected either directly or through a distribution transformer which further steps down the voltage to the utilization level, 120 volts for household appliances.

2.1.2 Distributed generation

Distributed generation refers to the notion of generating power using a set of small sized generators that produces power at low voltage levels and usually uses alternative fuel. The generators are mainly designed to be connected directly to the distribution network near load centers.

It is expected that distributed generation will have increasing importance for a number of reasons, [JA00] and [JOG00]:

- It allows for the independent production of electric energy to carry the full load or only the peak load and sell the excess energy at a profit.
- It has a potential of providing some of the ancillary services, which are electrical services provided other than real power.
    a) Reactive supply (absorption and injection) to achieve voltage control
    b) Power factor regulation

Different types of DG technologies

There are several types of distributed generators in the market. Some are conventional such as the diesel generators and some are new technologies such as the micro-turbines. The following section briefly describes major DG alternatives.

Fuel cells: A fuel cell is an electrochemical device that converts chemical energy directly into electrical energy. The fuel cell unit uses hydrogen and oxygen to perform the required chemical reaction and produce power. Fuel cells are inverter interfaced DGs, meaning the unit produces dc power that is converted to ac power via a 3-phase converter (Figure 1) [Hir98].

Micro-turbine: Micro-turbines are small gas fired turbines rotating at a very high rate of speed (90,000 rpm). A high rpm DC generator is used to generate dc power. The DC generator is coupled to a dc/ac power converter to produce voltages at the rated frequency [Sut01].

Photovoltaic cells: Photovoltaic cells convert solar energy directly into electrical energy. Like fuel cells, the power produced is dc power and a power electronics converter is needed to interconnect with the utility grid [JOG00].

Wind turbines: The wind turbine operates by extracting kinetic energy from the wind as it passes through the rotor. The wind turbine shaft is connected either to an induction or synchronous generator. A transformer is then used to step up the output voltage to the utility grid level [JA00].

Diesel generator: This is the most commonly used DG now. A small synchronous generator is coupled with a reciprocating piston engine to produce ac power. They are usually operated standalone during utility power outages.

In this study, we will be focusing only on the inverter interfaced DGs such as fuel cells, micro-turbines, and photovoltaic cells.

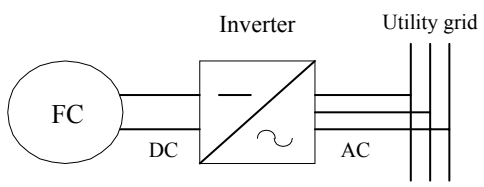

Figure 1: Fuel cell unit

2.1.3 Impact of DGs on distribution networks

The distribution network was designed to extract power from the transmission network and distribute it to the loads. It was not designed to have generators directly connected to it. The distribution network topology, control, and protection are all designed assuming that power is flowing in one direction, from transmission to loads. The connection of DGs to the feeders of the distribution network can cause the power flow to be bi-directional instead of uni-directional affecting the network performance and stability in a number of ways, [JA00], [Hir98], [Sut01] and [JOG00]. Through an extensive literature review, all suggested implications for connecting DGs to distribution networks have been studied. The most serious impacts that could not be resolved using conventional techniques were found to be

the impact of the DG on both the feeder voltage regulation and the feeder protection. In the following two subsections, these two implications will be discussed in more detail.

2.2 Impact of DG on feeder voltage regulation

When a DG is connected to a feeder, it will affect the voltage regulation of the feeder depending on the location, size, and operating scheme of the DG. In the following section, the conventional voltage regulation will be discussed, followed by the impact of the DG's presence on such voltage regulation technique.

2.2.1 Conventional feeder voltage regulation

A distribution network consists of a number of substations which steps down the voltage level and feeds a number of feeders. As shown in Figure 2, the feeder starts from the substation bus and loads are tapped off at every node. Each feeder is equipped with a HV/MV on-load tap changing transformer that has the ability of changing the voltage level of the feeder at the substation bus. The voltage drop along the feeder depends on the feeder loading as illustrated in Figure 3, where the maximum voltage drop occurs during peak load. The on-load tap changing transformer (LTC) and its associated voltage regulator (VR) regulates the voltage at the substation end to compensate for the voltage drop due to the change in loading. The aim is to always keep the voltage along the feeder within ± 5 percent of the nominal voltage.

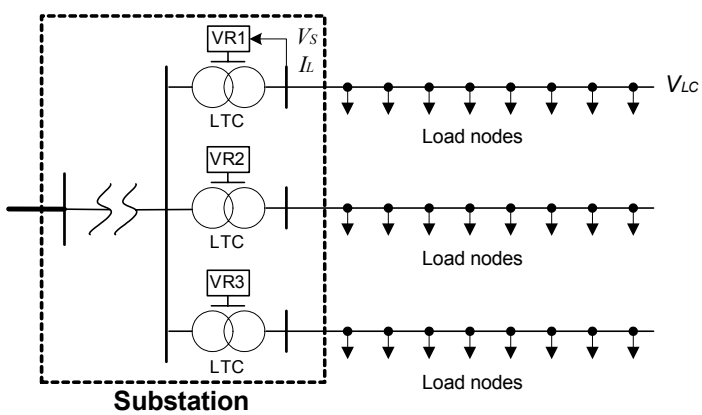

Figure 2: Conventional distribution network

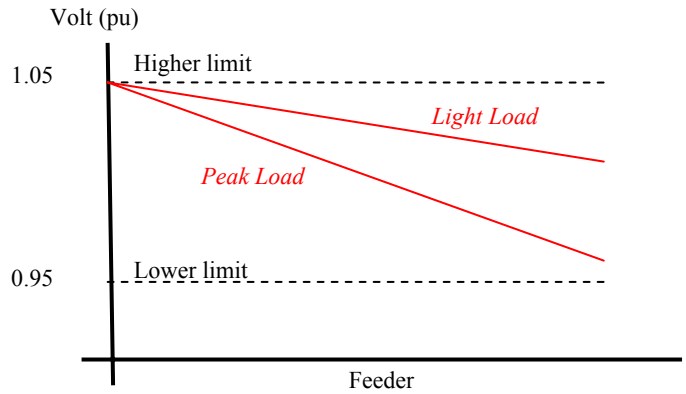

Figure 3: Voltage level along the feeder

VR control with line-drop compensation:

The aim of line-drop compensation is to keep the voltage constant, not at the feeder's substation bus, but at some remote load center. Normal practice is to sense the load current (local to the transformer) and use this to estimate the voltage drop on the feeder at the remote load center according to the following equation.

$$V_S^{des} = V_{LC}^{set} + I_L\left[R_{set} + jX_{set}\right]$$

Where I_L = load current, V_S = substation bus voltage, and V_{LC} = voltage required at the remote load center. R_{set} and X_{set} inside the relay are adjusted to correspond directly to the feeder's impedance. Thus the substation bus voltage is adjusted to insure that the remote load center voltage is within acceptable limits.

2.2.2 Impact of DG on feeder voltage regulation

The following two subsections illustrate the impact a DG has on the feeder voltage regulation under two conditions, normal and emergency. To demonstrate such conditions, a seven node prototype feeder (Figure 4) is simulated under different scenarios. The feeder load is assumed to be equally distributed along the feeder, and the feeder is protected with an OC relay. (Relevant data in Appendix A)

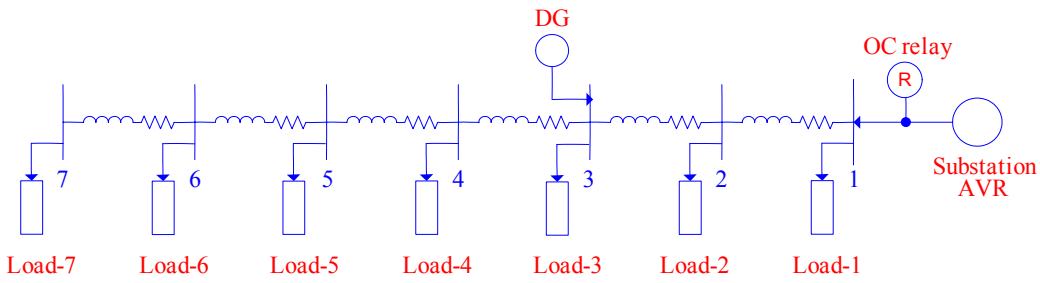

Figure 4: Prototype Feeder

A) Impact of DG on the VR during normal operation

As previously indicated, in a conventional feeder the voltage level is regulated by the VR, which estimates the voltage drop over the feeder by measuring the feeder current at the substation end. However, this depends mainly on the simple fact that the power is uni-directional from the substation bus (where the VR is located) flowing into the end of the feeder. The presence of DGs makes the power bi-directional, and if the DGs connected to a feeder are carrying most or all the feeder load, then the voltage profile along the feeder depends mainly on the DGs' location, power generated, and the DG power factor. This creates an unpredicted and uncontrolled situation where the voltage level of all nodes might or might not be within acceptable limits.

To illustrate such a problem, consider the prototype system in the following three scenarios:

Case 1: feeder without DGs and the voltage along the feeder is within acceptable limits.

Case 2: feeder with three DGs at nodes 2, 3, and 6 carrying the whole feeder load.

Case 3: feeder with one DG at node 2 carrying the whole feeder load.

Figure 5 shows the voltage profile along the feeder for the three different cases. For cases 2 and 3, the current flowing from the on-load-transformer is almost zero. The VR will assume that both cases are the same with the feeder's load at the minimum level, therefore it will adjust its voltage level to 1.00 p.u. The voltage profile in case 2 is within the limits because the DGs are distributed along the feeder, unlike the third case, where the feeder loads are carried by a localized DG. This shows that, although the VR treated both cases

similarly, the voltage profile along the feeder is totally different and depends on the number and location of the DGs carrying the load.

It could now be concluded that the conventional VR technique cannot properly adjust the voltage level of a feeder with various DGs connected to it, since it depends solely on measuring the feeder's current at the substation end, which is no longer a good indication of the feeder status. Therefore, a new technique must be developed to facilitate the coordination between DGs and the VR for better feeder voltage regulation.

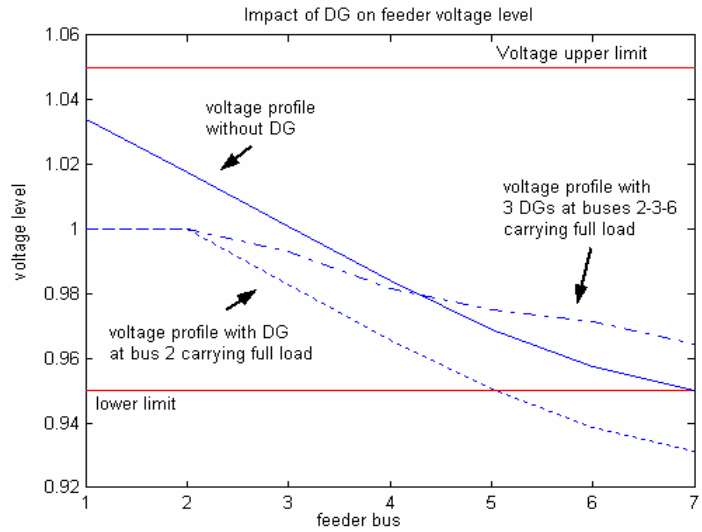

Figure 5: Impact of DG on the VR control

B) Voltage regulation under emergency conditions of sudden disconnection of a DG

If the DG connected to a feeder operates without considering the impact of its operation on its neighboring nodes, one potential problem that may arise is that the sudden disconnection of a DG may cause an undesirable tripping of other generators connected to the same feeder. The location of the DG, the feeder loading, and the DG power generated are key factors in the impact of the sudden disconnection of that generator [SJR93].

To illustrate this potential problem, consider the prototype system with a DG connected to node three and operating at its maximum capacity carrying 30 percent of the total feeder load. The solid curve in Figure 6 represents the voltage profile along the feeder with the DG connected. The effect of suddenly disconnecting this DG is shown in the lower curve,

where the voltage level of the last portion of the feeder (around 40 percent of the feeder length) falls below the lower permissible limit. This will trigger the undervoltage relay protecting the DGs located in this portion of the feeder to trip. Although the VR will adjust the feeder voltage level (upper dashed curve), its slow response time will make its action useless. The VR takes about 10 seconds to move one tap which corresponds to about 0.05 pu voltage change (assuming a 16 tap VR for ±5 percent voltage regulation) [ABB]. On the other hand, the DGs are quite sensitive to voltage sags, as they usually employ undevoltage/overvoltage protection schemes to protect the device against the external faults [IEEE929], [IEEE47]. These protection schemes are usually fast, typically set to trip the DG within two seconds if the voltage level is below the acceptable limit, and trip within 0.16 seconds if the voltage level is less than 50 percent of nominal voltage. Therefore, the VR cannot provide the quick voltage support needed to restore the voltages following a sudden disconnection of the DG, because the response of the VR is much slower than needed.

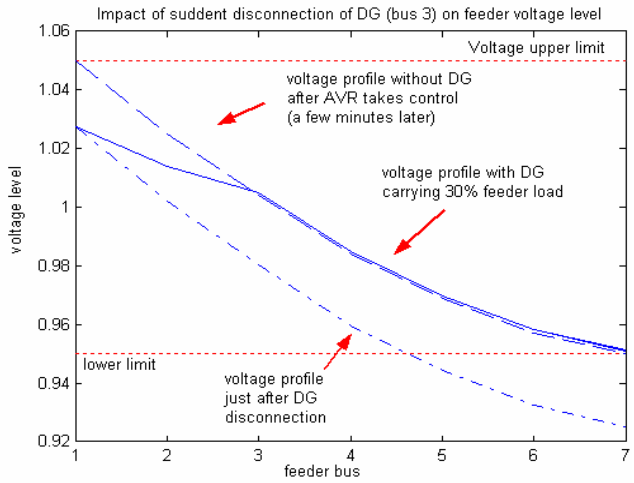

Figure 6: Impact of the sudden disconnection of the DG

2.3 Impact of DG on feeder protection

DG presence in a distribution network impacts the conventional feeder protection schemes. In the following two sections, we will discuss how the feeder is currently protected and the impacts of DG presence on such protection schemes.

2.3.1 Conventional feeder protection

Distribution feeders are usually radial with the loads tapped off along the feeder sections. The feeder protection strategy aims at optimizing the service continuity to the maximum number of users following a fault disturbance on the network. This means applying a combination of circuit breakers, automatic reclosers, and fuses to clear temporary and permanent faults. As shown in Figure 7, fuses are responsible for isolating permanent faults at point A and beyond. The automatic recloser clears faults on point B and beyond (it's downstream). The main circuit breaker at the beginning of the feeder is equipped with an OC relay to isolate any permanent fault along the main feeder. When the feeder current exceeds a certain pickup value, the OC relay sends the breaker a trip signal, and the speed of tripping the fault is inversely proportional with the fault current magnitude.

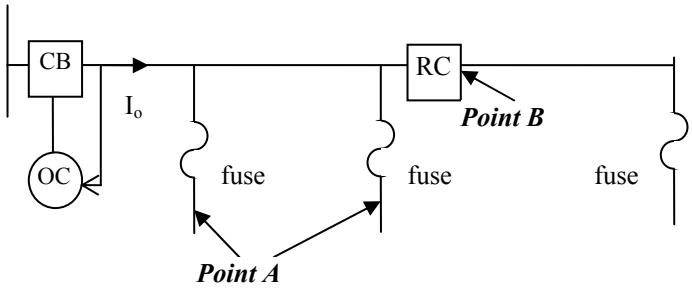

Figure 7: Radial feeder protection

2.3.2 Impact of DG on feeder protection

The conventional protection scheme of each feeder is designed, assuming the feeder is radial. But, as mentioned earlier, the presence of DGs on a feeder will cause bi-directional power flow, which means that part of the feeder will no longer be radial [GB01]. This will create several problems to the current protection schemes used, as shown in several papers including [SR01], [BD00], [Lop02] and [Wal01].

Ackermann in [AK02] shows that the presence of DGs will result in an increase in fault current levels, and that the detailed assessment of the impact DGs might have on fault currents is very challenging as the impact largely depends on a number of factors. Among these are "the technology of the DG, its operation mode, interface with the DG, system voltage prior to fault, etc…" In [GM02], Gomez claims that there is no concern with the

DG when its power is less than 10 percent of the minimum load demand by the feeder. The most immediate consequence is the need for verification of the protective device breaking capacity, which might not be enough due to the increase of the available short-circuit power. As mentioned by Barker in [BD00], the fault contribution from a single small DG unit is not large, however, the aggregate contributions of many small units, or a few large units, can alter the short-circuit levels enough to cause protective devices to malfunction.

The main impacts of DG on the feeder protection connection are in three different areas: the OC relay performance, the recloser operation, and the islanding protection.

A) Over-current relay performance

One of the DG impacts on feeder protection is on the OC relay, as the current contribution from the DG will affect the "*reach of the relay*". OC relays are set to protect a certain part of the feeder, which is sometimes referred to as the "*reach*". The reach of the relay is determined by the minimum fault current it is set to react to, the so-called *pick-up current*. The presence of a DG will reduce the reach of the OC relay [Dug02], thus leaving medium impedance faults at the end of the feeder undetected (Figure 8). The reduction in reach is due to the fact that the DG contributes to the fault current, thus decreasing the fault current seen by the OC relay for the same fault resistance (R_f).

To understand the effect of DGs on reducing the reach of the feeder's OC relay, a study is presented in Chapter 6. The influence of the DG's location and power level on the relay effectiveness is also shown. Moreover, a method designed to mitigate the problem is presented in the same chapter.

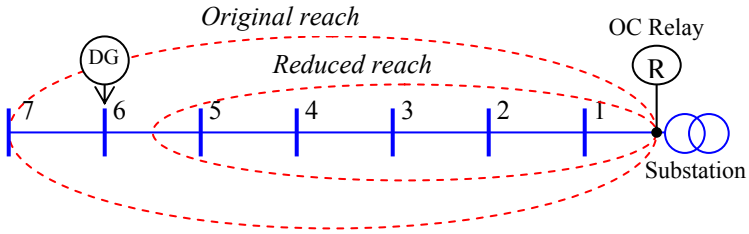

Figure 8: Relay reach with and without DG

B) Recloser operation

The DG contribution to feeder faults impacts the operation of the recloser in three different ways: 1) the recloser might be exposed to high mechanical and thermal stresses beyond its rated limits, 2) the recloser-fuse coordination can be affected, and 3) the recloser might trip for upstream faults. In the sections below, we will discuss these impacts in more detail.

1) Exposing the recloser to high mechanical and thermal stresses [Doy02]

Reclosers are designed to withstand and interrupt the high fault currents. One of the important parameters of a recloser is the maximum current the recloser can withstand. This is called the *maximum withstand current*. With DGs connected as shown in Figure 9, the fault current seen by the recloser (I_{RC}) will increase. This would not normally cause a problem as long as the new I_{RC} does not exceed the recloser maximum withstand capability. However, if $I_{RC} > I_{max}$ the recloser will be exposed to mechanical and thermal stresses, especially in the first one and a half cycles, which might cause a recloser failure.

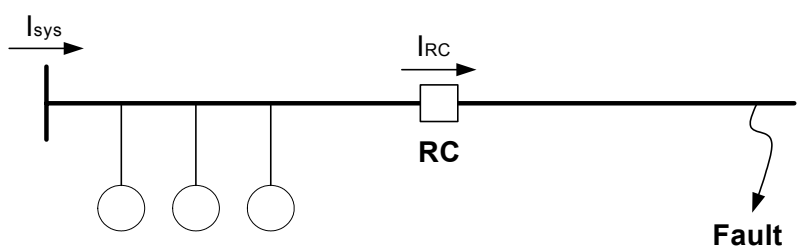

Figure 9: DGs are located upstream, fault located downstream

2) Recloser-fuse coordination

The philosophy of feeder protection is that a fuse should only operate for permanent faults within its reach. But for temporary faults, the recloser should disconnect the circuit with fast operation and give the fault a chance to clear. Only if the fault is permanent, should the fuse be allowed to open. As mentioned by [GB01], for the feeder topology as the one shown in Figure 10, the fault current flowing through the fuse is greater than that flowing through the recloser. This might cause the fuse to trip faster than the recloser for

temporary faults. And since temporary faults account for 70 to 80 percent of feeder faults [GB01], the miss coordination between fuse and recloser will impact the feeder's reliability considerably.

Another condition that may cause the fuse to trip faster than the recloser under temporary faults was presented by [BD00] and [Doy02]. As suggested in [BD00], if DG units are added to the feeder topology shown in Figure 9, the fault current may become large enough that the lateral fuse no longer coordinates with the feeder circuit breaker during faults. This would lead to unnecessary fuse operations. [Doy02] points out that it is very likely that coordination between the recloser and any down-line fuses will be lost. Because both the recloser and fuses operate faster at higher fault currents, the required margins between the recloser fast curve and the fuse minimum melt curve could be reduced enough to lose coordination.

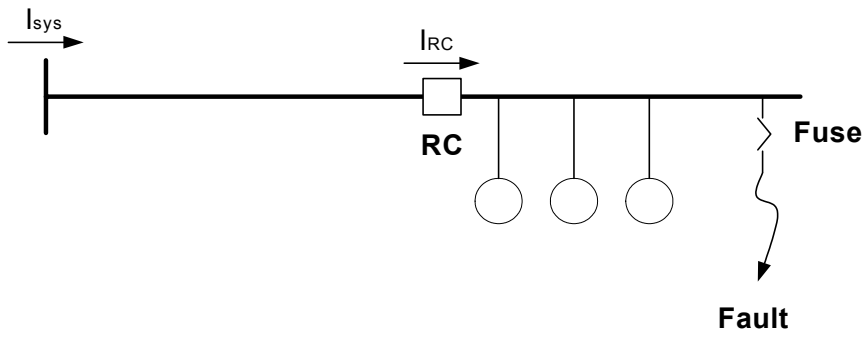

Figure 10: DGs and fault are located downstream

3) Recloser tripping for upstream faults [Doy02]

When there are DGs downstream of a recloser as illustrated in Figure 11, then the recloser will see fault currents in the reverse direction, if the fault is upstream of the recloser. It may even be possible that the I_{RC} exceeds the minimum tripping value of the recloser, and thus the recloser will trip for faults upstream, which is unacceptable.

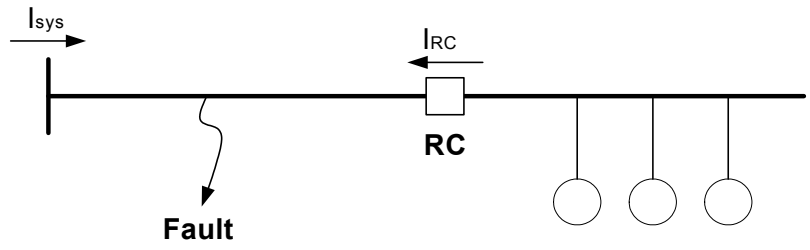

Figure 11: DGs are located downstream, fault located upstream

The solution for the recloser tripping problem for upstream faults can be achieved by upgrading the recloser's conventional OC relay by a directional OC relay. This will make the recloser trip only if the I_{RC} exceeds the minimum tripping value in a certain direction.

While solving the first two problems (1 & 2) related to the recloser operation is not that simple, the solution involves estimating the contribution of the DG into the fault current. This fault current contribution is needed to properly size reclosers and correctly set the recloser-fuse coordination parameters. In [BD00], [BJ02], and [AK02], Barker and Ackermann agree that the only accurate approach for solving such problem is to perform a software-based analysis, which correctly models the DG behavior to fault events. Therefore, relatively accurate short-circuit models of different types of DGs are needed to assess the impact of its fault contribution during the time frame from about one-cycle up to several seconds into a fault event. Chapter 5 presents a technique that was developed to facilitate the integration of inverter interfaced DGs into conventional fault analysis studies of distribution networks.

C) Islanding protection

Islanding on a feeder occurs when a protection device – breaker, fuse or an automatic recloser – isolates a section of the feeder to isolate a fault, thus creating an island. Islanding becomes a concern when there is a DG on the islanded part of the feeder, as the DG will try to energize the island (Figure 12). Due to the serious problems of islanding, which includes threatening the safety of utility repair personnel, utilities and standard-

making bodies require that DGs be equipped with anti-islanding protection, so DGs that are on the islanded part of the feeder can be disconnected as soon as possible.

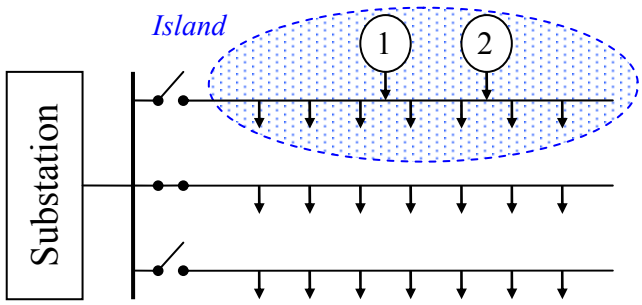

Figure 12: Islanding

[BD00], [RB99], and [Rop00] show that none of the current islanding detection methods are capable of detecting the island under all possible conditions. The main reason for such a drawback is that the current methods use only their local measurements, such as the DG's voltage and current. For protecting the feeder at all conditions, further research is needed to either develop a new technique or improve the current techniques.

Although islanding protection is not one of the problems this dissertation focuses on, it was presented to show that the islanding protection can be addressed more effectively once a communication network is adopted at the distribution level, the same communication network that is needed for addressing the problems associated with integration of DG into distribution network.

2.4 Summary

This chapter began with a brief introduction to distribution networks, distributed generation, and the impact of distribution generation on distribution networks. It then examined the impact of DGs on conventional feeder voltage regulation, under both normal and emergency conditions.

The impact of DG on feeder protection was examined and the impact on the OC relay performance and recloser operation was illustrated. Finally, the islanding phenomenon was explained.

CHAPTER THREE

Supervisory Control Scheme for Feeder Voltage Regulation

This chapter presents a supervisory controller designed to regulate the voltage along a feeder with the presence of DGs. The chapter starts by defining the feeder voltage regulation problem and the proposed supervisory controller objectives. The proposed supervisory controller design and architecture are then presented. Finally, test results are shown to prove that the proposed controller can successfully regulate the voltage of a distribution feeder with DGs connected to it.

3.1 Problem definition

As mentioned in the previous chapter, regulating the voltage of a feeder with DGs (Figure 13) cannot be done using the conventional VR scheme. This is because of two main shortcomings, the current VR scheme depends only on the local current measurement and the VR is a relatively slow responding device.

The goal taken in this study is to enhance the current voltage regulation scheme that can address these shortcomings. It is contented that this can be accomplished as follows:

- Provide a communication link between the VR and the DGs. This communication link will enable the VR to collect the additional data it needs in order to be able to estimate the voltage drop on the feeder and thus provide better voltage regulation. The communication will also provide the coordination between the VR and the DGs.

- Use DGs for reactive power support needed during the voltage sag conditions that are too short for the VR to react. This will provide the fast voltage regulation needed during voltage sag conditions due to the sudden drop of a DG as well as large motor start-ups. This uses the capability of DGs to provide reactive power support during emergency conditions. The majority of the DGs, microturbines and even the fuel cells, can provide this service. DGs are usually equipped with their own controller which controls the DG's output active and reactive power.

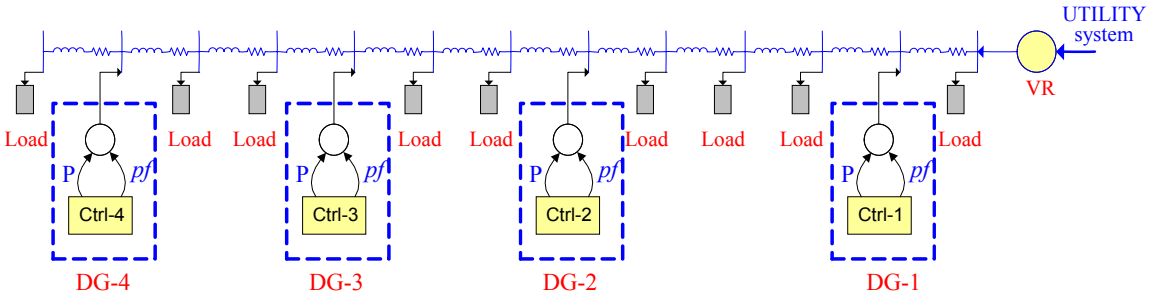

Figure 13: Feeder with DGs and loads

3.1.1 DG model

Inverter interfaced DGs consist of a power generating unit that produces dc power and an inverter unit to convert that power to ac power. The power generating model depends on the type of the DG, microturbine, fuel cell ... etc. In appendix A, the microturbine model as well as the fuel cell model is presented. In Figure 14, the inverter model is presented, showing the inverter's input and output filters and the six Intergate Bipolar Transistor (IGBT) switches used to convert the input from dc voltage to an ac voltage.

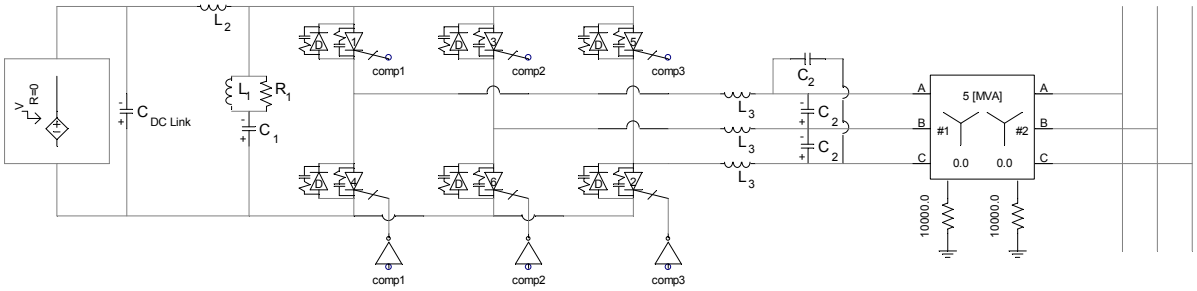

Figure 14: DG's inverter with input and output filters and step-up transformer

As shown in Figure 15, two PI controllers are used to regulate the DG's output active and reactive power, via regulating the magnitude and angle of the inverter's ac output voltage. The correct pulse sequence given to the IGBT switches - that will yield the required voltage magnitude and angle – are generated using the Pulse Width Modulation (PWM) technique.

It is important to mention that the DG's controller adopts a constant power factor control scheme. Such a scheme uses the active power setpoint-command signal to determine the corresponding reactive power setpoint signal in order to maintain the power factor constant. This means that the two parameters that are regulated to match their setpoints are the active power output *"P_{set}"* and the power factor *"$pf_{set.}$"* Depending upon these parameters, the reactive power output is determined.

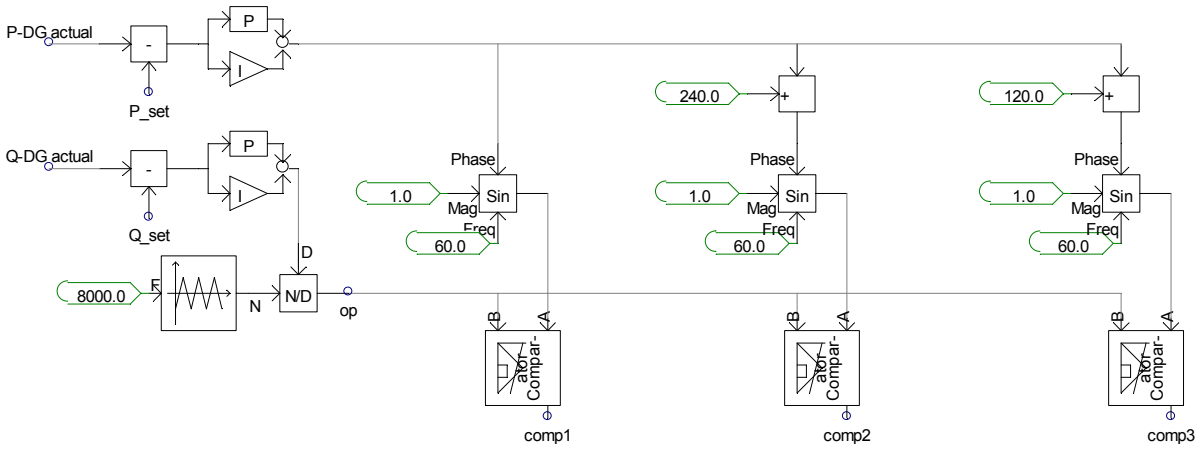

Figure 15: DG's control model and inverter pulse generator

3.2. Supervisory controller

In order to coordinate control actions between the VR and the DGs, there will be a supervisory controller at the distribution substation with communication links between the controller and the field devices, i.e, the VR and the DGs on the feeder. The supervisory controller will gather data from the feeder at the monitoring points, which are mainly the DG locations, but could also include other points on the feeder, and send the corrective set-point signals for the VR and the DGs. Figure 16 illustrates this proposed supervisory control scheme.

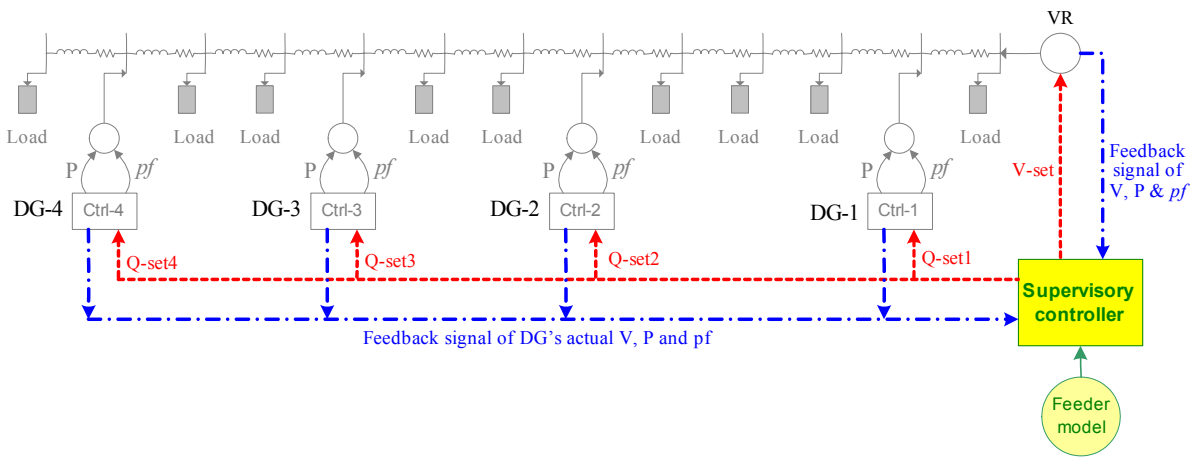

Figure 16: Feeder with DGs and loads and proposed supervisory controller

This supervisory controller will accomplish the following objectives:

- The feeder voltage levels should be recovered to acceptable levels (which are usually between 0.95 and 1.05 pu) as fast as possible.
- The total reactive power support from DGs should be kept as small as possible. This will minimize the cost of reactive power support from DG, especially if the utility will pay the DG-owners for their reactive power support.
- The reactive power support from DGs should be requested *if and only if* the VR is incapable of supporting the feeder voltage.

Note that the supervisory controller interfaces with DGs by adjusting their power factors. This is because the controllers for the DGs have two set-points, "P_{set}" and "$pf_{set.}$" The power setting P_{set} is determined by the DG owner and is usually based on economic factors, while the pf_{set} is normally set to unity since DG owners get paid for their active power output. The pf_{set} can, however, be adjusted for voltage support, since the power factor determines the DGs reactive power output, which in turn affects the voltage level on the system.

Based on these objectives and constraints the ideal controller response is illustrated in Figure 17, which shows the desirable actions of the DGs and the VR in response to a sudden voltage drop (event) in one of the feeder's nodes. The time axis is divided into four intervals, A, B, C and D, with each determining a certain operating condition.

Interval A represents the feeder operation just before the event. The feeder is operating with its minimum node voltage at 0.95 volts, the VR voltage is constant, and the DGs are operating at unity power factor.

Interval B starts when a DG disconnects causing the minimum node voltage to drop below 0.95 as shown in the figure. The VR and the remaining DGs start acting to recover the feeder's voltage level. By the end of interval B, the feeder's voltage level returns to 0.95 due to the fast reaction of the DGs connected to the feeder. The DGs respond to the sudden event by quickly decreasing their power factor in order to inject enough reactive power to support the voltage.

Throughout interval C, the voltage level along the feeder is within limits, but the VR is slowly picking up the burden of supporting the voltage and relieving the DGs, who slowly return to unity power factor operation.

Interval D shows the feeder at a steady state after recovering from the event. The minimum node voltage is 0.95, the DGs are operating at unity power factor, and the VR voltage set point moved to a higher level.

The bar chart at the bottom of Figure 17 shows the desirable contribution and coordination between the DGs and the VR to ensure fast system recovery from a sudden under voltage event. At the beginning, the DGs fully support the feeder voltage, while the VR is not contributing. This gradually changes until the VR fully supports the feeder voltage and relieves the DGs.

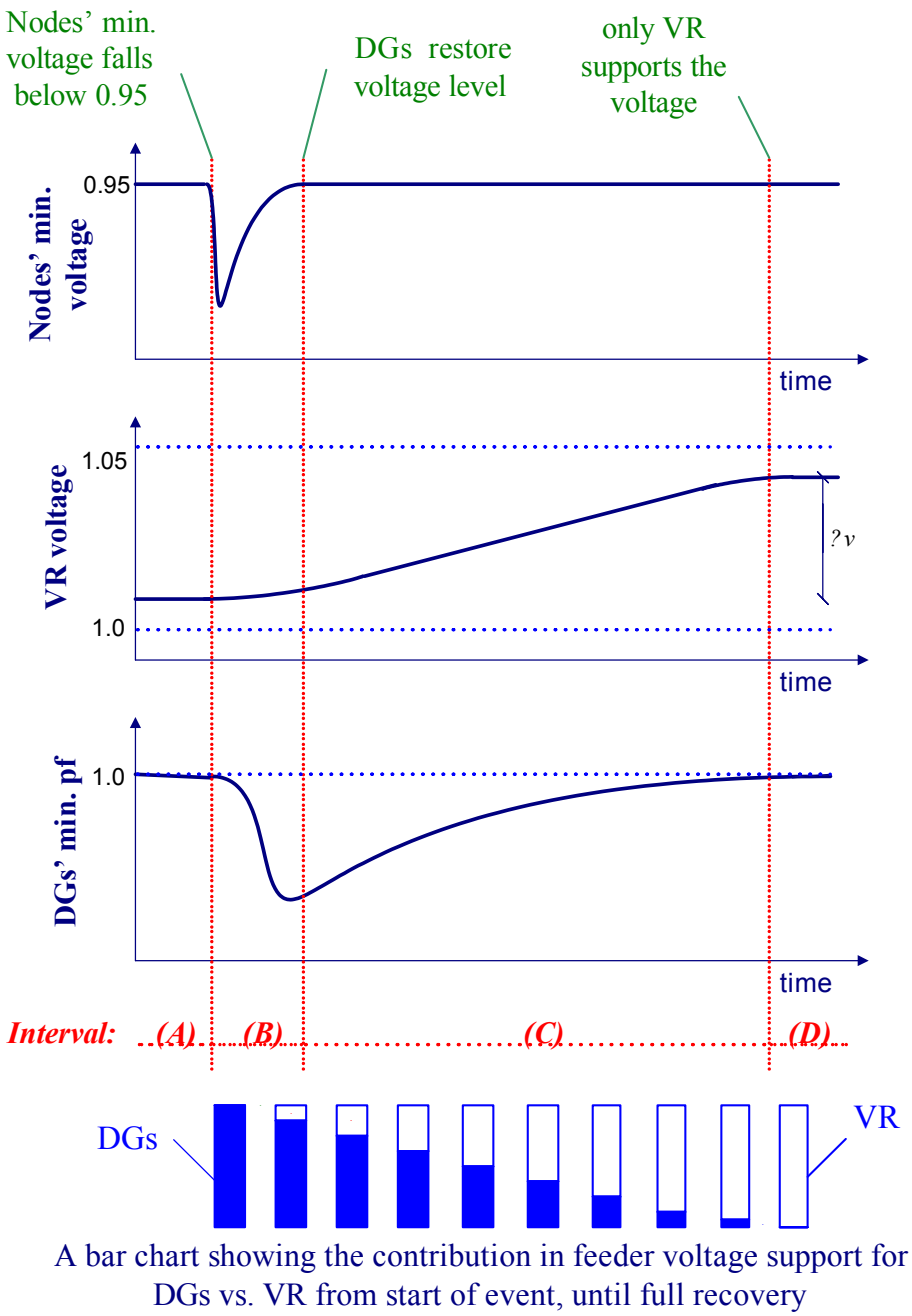

Figure 17: DG and VR response to a sudden voltage drop event

3.3 Controller design

The supervisory controller in Figure 16 will use feedback signals from the DGs and the VR and send the required change in the DGs' reactive power and VR's tap setting to the DGs and the VR. The architecture of the proposed supervisory controller is shown in Figure 18. The supervisory controller consists of two controllers running in parallel. The C-2 controller supervises the VR while the C-1 controller will supervise the DGs. The two controllers need feedback signals from the feeder about the voltage and power values for all DGs and load nodes. As mentioned earlier, the load nodes' system parameters need to be estimated, with this task being accomplished by the estimator block (E-1).

The details of controllers C-1 and C-2 and the estimator E-1 are elaborated in the following subsections.

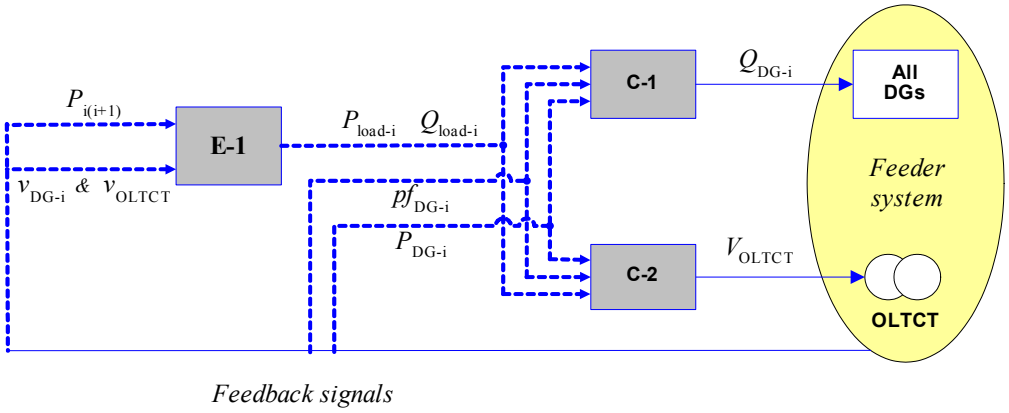

Figure 18: Supervisory controller block diagram

3.3.1 The Estimator (E-1)

The estimator will gather data from the feeder and construct an approximate feeder model to be used by the controllers. The goal here is to develop a feeder model that can use the real-time data available from the feeder. Since there would be only limited data available, we need to approximate the feeder model accordingly. We assume that at certain locations on the feeder, at DG points for example, power flow measurements are available. These power flow measurements can then be used to determine the approximate load served between the two measurement points, as the load would be simply the difference between the two flow

measurements. This is illustrated in Figure 19. The total load between the measurements of P_{12} and P_{23} for example would be $P_{L2} = P_{12} - P_{23}$. The approximate model is then obtained by lumping these total loads in the middle of the sections defined by the flow measurements, which is illustrated in Figure 19b.

Note that in this approximate feeder representation, we have the active and reactive power measurement at each node. Therefore, we can use the power flow equations to represent the feeder. For a radial feeder, these equations would be of the following form per phase (we neglect the line mutual coupling effects) [Ber86].

$$P_i + jQ_i = V_i^2\left[Y_{i(i+1)} + Y_{i(i-1)}\right] - V_i\left[V_{i+1}Y_{i(i+1)} + V_{i-1}Y_{i(i-1)}\right]$$

Where $Y_{i(i+1)}$ is the admittance of the segment connecting node i to node $i+1$.

The estimator module uses the power flow equations to calculate the voltage levels on the feeder. The estimator then passes the approximate feeder model and the voltage data to the control modules. Control modules use the model to determine the effect of their control actions on the feeder voltage levels.

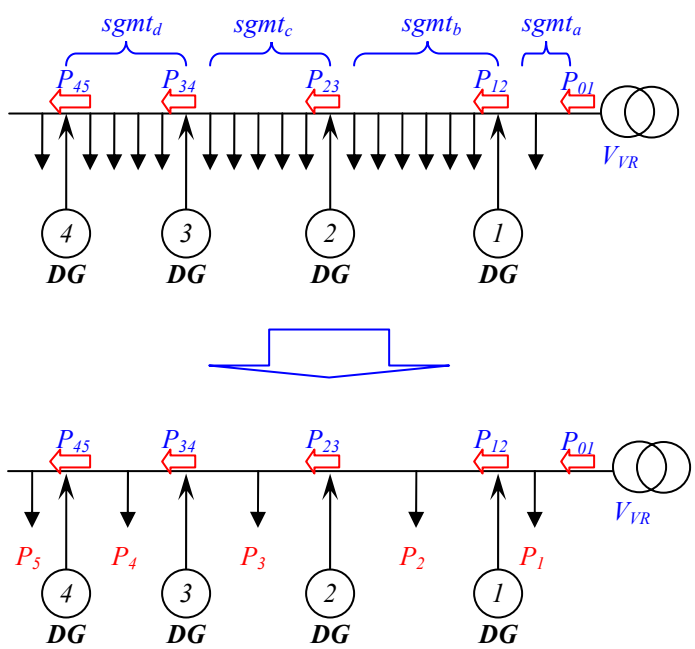

Figure 19: Combining neighboring loads to determine approximate feeder model

3.3.2 DG controller (C-1)

This controller determines the reactive power needed from each DG in order to keep the feeder within voltage limits. The controller will solve the constrained minimization problem formulated below. The objective function represents the cost of dispatch, which is the total amount of reactive power needed from all DGs. The power factor constraints ensure that the reactive power support from the DGs will be within their capabilities, as they will limit the DGs reactive power values based on their real power outputs.

The DG controller will run this optimization every update cycle, for example at every second, only during the emergency period, which is determined by the VR controller. Once the new reactive power dispatch values are determined, the controller sends them to the DGs as new set points.

Min $Cost = \sum_{i=1}^{m} Q_{DG-i}$

s.t.

- *Feeder model*: a model of the feeder configuration that represents the relationship between power flow, DG power injected, load distribution, and nodes voltages.

$$V_{i+1} = V(v_i, P_i, Q_i)$$

- *Node voltage constraints*: ensures that all node voltages are within acceptable voltage limits.

$$0.95 \le v_i \le 1.05 \qquad i=1, 2..., n \qquad \text{for } n \text{ nodes}$$

- *Power factor constraints*: ensures that the reactive power dispatched to each DG is within its capabilities and depends upon the amount of power injected by the DG into the system.

$$0.5 \le pf_i \le 1.0 \qquad i=1, 2..., m \qquad \text{for } m \text{ DGs}$$

3.3.3 VR controller (C-2)

The controller for the VR tries to adjust the set point of the VR, which is the output voltage of the regulator; in such a way that the voltages on the feeder will remain within their limits

and the reactive power support from the DGs is minimum. For this, at the beginning of each update cycle, the controller checks if the voltages are within limits. If not, then the controller determines if the VR alone can restore the voltages without support from the DGs. This is done by solving the following optimization problem:

$$
\begin{aligned}
&\textbf{\textit{Min}} \quad v_{OLTCT} \\
&\textbf{\textit{s.t.}} \quad V_{i+1} = V(v_i, P_i, Q_i) && \text{---------- } \textit{(feeder model)} \\
&\qquad 0.95 \le v_i \le 1.05 && \text{---------- } \textit{(n- voltage constraints equations, for n nodes)} \\
&\qquad pf_i = 1.0 && \text{---------- } \textit{(m- pf-voltage relation equations, for m DGs)}
\end{aligned}
$$

Note that the power factors of the DGs are set to unity to prevent the reactive power support from the DGs. The output of this optimization gives the minimum set point the VR needs to restore the voltages on the feeder. If the new set point is outside the limits of the VR, which are usually between 0.95 and 1.05, it indicates that the VR alone cannot provide voltage regulation. In this case, the controller sets the new set point to the limit value. The controller sends the new set point to the VR and waits (i.e. does not run) until it gets the feedback from the VR confirming that the VR moved the voltage to the desired level. This waiting provides the coordination between the two controllers by letting the DGs provide emergency support while the VR is taking the corrective action.

3.4 Test results

In order to evaluate the effectiveness of the proposed supervisory controller, a prototype distribution feeder is used with three DGs. The controller performance and its ability to keep all DGs within limits will be monitored for three cases, sudden increase in feeder load, sudden disconnection of a DG, and under severe contingency.

3.4.1 Test System

The feeder simulated is the IEEE 34 node prototype feeder [IEEE34], which represents a long feeder serving a mixed set of loads. The feeder is modified by adding three DGs on the main feeder. With the DGs supplying most of the load, two VRs on the original feeder are replaced by the substation VR as it provides enough voltage regulation on the feeder. The VR is assumed to move its taps in 180 seconds for a ±5 percent voltage regulation. The three DGs are modeled as fuel cells with a controller to regulate the DG's active power and power factor (P_t, pf) (DG model details are given in [BE02]). It is assumed that every DG location also provides the power flow measurements from the feeder. The approximate feeder used by the controller is therefore an 8 node feeder as given in Figure 20. The feeder is simulated using PSCAD and is shown in Figure 21. As indicated in the previous section, the loads in the reduced feeder correspond to the total load between the two measurement points (Table 1). In the simulation, the loads are represented by their equivalent impedance and are assumed to be constant power loads.

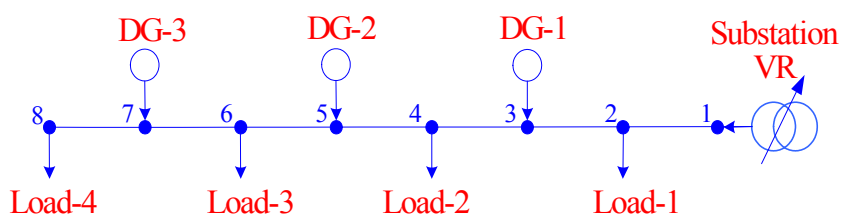

Figure 20: Approximate feeder for the controller

Table 1: Feeder loads

Node	*P (kW)*	*Q (kVar)*
2	80	40
4	180	80
6	500	170
8	950	0

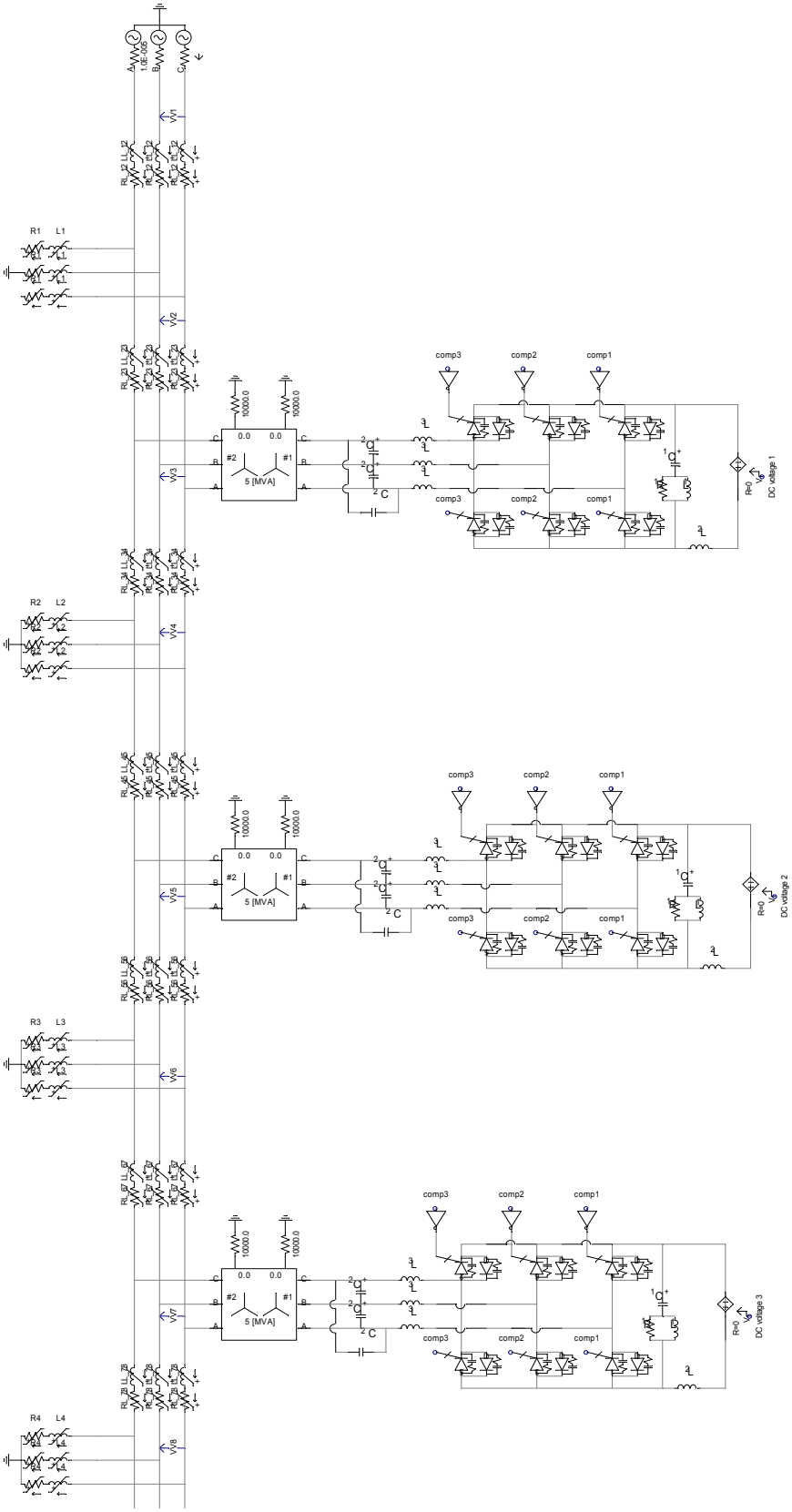

Figure 21: Tested feeder model in PSCAD

3.4.2 Simulation platform

To simulate the supervisory controller and the feeder model, two different simulation platforms were incorporated, the PSCAD/EMTDC platform and the Matlab platform (Figure 22). The PSCAD platform [Man] is perfect for simulating the actual feeder with its feeder impedances, loads, and DGs dynamic responses, but the PSCAD is not powerful enough to be used in designing our optimal controller. Therefore, the Matlab platform is utilized for designing and executing the controller. A special interface block in PSCAD is used to link both platforms. The interface block obtains the required feeder data and sends it at every interval Δt to the controller in Matlab. The controller in Matlab runs and generate optimal output commands for each DG and the VR. Those output set points are received by the interface block and sent to its corresponding device. In the simulation, the Δt is set to 1.5 seconds, which means that every 1.5 seconds the supervisory controller generates new set points to the VR and the DGs.

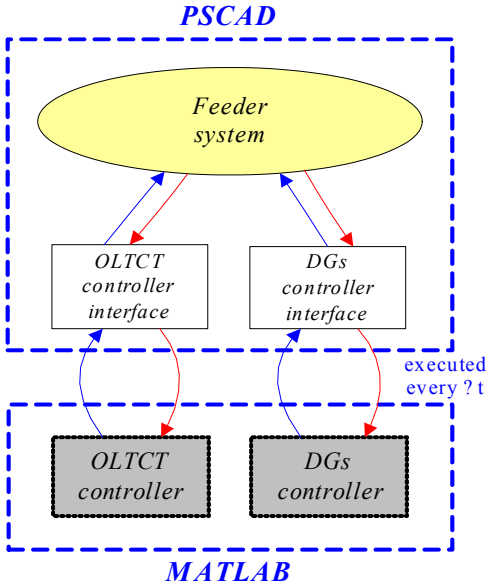

Figure 22: Simulation platform

3.4.3 Test results

Three *operating* conditions have been simulated on the prototype system. Details about these three cases are given below.

Case 1- Change in Feeder Load

This case illustrates the controller response to a load change on the feeder. The load change has been simulated by increasing every load on the feeder by 10 percent. The DG contributions in this case are set to 750 kW for DG1 and DG2, and 250 kW for DG3, with each operating at unity power factor. The simulation results are given in Figure 23. The top plot shows the minimum voltage profile (at node 8), the middle plot shows the set points for VR calculated by the supervisory controller versus the VR actual output voltage, and the bottom two plots show the pf settings calculated by the supervisory controller and the corresponding reactive power output of DGs. From the figures, the four different stages of the response to the load change can be seen:

Stage 1 (0 – 1.5 sec):

This is the pre-event period during which the VR has set its output to 1.02 p.u. to keep the feeder node voltages within acceptable limits (1.05-0.95), as the minimum voltage at node 8 is 0.951 p.u. During that period, the power factor of the three DGs is unity.

Stage 2 (1.5 – 2.4 sec):

This period starts with the load increase at 1.5 seconds. The voltages drop temporarily to about 0.92 p.u. as a result of this event. The controller notices the voltage drop with a time delay of 0.9 sec. (Note that the controller gets the updated data at every 1.5 sec).

Stage 3 (2.4 – 55.2 sec):

This is the emergency period. At t = 2.4 seconds, the supervisory controller notices that there are low voltages on the system and starts sending new corrective signals (set points) to the VR and the DGs. As indicated in the figure, the controller determines the new set point for the VR at 1.044 p.u. and the VR starts increasing its output voltage accordingly (with a constant rate determined by VR speed of operation). The controller sets the pf of the DGs originally to 1.0, 0.97, and 0.9 for DG1, DG2, and DG3, respectively. The bottom two figures show how the controller updates these set points as the VR changes its output voltage at every 1.5

seconds and how the DGs adjust their reactive power support accordingly. It is important to notice that throughout this period the minimum voltage at node 8 is kept constant at 0.95 p.u. as the top figure shows. This period ends, in this case, with the VR reaching its new set point at 55.2 second and the DGs returning to their normal operation (unity power factor) with no reactive power support for voltage regulation.

Stage 4 (55.2 – 80 sec):

This period shows the new steady state operating point the feeder has reached due to the 10 percent step increase in load.

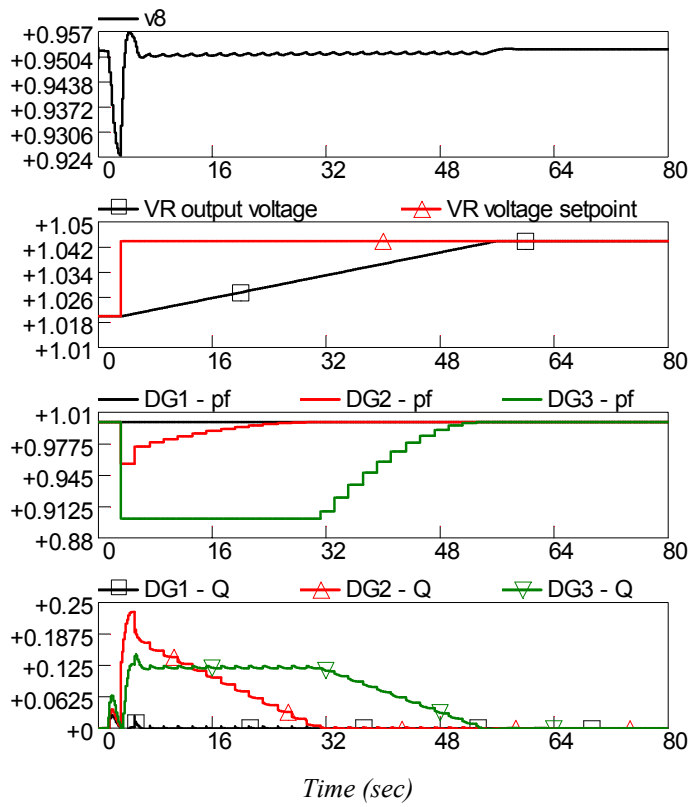

Figure 23: Simulation results for Case 1

For an overall look at the feeder's eight nodes, Figure 24a shows the voltage levels of the eight nodes throughout the simulation period, and a zoomed in window on the first seven seconds is shown in Figure 24b. Both figures show how the proposed controller's actions impacted the voltage profile along the feeder, making all nodes operate within acceptable

voltage limits. The exact voltage level of each node at each stage is shown in Table 2.

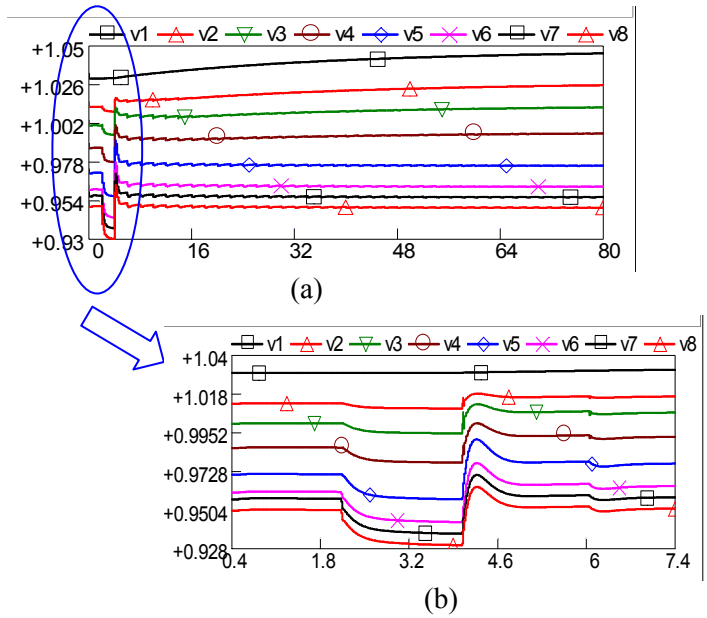

Figure 24: Voltage levels of the 8 nodes

Table 2: Node voltages at different time intervals

Node	voltage @ 0 - 1.5	voltage @ 1.5 – 2.4	voltage @ 2.4 - 80
1	1.03	1.03	1.047
2	1.012	1	1.03
3	1.0	0.995	1.021
4	0.987	0.978	1.001
5	0.971	0.956	0.991
6	0.961	0.943	0.969
7	0.957	0.936	0.96
8	0.95	0.93	0.95

To conclude, the plots illustrate that the controller has performed as desired. The controller quickly identifies the new set point for the VR and while the VR moves towards this new set point, the controller uses the DGs to keep the voltages within acceptable levels. The controller lets the DGs return to their normal operating point as soon as the VR lifts the voltage level of the feeder above the minimum level.

Case 2- Sudden Disconnection of a DG

This case shows the effect of a sudden disconnection of a DG on the feeder voltage level and the response of the controller to this event. The feeder is assumed to be operating at the nominal load level considered in Case 1 with the three DGs providing the same power support before the event. The simulation results are given in Figure 25, which shows the feeder voltages and controller response as in Figure 23. The figure shows again the three stages of response. The event, the disconnection of DG3, occurs at 2.08 sec. and causes the voltages to drop. This time the lowest voltage drops to 0.914 p.u. The controller senses the voltage violation again about 1.12 seconds later (at 3.2 seconds in the simulation) and starts taking the corrective action. The controller calculates the new set point for the VR as 1.05 p.u. The initial set points for the remaining DG1 and DG2 are calculated as 0.97 and 0.9, respectively. During the emergency period, as in Case 1, the VR moves its taps towards the new set points while the DGs provide the reactive power to keep the voltage levels within acceptable limits. The emergency period in this case is a little longer (about 66 seconds) as it takes more time for the VR to move its tap to the higher set point of 1.05 p.u. The emergency period also ends in this case when the VR reaches its new set point (at 68.8 second). At this point, the VR can keep the voltages within limits without the support of the DGs (as indicated in the figure by the two DGs returning to the unity power factor operation). These results again illustrate that the supervisory controller performs as desired following the event of a DG connection. The controller keeps the voltages within acceptable levels all the time, except during the short period at the beginning, which corresponds to the time-lag period mainly determined by the data update rate. Note that in this case the DG disconnection does not cause severe voltage drop for the undervoltage protection of the remaining DGs to be activated, as the voltages remain above 0.9 p.u. all the time.

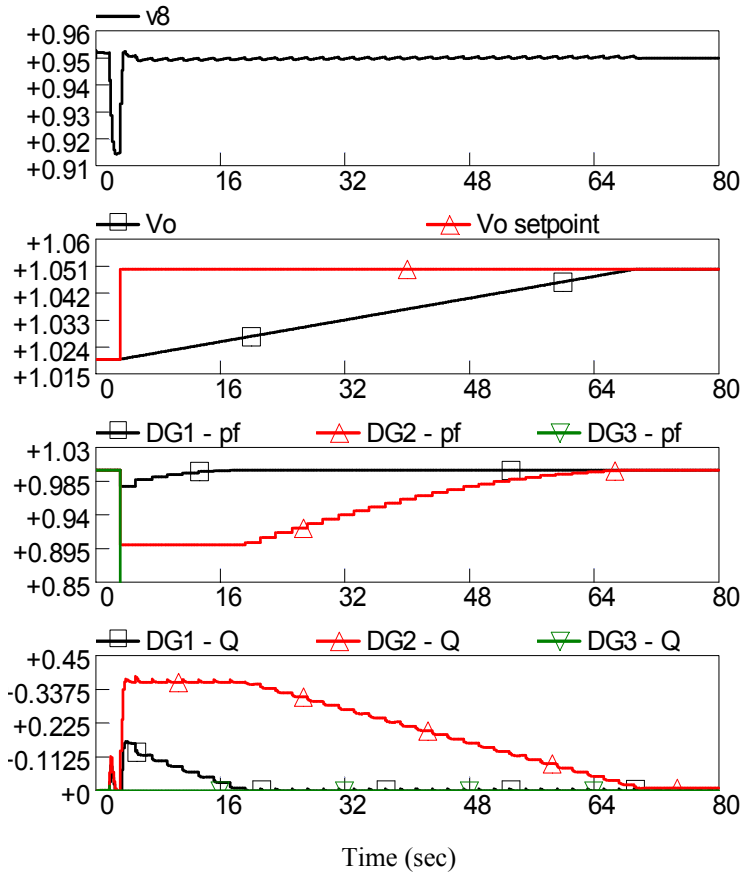

Figure 25: Simulation results for Case 2

Case 3- Severe Contingency:

This case simulates a more severe contingency than Case 2. This is created by changing the power support from the DGs. In this case, the DG1 and DG3 are assumed to provide 500 kW and DG2 to provide 700 KW. As in Case 2, contingency corresponds to disconnection of DG3. The simulation results for this case are given in Figure 26. The three stages of response are seen in the figure. The disconnection of DG3 (at 1.75 sec.) causes the voltages to drop. This time, the lowest voltage drops to 0.86 p.u. The controller senses the voltage violation about 0.8 seconds later (at 2.57 seconds in the simulation) and starts taking the corrective action. The controller calculates the new set point for the VR at the maximum level of 1.05 p.u.. Similarly, the initial set points for the remaining DG1 and DG2 are set to their lowest limit of 0.85 in order to get the maximum reactive power support. This reactive power support from the DGs boosts the minimum voltage level to 0.92. The DGs maintain this maximum support during the emergency period until the VR

raises its output voltage enough so that the minimum voltage reaches the minimum level (at 50 sec.). The emergency period in this case ends at about 93 seconds with the VR reaching its new set point. But in this case, the VR alone cannot raise the minimum voltage above the minimum level. Therefore, the DGs are set to provide reactive power even after this point.

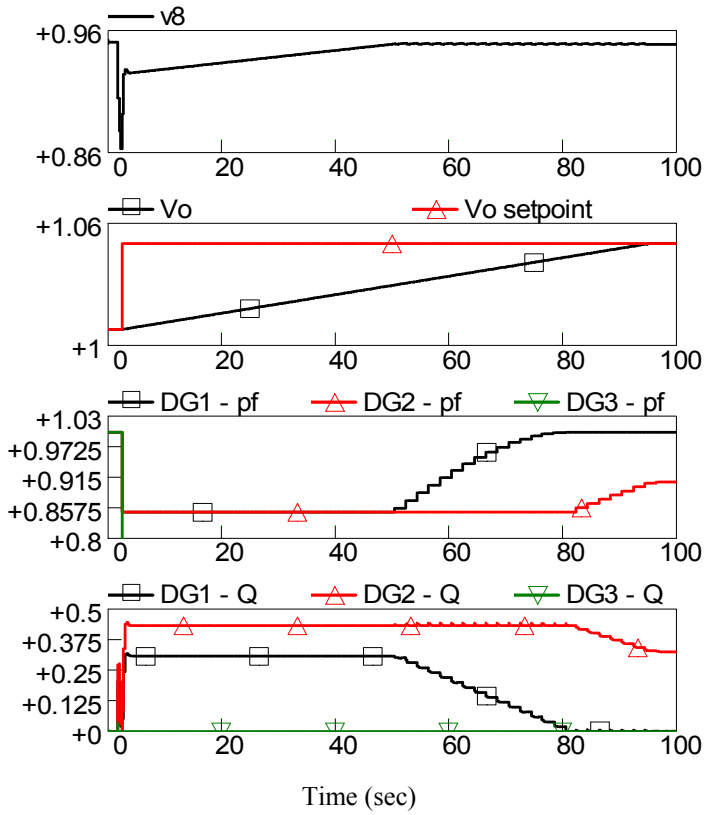

Figure 26: Simulation results for Case 3

Note that in this case the DG disconnection does cause severe voltage dip at nodes 6, 7 and 8. The voltage dip is low enough to activate the undervoltage protection of DG2 (0.876 p.u.). However, since the controller restores the voltage level above 0.9 p.u. in about 0.8 seconds (as shown in Figure 27), the controller action prevents the DG2 from tripping due to low voltage.

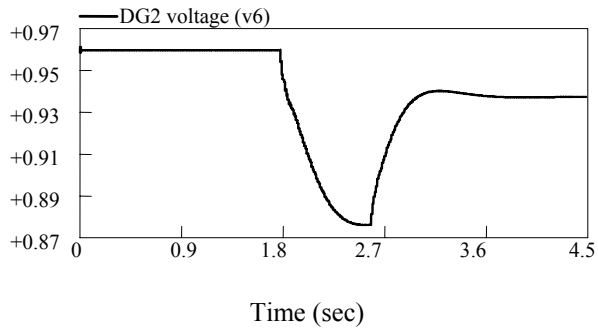

Figure 27: Voltage seen by DG2 in Case 3

3.5 Summary

This chapter presented a central controller designed to regulate the voltage along a feeder with the presence of DGs. The chapter started by defining and explaining the feeder voltage control problem, illustrating that the connection of multiple DGs on a feeder renders the voltage regulation on the feeder provided by a conventional VR ineffective and tighter voltage regulation is needed for the DGs to operate properly. The chapter identified that the two limitations of the conventional VR are the dependence on only the local measurement(s) and the slow response time, which need to be addressed in order to meet the new tighter voltage regulation requirements on the feeders.

An approach designed to keep all nodes on a given feeder within acceptable voltage limits when DGs are connected to that feeder is proposed. The proposed supervisory controller depends on employing DGs for the quick reactive power support needed especially under emergency conditions. Moreover, the proposed controller provides the necessary coordination between the feeder voltage regulator and the DGs. The details of the controller design and architecture were discussed in the chapter.

Finally, three case studies were simulated to test the performance of the proposed central voltage controller. They were a sudden increase in feeder load, a sudden disconnection of a DG, and a sever contingency. The test results indicated that the controller performs as desired because it provides a tight voltage regulation on the feeder at minimum reactive power cost under both normal conditions and also under the severe contingencies such as the sudden disconnection of a DG.

CHAPTER FOUR

Feeder Voltage Regulation using MAS

4.1 Introduction

This chapter presents an approach for solving the feeder voltage regulation problem in a distributed manner, with the goal of fulfilling the plug-and-play feature desired by manufacturers and regulatory bodies. The plug–and–play feature will enable customers to simply connect their DGs to the feeder, and through a MAS all DGs will cooperate with the feeder's VR to help maintain the feeder voltage level within limits at minimum cost.

4.1.1 Objective and approach

One approach to solve a complex optimization problem in a distributed manner using MAS, is to decompose the original problem into a series of smaller subproblems each assigned to a particular agent. Additional constraints or a supervisory (master) subproblem could be used to ensure that solving each subproblem independently will yield the same, or at least a similar, solution to the original problem [SW03], [TC00] and [DS90]. This methodology is not appropriate for the problem at hand, since it depends on knowing the explicit system model, which will be unavailable if we were to adopt the plug-and-play feature. Therefore, the objective of this chapter is to develop another approach that facilitates solving the feeder voltage regulation problem in a distributed manner without the need for the exact feeder system model.

The approach presented exploits special features and characteristics in the problem to determine simpler relationships between the overall goal and the available actions. As shown in section 4.2, these relationships will be used together with the ability of each agent to sense its local variables and reformulate the optimization problem in a distributed form. That distributed problem could be solved via MAS using the contract net protocol (CNP) and will yield the exact solution as the original optimization problem. The architecture of the MAS along with the CNP solving procedure and test results will also be presented.

4.2 Feeder Voltage Regulation

This section begins by presenting the feeder voltage regulation problem, and then attempts to linearize and decouple the problem in order to determine the input-output relationship. That relationship will then be utilized to reformulate the problem in a form that makes solving it in a distributed manner simpler to realize.

4.2.1 DG reactive power dispatch

As mentioned in the previous chapter, the aim is to determine the minimum reactive power needed from each DG in order to keep the feeder within voltage limits. The problem was formulated as an optimization problem as shown below:

Min $z = \sum \Delta Q_i = \Delta Q_3 + \Delta Q_5 + \Delta Q_7$

S.t
- $v_i = f(v_i, P_i, Q_i)$ *Feeder system model*
- $0.95 \leq v_i \leq 1.05$ *voltage constraints* for all nodes, $i=1 \ldots n$
- $0.85 \leq pf_i \leq 1$ *power factor constraint*, for DGs $i=1 \ldots m$

Where feeder model is $\vec{S}_i = P_i + jQ_i = \vec{V}_i^2 \left[Y_{i(i+1)} + Y_{i(i-1)} \right] - \vec{V}_i \left[\vec{V}_{i+1} Y_{i(i+1)} + \vec{V}_{i-1} Y_{i(i-1)} \right]$

The objective function represents the cost of dispatch, which is the total amount of reactive power needed from all DGs. The power factor constraints ensure that the reactive power support from the DGs will be within their capabilities, as they will limit the DGs' reactive power values based on their real power outputs. The node voltage constraint ensures that

the dispatched reactive power values will maintain the voltage level of all nodes within acceptable limits.

4.2.1.1 Dispatching as a Control Problem

The dispatching problem can also be viewed as a control problem. From the control perspective, the problem is a distributed control problem where controllers on DGs need to adjust the DGs reactive power outputs such that the voltage profile on the feeder remains within the limits. If we examine the voltage profile on a feeder with the DGs adjusting their outputs according to the desired optimal scheme (i.e., the DGs provide the optimal support), we see that the voltage profile, as illustrated in Figure 28, is monotonically decreasing from the substation towards the end of the feeder, and the voltage at the end of the feeder is at its lowest limit of 0.95 p.u. Therefore, it could be said that the goal of the control is to raise the low voltage at the end of the feeder, V_n, to the lower limit. In other words, for this control problem, the V_n is the output variable and the controllers will try to bring this variable to the desired level of 0.95 p.u. whenever the voltage goes below that value.

To design the controller, the first step is typically to determine the system model in a transfer function form, i.e., determine a relationship between the input variables (DGs reactive power outputs, Q_{DG}'s) and the output V_n. Determining the input output relation of the system is shown below.

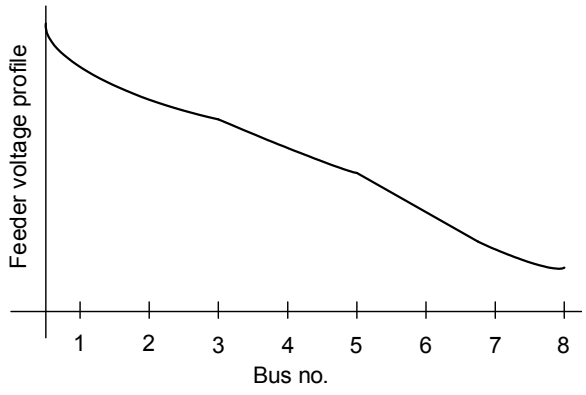

Figure 28: Monotonically decreasing voltage profile with DGs connected

Feeder Representation:

As noted previously, the power flow equations constitute the system model. They are, however, non-linear. Therefore, to get the desired input-output representation from these equations they will be linearized.

To illustrate the process, let us consider the 8 node prototype feeder in Figure 21. The power flow equations for each node and for each phase (neglecting the mutual couplings) are in the following form:

$$\vec{S}_i = P_i + jQ_i = \vec{V}_i^{\,2}\left[Y_{i(i+1)} + Y_{i(i-1)}\right] - \vec{V}_i\left[\vec{V}_{i+1}Y_{i(i+1)} + \vec{V}_{i-1}Y_{i(i-1)}\right]$$

By separating the real and imaginary components of the above complex power balance equation, sixteen nonlinear algebraic equations will be formed as follows:

$$\begin{aligned}
P_1 &= V_1^{\,2}G_{11} + V_1 \cdot V_2 \cdot G_{12} & Q_1 &= -V_1^{\,2}B_{11} + V_1 \cdot V_2 \cdot B_{12} \\
P_2 &= V_2^{\,2}G_{22} + V_2 \cdot V_1 \cdot G_{12} + V_2 \cdot V_3 \cdot G_{23} & Q_2 &= -V_2^{\,2}B_{22} + V_2 \cdot V_1 \cdot B_{12} + V_2 \cdot V_3 \cdot B_{23} \\
&\vdots & &\vdots \\
P_7 &= V_7^{\,2}G_{77} + V_7 \cdot V_6 \cdot G_{67} + V_7 \cdot V_8 \cdot G_{78} & Q_7 &= -V_7^{\,2}B_{77} + V_7 \cdot V_6 \cdot B_{67} + V_7 \cdot V_8 \cdot B_{78} \\
P_8 &= V_8^{\,2}G_{88} + V_8 \cdot V_7 \cdot G_{78} & Q_8 &= -V_8^{\,2}B_{88} + V_8 \cdot V_7 \cdot B_{78}
\end{aligned}$$

where B_{ij} , G_{ij}, are constants and correspond to the feeder line section impedance between nodes i and j. Let the line section impedance be $z_{ij} = R_{ij} + jX_{ij}$, and the admittance be $y_{ij} = z_{ij}^{-1} = g_{ij} + jb_{ij}$. It is important to note that b_{ij} has a negative value.

$$G_{ii} = \sum_{j=0}^{n} g_{ij} \;\;\&\;\; G_{ij} = -g_{ij} \qquad\qquad B_{ii} = \sum_{j=0}^{n} b_{ij} \;\;\&\;\; B_{ij} = -b_{ij}$$

The linearization of these equations around the operating point will result in the following set of linear equations (see Appendix B for details):

$$\begin{bmatrix} \Delta P \\ \Delta Q \end{bmatrix} = \begin{bmatrix} J_1 & J_2 \\ J_3 & J_4 \end{bmatrix} \cdot \begin{bmatrix} \Delta\theta \\ \Delta V \end{bmatrix}$$

where the Jacobian matrix gives the linearized relationship between the small changes in the voltage angle $\Delta\theta$ and magnitude ΔV, and the small changes in real and reactive power ΔP & ΔQ. Elements of the Jacobian are the partial derivatives with respect to θ and V at a given operating point.

These equations could be further simplified by using the well-known fact that real power is more sensitive to the $\Delta\theta$, and reactive power is more sensitive to ΔV, (i.e, the sensitivity terms in J_2 and J_3 are much smaller in magnitude than the terms in J_1 and J_4). Therefore, we can approximate $J_3 = J_2 \cong 0$ (see Appendix B for details). This will yield the following decoupled equations:

$$\Delta P = J_1 \Delta\theta \qquad \text{---------- (4.1)}$$

$$\Delta Q = J_4 \Delta V \qquad \text{---------- (4.2)}$$

Where $J_1 = \begin{bmatrix} \frac{\partial P_2}{\partial \theta_2} & \cdots & \frac{\partial P_2}{\partial \theta_n} \\ \vdots & & \vdots \\ \frac{\partial P_n}{\partial \theta_n} & \cdots & \frac{\partial P_n}{\partial \theta_n} \end{bmatrix}$ and $J_4 = \begin{bmatrix} \frac{\partial Q_2}{\partial V_2} & \cdots & \frac{\partial Q_2}{\partial V_n} \\ \vdots & & \vdots \\ \frac{\partial Q_n}{\partial V_n} & \cdots & \frac{\partial Q_n}{\partial V_n} \end{bmatrix}$

To get the input-output relationship, the injection terms in the above equations will be considered. The power injections at the load nodes will not change substantially, as the load will not change substantially during the control period. Moreover, the real power output of the DGs will not change. Therefore, we can approximate the real power injection terms in (4.1) as zero, and use Eq (4.2) to get the transfer function.

For the 8 node feeder, Eq (4.2) is of the following form:

$$\begin{bmatrix} \Delta Q_2/V_2 \\ \Delta Q_3/V_3 \\ \Delta Q_4/V_4 \\ \Delta Q_5/V_5 \\ \Delta Q_6/V_6 \\ \Delta Q_7/V_7 \\ \Delta Q_8/V_8 \end{bmatrix} = -\begin{bmatrix} B_{22} & B_{23} & 0 & & \cdots & & 0 \\ B_{23} & B_{33} & B_{34} & & & & \\ 0 & B_{34} & B_{44} & B_{45} & \ddots & & \vdots \\ & & B_{45} & B_{55} & B_{56} & & \\ \vdots & & \ddots & B_{56} & B_{66} & B_{67} & 0 \\ & & & & B_{67} & B_{77} & B_{78} \\ 0 & & \cdots & & 0 & B_{78} & B_{88} \end{bmatrix} \cdot \begin{bmatrix} \Delta V_2 \\ \Delta V_3 \\ \Delta V_4 \\ \Delta V_5 \\ \Delta V_6 \\ \Delta V_7 \\ \Delta V_8 \end{bmatrix} \qquad \text{---------- (4.3)}$$

Since the ΔQs are zero at the load nodes, these equations could be rearranged by regrouping the load nodes and DG nodes separately:

$$\begin{bmatrix} 0 \\ 0 \\ 0 \\ 0 \\ \hline \Delta Q_3/V_3 \\ \Delta Q_5/V_5 \\ \Delta Q_7/V_7 \end{bmatrix} = -\left[\begin{array}{cccc|ccc} B_{22} & 0 & & 0 & B_{23} & 0 & 0 \\ 0 & B_{44} & & & B_{34} & B_{45} & 0 \\ & & B_{66} & 0 & 0 & B_{56} & B_{67} \\ 0 & & 0 & B_{88} & 0 & 0 & B_{78} \\ \hline B_{23} & B_{34} & 0 & 0 & B_{33} & & 0 \\ 0 & B_{45} & B_{56} & 0 & & B_{55} & \\ 0 & 0 & B_{67} & B_{78} & 0 & & B_{77} \end{array}\right] \cdot \begin{bmatrix} \Delta V_2 \\ \Delta V_4 \\ \Delta V_6 \\ \Delta V_8 \\ \hline \Delta V_3 \\ \Delta V_5 \\ \Delta V_7 \end{bmatrix} \qquad \text{---------- } (4.3')$$

In general these equations could be written as

$$\begin{bmatrix} 0 \\ \hline \Delta Q_i/V_i \end{bmatrix} = -\left[\begin{array}{c|c} A_1 & A_2 \\ \hline B_1 & B_2 \end{array}\right] \cdot \begin{bmatrix} \Delta V_L \\ \hline \Delta V_G \end{bmatrix} \qquad \text{---------- } (4.4)$$

where ΔV_L and ΔV_G correspond to the voltages at the load and generator nodes, respectively. Note that the equations correspond to the nodal equations of an equivalent DC circuit with branch conductance of b_{ij} and node current injections of Q_i. It is also important to mention that $B_{88} = -B_{78}$, therefore from the fourth row in the matrix Equation (4.3') we can observe that $\Delta V_7 = \Delta V_8$, which will later be shown to be very useful.

By manipulating the Equation (4.4), the desired input-output relationship between the ΔQ_i and ΔV_G is obtained:

$$\left(B_1 A_1^{-1} A_2 - B_2\right)\Delta V_G = \Delta Q/V$$

For the prototype feeder, these equations can be written explicitly as:

$$\begin{bmatrix} \Delta Q_3/V_3 \\ \Delta Q_5/V_5 \\ \Delta Q_7/V_7 \end{bmatrix} = \left[\begin{bmatrix} B_{23} & B_{34} & 0 & 0 \\ 0 & B_{45} & B_{56} & 0 \\ 0 & 0 & B_{67} & B_{78} \end{bmatrix} \cdot \begin{bmatrix} 1/B_{22} & 0 & 0 & 0 \\ 0 & 1/B_{44} & 0 & 0 \\ 0 & 0 & 1/B_{66} & 0 \\ 0 & 0 & 0 & 1/B_{88} \end{bmatrix} \cdot \begin{bmatrix} B_{23} & 0 & 0 \\ B_{34} & B_{45} & 0 \\ 0 & B_{56} & B_{67} \\ 0 & 0 & B_{78} \end{bmatrix} - \begin{bmatrix} B_{33} & 0 & 0 \\ 0 & B_{55} & 0 \\ 0 & 0 & B_{77} \end{bmatrix} \right] \cdot \begin{bmatrix} \Delta V_3 \\ \Delta V_5 \\ \Delta V_7 \end{bmatrix}$$

$$\begin{bmatrix} \Delta Q_3/V_3 \\ \Delta Q_5/V_5 \\ \Delta Q_7/V_7 \end{bmatrix} = \underbrace{\begin{bmatrix} -B_{33} + \frac{B_{23}^2}{B_{22}} + \frac{B_{34}^2}{B_{44}} & \frac{B_{34}B_{45}}{B_{44}} & 0 \\ \frac{B_{34}B_{45}}{B_{44}} & -B_{55} + \frac{B_{45}^2}{B_{44}} + \frac{B_{56}^2}{B_{66}} & \frac{B_{56}B_{67}}{B_{66}} \\ 0 & \frac{B_{56}B_{67}}{B_{66}} & -B_{77} + \frac{B_{67}^2}{B_{66}} + \frac{B_{78}^2}{B_{88}} \end{bmatrix}}_{M} \begin{bmatrix} \Delta V_3 \\ \Delta V_5 \\ \Delta V_7 \end{bmatrix}$$

Let the coefficient matrix be M, therefore the desired input-output representation will be:

$$\Delta V_G = \mathbf{M}^{-1}\Delta\mathbf{Q}$$

Note that the coefficient matrix M is symmetric and is of the following form, for proof see Appendix B section B3:

$$M = \begin{bmatrix} a & -m & 0 \\ -m & b & -c \\ 0 & -c & c \end{bmatrix}$$

where *a, b, c, m,* and *p* are all positive constants, as $B_{ij} = -b_{ij}$ terms are positive and $B_{ii} = \sum_{j=0}^{n} b_{ij}$ are negative. Furthermore, $b = m + c$, then M^{-1} will always have the following form, for proof see Appendix B section B4:

$$\begin{bmatrix} \Delta V_3 \\ \Delta V_5 \\ \Delta V_7 \end{bmatrix} = \begin{bmatrix} k & k & k \\ k & n & n \\ k & n & p \end{bmatrix} \begin{bmatrix} \Delta Q_3/V_3 \\ \Delta Q_5/V_5 \\ \Delta Q_7/V_7 \end{bmatrix} \qquad \text{---------- } (4.5)$$

and the constants have the property that $k > n > p$. This special form will be used in development of the controller in the next section.

4.2.2 Controller Design

The input-output equation (4.5) shows how much the output (the voltage V_i) will change for a given change in the input (the reactive power injection ΔQ_i from DGs). From the structure of equation (4.5), several observations could be developed, which will help in designing the controller that is suitable for the distributed implementation.

4.2.2.1 Impact of a DG support on node voltages

Let, for example, DG_3 increase its Q output by ΔQ_3, while the other DGs do not (therefore $\Delta Q_5 = \Delta Q_7 = 0$). This Q support will result in the node voltage increase on the feeder, and the following equations, (4.6) - (4.8), estimate the resulting voltage boost at the DGs' nodes and the last node (output).

$$\Delta V_3)_{due-to-Q3} = k \cdot \Delta Q_3 / V_3 \qquad \text{---------- (4.6)}$$

$$\Delta V_5)_{due-to-Q3} = k \cdot \Delta Q_3 / V_3 \qquad \text{---------- (4.7)}$$

$$\Delta V_7)_{due-to-Q3} = k \cdot \Delta Q_3 / V_3 \qquad \text{---------- (4.8)}$$

The first equation, equation (4.6), shows the sensitivity of the voltage at a DG node due to the Q injected by the node's DG.

$$k_i = V_i^0 \frac{\Delta V_i}{\Delta Q_i}$$

where k is constant and depends mainly on the location of the DG along the feeder, and V_i^0 is the node voltage before injecting ΔQ_i. These sensitivity factors can be obtained by the DGs based on the local observations, i.e. by measuring the voltage boost at their nodes following an increase in their Q output.

The other equations, equations (4.7, 4.8), also indicate that the voltage boost at the nodes that are downstream of node 3, at which Q is injected, will be the same as that of the node 3. Similarly, if only the DG at node 5 is injecting ΔQ_5, from equation (4.5) we find that,

$$\Delta V_5 = \Delta V_7 = n \cdot \Delta Q_5 / V_5$$

This confirms that the voltage boost in node 5 is equal to that in node 7, due to an increase in the reactive power injected at node 5 by a value of ΔQ_3.This observation will hold in general. Therefore, we can claim the following:

<u>*Claim:*</u>

The voltage boost a DG will provide, on its node's voltage and the voltages of downstream nodes, via increasing its Q output by ΔQ, *can be estimated using local measurements.*

<u>*Proof:*</u>

As shown in appendix B section B4, the general form of the coefficient matrix, M, relating reactive power of a DG, ΔQ_G, to the corresponding boost in the node voltages of the DGs, ΔV_G, for "n" number of DGs, will be as follows:

$$\begin{bmatrix} \Delta V_{G1} \\ \Delta V_{G2} \\ \vdots \\ \\ \\ \Delta V_{Gn} \end{bmatrix} = \begin{bmatrix} k & \cdots & & & k \\ k & n & \cdots & & n \\ k & n & p & \cdots & p \\ k & n & p & \ddots & \\ k & n & p & & \\ \vdots & \vdots & \vdots & & r \end{bmatrix} \begin{bmatrix} \Delta Q_{G1} \\ \Delta Q_{G2} \\ \vdots \\ \\ \\ \Delta Q_{Gn} \end{bmatrix}$$

Therefore, if DG-*i* injects ΔQ_i into the feeder, then

$$\Delta V_i = M(i,i)\ \frac{\Delta Q_i}{V_i}$$

and $\Delta V_{i+1} = M(i+1,i)\ \dfrac{\Delta Q_i}{V_i}$

and $\Delta V_{i+2} = M(i+2,i)\ \dfrac{\Delta Q_i}{V_i}$

up to $\Delta V_n = M(n,i)\ \dfrac{\Delta Q_i}{V_i}$

From the structure of *M* shown above, we find that

$$M(i,i) = M(i+1,i) = M(i+2,i) = \cdots\cdots = M(n,i)$$

Therefore, $\Delta V_i = \Delta V_{i+1} = \Delta V_{i+2} = \cdots\cdots = \Delta V_n = M(i,i)\ \dfrac{\Delta Q_i}{V_i}$

For example if DG3 is injecting ΔQ_{G3}, then the voltage boost on node 3 and the down-stream nodes will be:

$$\Delta V_{G3} = \Delta V_{G4} = \Delta V_{G5} = \cdots\cdots = \Delta V_n = p\ \frac{\Delta Q_{G3}}{V_{G3}}$$

Therefore, we can conclude that the reactive power injection of a DG will boost the voltage level of its local node and the down-stream nodes on the feeder by the same value. Moreover, the voltage boost value could be determined using the local measurements of the DG, which is the DG's sensitivity factor and local node voltage.

Figure 29 shows the voltage profile along an 8 node feeder without having any of the DGs inject reactive power. If DG at node 3 injects reactive power that result in an increase in its local node voltage by a value of "Δv" volts, according to our claim, the voltage level at the end of the feeder will increase by the same value "Δv" volts, which is shown in Figure 30.

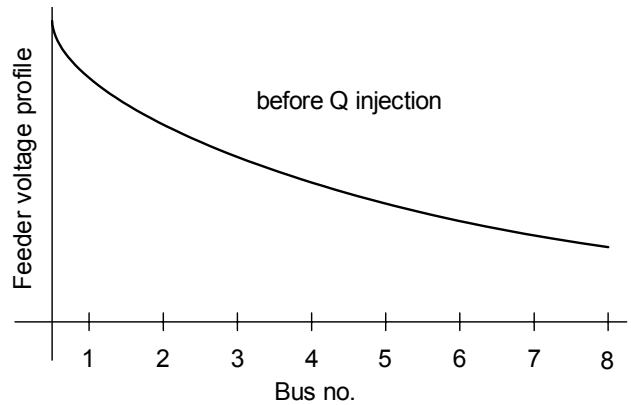

Figure 29: Eight node feeder voltage profile

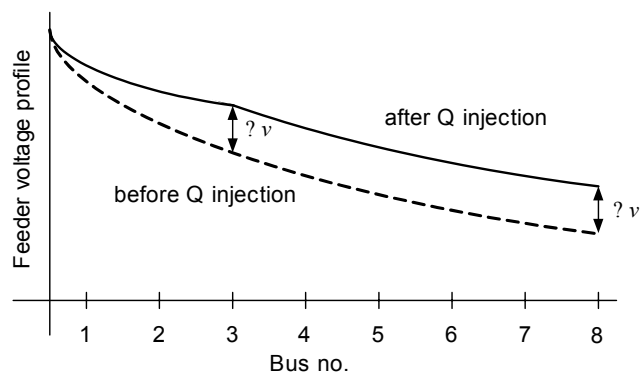

Figure 30: Feeder voltage profile with Q injected at node 3

The significance of this observation is that the DG can estimate how much voltage boost it can provide based on its local data. Furthermore, the linear model of equation (4.5) indicates that the total voltage boost due to reactive power support from the available DGs can be estimated by superposition. In other words, the increase in voltage at the end of the feeder will be equal to the total change in the nodes' voltages due to contributions by the DGs that provided the support. For the example considered, if the three DGs connected at nodes 3, 5 and 7, provides Q support, then the voltage boost at the end of the feeder is:

$$\Delta V_8 = k\frac{\Delta Q_3}{V_3} + n\frac{\Delta Q_5}{V_5} + p\frac{\Delta Q_7}{V_7} \qquad \text{---------- } (4.9)$$

This is illustrated by the simulation in Figure 31. Note that each term in the above equation corresponds to the contribution of the corresponding DG and can be calculated by the DGs local information.

For the DG agent to know its sensitivity factor, k_i, a simple test has to be done when the DG is first connected to the network. Each DG will inject a certain amount of reactive power (ΔQ_i) and the local node's voltage level will be measured before and after the ΔQ_i injection. Form the difference between the two voltage measurements (ΔV_i), and the node's voltage level before the reactive power was injected V_i, the DG agent can evaluate its k_i by simply dividing the measured, $V_i \cdot \Delta V_i$, by the injected ΔQ_i.

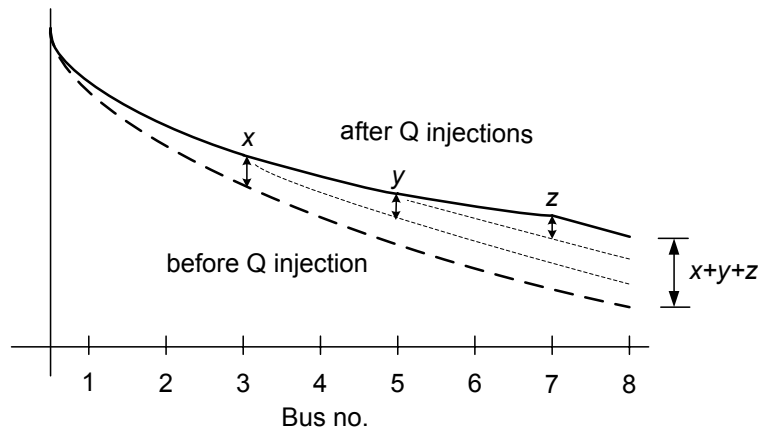

Figure 31: Feeder voltage profile with Q injected at nodes 3, 5 & 7

4.2.2.2 DG reactive power dispatch

Now, using the input-output function, the control problem can be rewritten as:

$$Min \quad \sum \Delta Q_i$$

$$\text{S.t} \quad \bullet \quad \Delta V_8 = \frac{k_3}{V_3}\Delta Q_3 + \frac{k_5}{V_5}\Delta Q_5 + \frac{k_7}{V_7}\Delta Q_7 = 0.95 - V_8 \quad \text{----------} \; (4.10)$$

$$\bullet \quad 0 \le \Delta Q_i \le Q_{\max - i}$$

This problem is similar to the generator real power economic dispatch problem. In this case, the power to be dispatched is the reactive power, and the power balance equation is replaced

with the voltage limit constraint. The optimality conditions for this problem would be the same as that of the real power economic dispatch, and thus should satisfy the optimality condition (neglecting the Q limit constraints):

$$\lambda = 1/a = 1/b = 1/c$$

where λ is the Lagrange multiplier associated with the voltage constraint and indicates incremental cost of dispatch, and terms 1/a, 1/b and 1/c correspond to the penalty factors. The optimality condition in (4.10) cannot be satisfied as written, but what it indicates is that the DG with the smallest penalty factor should be dispatched first, i.e $\lambda = \min(1/a, 1/b, 1/c)$. For example, if DG_3 is the DG with the minimum penalty factor, then it will be dispatched up to its maximum limit $Q_3 = Q_{3max}$. If dispatching DG_3 is not enough to satisfy the constraint, then the unit with the second smallest penalty factor should be dispatched, and so on, until the Q support from the units is enough to satisfy the voltage constraint (i.e. provide enough voltage boost at the end of the feeder).

The optimality conditions indicate that the dispatching can be achieved by following the simple ordering determined by the DGs penalty factors. More importantly, dispatching does not need to be done in a centralized manner. The dispatching can be implemented in a distributed fashion that will satisfy the plug-and-play rules. To achieve this, it is proposed that the MAS distributed domain be used by using the CNP. The following section will show that the architecture proposed will ensure that the MAS will reach the optimal solution.

4.3 Overview of multi-agent systems

The interest for MASs has grown in the last few years [Sch01]. MASs are used in a great variety of applications such as electronic commerce, air traffic control, and process control. The popularity of MAS is due to the fact that it presents a means for naturally understanding, designing, and implementing several classes of complex distributed control problems. This growing attention to multi-agent technology has been more emphasized with the increase in Internet computing, which presents a space in which autonomous agents can

roam and interact with one another. Since MAS consists of several agents, then we first need to understand what is an agent.

4.3.1 What is an agent?

An agent is anything that can be viewed as perceiving its environment through sensors and acting upon that environment through actions. Wooldridge and Jennings [IL01] describe a *weak notion* of agency that involves *autonomy* or the ability to function independently, *social ability* by which agents interact with each other, *reactivity* allowing agents to perceive and respond to changes in environment, and *pro-activeness* through which agents behave in a goal-directed fashion. They also describe a *strong notion* of agency, prevalent in AI which, in addition to weak notion also uses mental components such as belief, desire, intention, and knowledge, and so on.

4.3.2 Multi-agent system (MAS)

As indicated by its name, a MAS is a macro-system comprising multiple agents, each of which is considered a micro-system. MASs result from the organization of multiple agents within an environment. For all independent problem solving agents to come together to form a coherent whole, they need to *coordinate* their activities and *cooperate* with each other in order to avoid duplication of effort, avoid unintentionally hindering other agents in achieving their goals, and to exploit other agents' capabilities [IL01].

Schumacher in [Sch01] points out three main characteristics for MASs:

- In MASs, every agent has a subjective view. It can only have incomplete information of the system, because its view point is limited.
- As a consequence of the first characteristics, no global control is applied. Each agent has its proper state that is not accessible by other participants in the system.
- The data is fully decentralized and is distributed in the participating agents and the environment.

The advantages of a MAS in comparison to single-agent systems are as follows [Sch01, Jen96]:

- The implementation of problems that ask for distributed data and control are more naturally realized using MASs.
- *Faster problem solving* by exploiting parallelism.
- *Decrease communication* by transmitting only high level partial solutions to other agents rather than raw data to central site.
- *More robustness and reliability because* the failure of an agent can be overcome if another agent takes over the uncompleted work.
- *More flexibility* by having agents with different abilities dynamically team up to solve a problem.
- *Scalability because* a MAS could easily be extended by adding new agents.

4.3.3 Design of MAS

When analyzing the MAS, we find that the central issue is how agents cooperate and coordinate their actions. Coordination is the process by which an agent reasons about its local action and the (anticipated) actions of others to try and ensure the community acts in a coherent manner. Without coordination, the benefits of decentralized problem solving vanish and the community may quickly degenerate into a collection of chaotic, incohesive individuals [Jen96]. In MAS coordination, two issues are important. The first is plan construction, which includes problem decomposition and conflict resolution, and the second is the means of communication. These issues will be discussed next.

4.3.3.1 Multi-agent Planning

A multi-agent plan is a plan which has been generated for multiple executing agents. With multi-agent planning techniques, agents build a plan and commit to behave in accordance with it. This plan describes all actions needed to achieve the respective goals of the MAS. Von Martial (1992) distinguishes two classes of distributed MAS planning:

- *Task driven planning (Task allocation)*

  In this planning system, there is an initial goal or task that is decomposed into sub-goals or sub-tasks and is assigned to several agents. On one extreme, the designer can make the task assignments in advance, thus creating a non-adaptive, problem-

solving organization [Syc98]. This approach is limiting and inflexible for dynamic and open environments. However, one can do task allocation dynamically and flexibly. Davis and Smith's [Syc98, JH98] work on flexible allocation of tasks to multiple agents resulted in the well-known CNP. This protocol will be briefly explained later.

- *Plan coordination*

  In contrast to the previous planning system, plan coordination deals with situations in which agents' plans preexist and the problem is to reconcile the given plans before they are performed in a common environment.

Generally, multi-agent planning needs some kind of synchronization. Agents' plans may be conflicting, but such conflicts can be solved by a particular agent (coordinator) or a solution may be reached through negotiations.

CONTRACT NET PTOTOCOL (CNP) [Syc98]

In this protocol, agents can take two roles: manager or contractor. Given a task to perform, an agent first determines whether it can break it into subtasks that can be performed concurrently. It utilizes the protocol to announce the tasks that could be transferred and requests bids from agents that could perform any of these tasks. An agent that receives a task announcement message replies with a bid for the task, indicating how well it thinks it can perform the task. The contractor collects the bids and awards the task to the best bidder. The CNP allows nodes to broadcast bid requests to all others. Although the CNP was considered by Davis, Smith, and many DAI researchers to be a negotiation principle, it is a coordination method for task allocation. CNP enables dynamic task allocation, allows agents to bid for multiple tasks at a time, and provides natural load balancing (busy agents need not bid). Its limitations are that it does not detect or resolve conflicts, the manager does not inform nodes whose bids are refused, there is no preemption in task execution (time critical tasks may not be attended to), and it is communication insensitive. It is important to mention that extensions have been made to mitigate some of these limitations, as shown by Sandholm in [San96].

4.3.3.2 Communication and interaction

Interaction between agents is essential in a MAS. If agents are unable to interact with one another, no global behavior in the MAS is possible [Sch01]. Agents communicate by exchange information-carrying messages with each other to coordinate their activities. In MASs, two main strategies may be used to support communication. Agents can exchange *messages* directly or they can access a shared data repository (called a *blackboard*) in which information can be posted and retrieved. Message passing and communication through blackboard may be combined in complex systems [Sch01].

The interaction between agents is based on specific communication means that can be classified into four basic paradigms [Sch01].

a) *Peer to peer* communication: messages are sent directly to a specific agent.
b) *Broadcast* communication: a message is sent to everybody in the MAS.
c) *Multicast* communication: a message is sent to a specific group of agents.
d) *Generative* communication: agents generate messages on a blackboard, which can be read by other agents.

4.4 MAS for Feeder Voltage Regulation

This section discusses how the MAS approach is designed and used to implement the algorithm developed earlier, such that the feeder voltage regulation problem can be solved in a distributed manner.

4.4.1 MAS architecture

The MAS will consist of several heterogonous agents, of which there are four different types, as shown in Figure 32. These agents will collaborate to maintain the voltage level along the feeder within acceptable limits, each operating at its own speed.

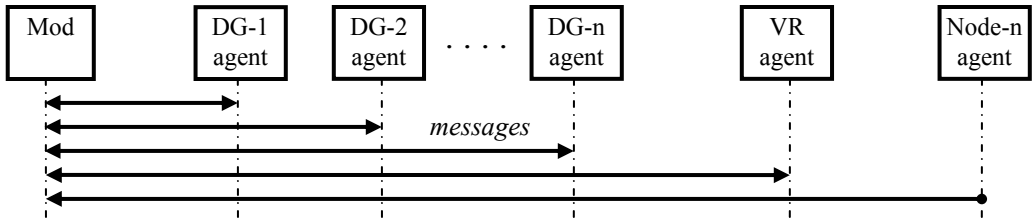

Figure 32: Different types of agents in the MAS

<u>*Agents and their role*</u>

Moderator: The moderator agent's role is to manage the bidding process by issuing request for proposals (RFP) and assigning bids to winning bidder.

DG agent: The DG agent will respond to the RFP sent by the moderator by sending a proposal containing its cost and maximum capability. When an agent is assigned a task, it will implement it via its associated DG.

Node-n agent: Node-n agent is located at the end of the feeder. It will measure the voltage level of the last node and thus decide on the voltage boost needed to maintain the voltage level within acceptable limits. The node-n agent will then report the amount of voltage needed to the moderator agent, which will use it to issue a RFP.

VR agent: When the VR agent receives a message from the moderator indicating the amount of increase in voltage level needed, the agent will adjust the VR accordingly.

4.4.2 Reactive power dispatch

For the MAS to correctly dispatch the reactive power over the DGs, each DG agent will need to know its sensitivity factor k_i and its local node voltage V_i in order to actively participate in the bidding process mentioned in the previous section. Each DG agent will also have to be aware of the maximum available reactive power its DG can supply. As mentioned previously, by knowing k_i each DG agent can estimate the voltage boost in its local node and down-stream nodes, for a specific reactive power output, the coordination of

such voltage support from all agents is achieved through the moderator agent. Figure 33 shows the overview of the MAS, where the moderator agent will coordinate the actions of agents to ensure optimum reactive power dispatch.

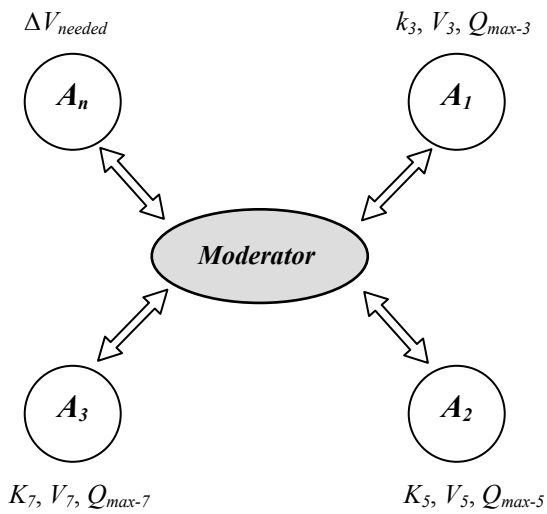

Figure 33: Overview of MAS

Figure 34 illustrates the solution process, which starts with the Node-n agent sending the moderator a message with the overall goal, that is the voltage boost needed at the end of the feeder. The moderator will then issue a RFP to each DG agent. Each DG agent will reply with its penalty factor β_i (where $\beta_i = V_i / k_i$) and maximum available action value ($\Delta Q_{i\text{-}max}$). The moderator will award each agent a contract instating how much Q support is needed from each agent. This assignment will be according to the optimality rules, as previously discussed.

In the example in Figure 34, the overall voltage boost requested by the node-n agent is 0.1 p.u. The moderator will award the agent with the lowest penalty factor, A3 with penalty factor of 5, a contract for its maximum available Q, 0.3 MVARs. But since the voltage boost resulting from such contract, 0.3 ÷ 5 = 0.06 p.u., is still smaller than the required overall voltage boost. The moderator will award a second contract to A2 with a value 0.4 MVAR. This awarded contract will result in an additional voltage boost equals to 0.4 ÷ 10 = 0.04 p.u., which when added to the voltage boost from A3, will be enough to achieve the requested voltage boost of 0.1 p.u.

Such process is called the reactive power dispatch update, where the moderator updates the values of the reactive power dispatched to each DG agent according to the overall goal requested by the Node-n agent. For regulating the feeder's voltage throughout the contingency period, successive reactive power dispatch updates are needed. This will be illustrated later in the test result.

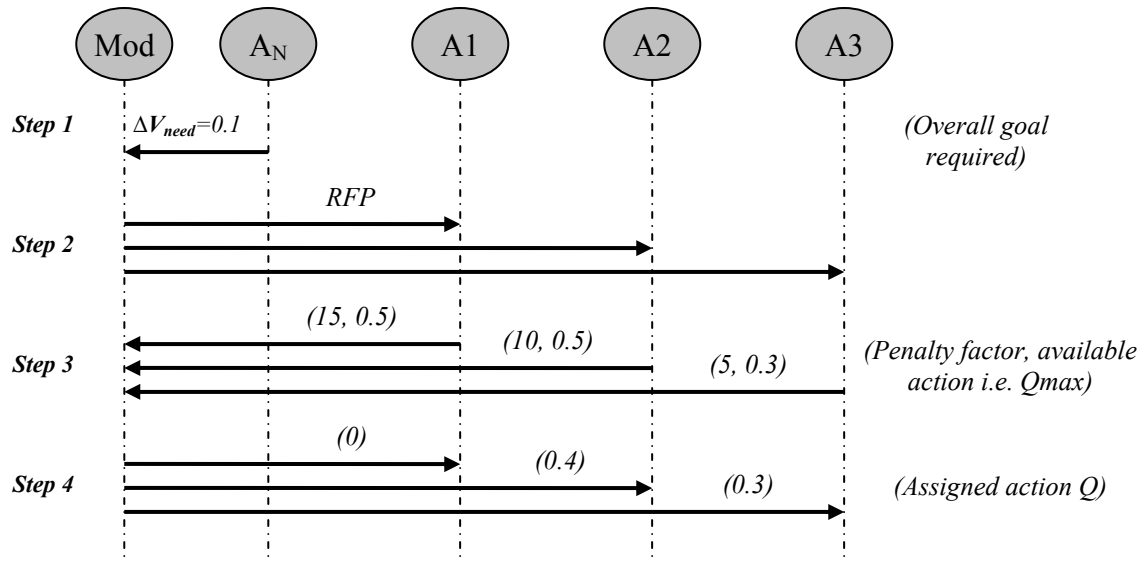

Figure 34: Solution process for a single reactive power dispatch update

Test results

The feeder used in Chapter 3 (section 3.4.1) is used to test the proposed distributed controller. The reactive power dispatched for each generator and the resulting voltage level at the end of the feeder is presented in Figure 35.

This test corresponds to the case of the sudden disconnection of DG_3, which caused the node voltage at the end of the feeder (node 8) to drop to 0.9202 p.u. The optimum solution reached by the central controller for the reactive power dispatched for the remaining two DGs is:

Q_{DG1} (@ node 3) = 0.0726 MVAR

Q_{DG2} (@ node 5) = 0.3632 MVAR

That reactive power dispatched boosted the voltage level of node 8 to 0.95 p.u.

The MAS-based scheme solved the problem in three iterations. The assigned reactive power for each DG and the corresponding voltage level at node 8 for each iteration is presented in Table 3. Notice that by the second iteration the MAS scheme reached an acceptable solution. For the program flow refer to Appendix B.

Table 3: Distributed controller output for each iteration

Iteration	***Q_{DG1} (@ node 3)***	***Q_{DG2} (@ node 5)***	***V node 8***	***|Δ error|***
Event start	0	0	0.9202	0.0298
1	0.1219	0.3632	0.9527	0.0027
2	0.0647	0.3632	0.9496	0.0004
3	0.0724	0.3632	0.95	0.00

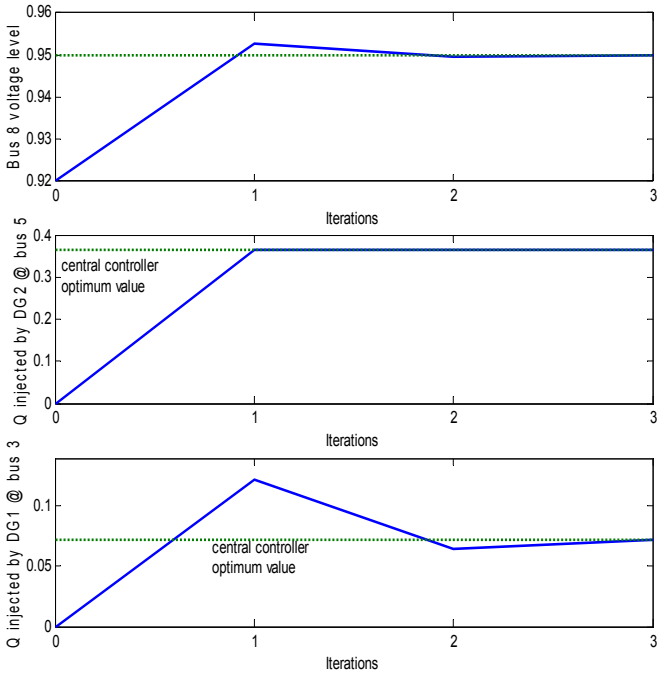

Figure 35: Distributed approach solution

4.4.3 Feeder voltage regulation

For the MAS to solve the feeder voltage regulation problem, it will have to operate in two phases. The first phase of the problem is when the MAS needs to coordinate the *contribution* of the DGs in order to ensure a fast and optimum voltage regulation. The second phase starts

when the VR begins picking up the voltage support for the feeder, and the MAS needs to coordinate the *relief* of the DGs from their voltage support in a slow and optimum manner.

Phase 1: Full dispatch of DGs for voltage support

This phase starts when *node-n agent* reports to the moderator the need for ΔV_n as soon as a contingency occurs. The moderator takes two actions in parallel:

a) The moderator broadcasts a RFP for all DGs and they respond in the manner discussed previously to quickly resolve this problem.
b) The moderator will forward the message to the *VR agent.*

The *VR agent* will then adjust the voltage set point at the substation end of the feeder according to the received message and reply with a message that it is starting to resolve the problem

Phase 2: Ramped-down dispatch of DGs for voltage support

As the VR agent starts to contribute to the voltage support by increasing the voltage level of the feeder at the substation end, DGs will need to be gradually relieved from reactive power support. The ramping down of the DGs' reactive power dispatched is done as follows. As the VR starts contributing, the voltage at the end of the feeder will exceed the *0.95* p.u. level. When the voltage level increases by a value more than ε over the *0.95* p.u. level, the *node-n agent* will report such an increase in voltage level as ΔV_{over}. The *moderator agent* will check if the *VR agent* is still increasing its output voltage and some DGs are still injecting reactive power. If yes, then it will send the *DG agents* a request for relief (RFR). This procedure is exactly like the RFP procedure, except that the DG with the highest cost will be granted the relief first until it isn't injecting any more reactive power, then the next expensive DG is relieved and so on.

4.5 Test results

In order to evaluate the effectiveness of the proposed MAS based control scheme, a prototype distribution feeder is simulated with three DGs. The simulated feeder is the IEEE 34 node prototype feeder [IEEE34] represented in section 3.4.1. The MAS performance is tested by simulating the second and third cases discussed in section 3.4.3, which simulate the events of sudden disconnection of a DG and under severe contingency. In both cases, the MAS is assumed to update the reactive power dispatched to the DGs at every 1.5 seconds, until the VR restores the feeder voltage to an acceptable level. In each update only one iteration is executed, and reaching the optimum solution depends on the successive updating. The performance of the MAS will be compared with that of the central controller to evaluate the effectiveness of the proposed MAS.

4.5.1 Test results for case A: *sudden disconnection of a DG*

This case illustrates the effect the sudden disconnection of a DG has on the feeder voltage level and the response of the proposed MAS to this event. Before the event, the DG contributions are set to 750 kW for DG1 and DG2 and 250 kW for DG3 with all three operating at the unity power factor. The event, the disconnection of DG3, occurs after 9.5 seconds from the start of the simulation and causes the voltages to drop, making the lowest voltage level drop to 0.914 p.u. The simulation results are given in Figure 36 with the top plot showing the minimum voltage profile (at node 8), the middle plot showing the set point for the VR versus the VR actual output voltage, and the bottom plot showing the reactive power outputs of the two remaining DGs. From the figure, the four different stages of the MAS response to the DG disconnection event can be seen:

Stage 1 (0 – 9.5 sec):

This is the pre-event period during which the VR has set its output to 1.02 p.u. to keep the feeder node voltages within acceptable limits. During that period, the reactive power contribution from the three DGs is equal to zero.

Stage 2 (9.5 – 11.0 sec):

This period starts with the disconnection of DG3 at time 9.5 sec., causing the minimum voltage level to drop to about 0.914 p.u. The MAS is assumed to start reacting to the voltage drop with a time delay of 1.5 sec.

Stage 3 (11 – 76 sec):

This is the emergency period. At t = 11 seconds, MAS collaborates according to the procedures mentioned previously in section 4.4 and starts dispatching reactive power to DG-agents, and the VR agent uses the message sent by the node-n agent to adjusts the VR's set point. The VR agent determines the new set point for the VR to be 1.05 p.u., and the VR starts increasing its output voltage accordingly (with a constant rate determined by VR speed of operation). Initially the MAS dispatches 229 kVAR and 362 kVAR to DGs 1 and 2 respectively. This dispatch increases the voltage level of node 8 to 0.956 p.u., which is slightly above the minimum allowable voltage limit (0.95 p.u.). In the second dispatch update, which is 1.5 seconds later, the MAS adjust the reactive power dispatch depending on the new voltage, 0.956 p.u., sent by the node-n agent located at the end of the feeder. Thus the new dispatched reactive power to DG1 declines to 130 kVAR, while DG2's reactive power is kept constant. With this update, the MAS successfully brings the voltage level at the end of the feeder to 0.95 p.u.

During the successive updates in this stage, the agents of the MAS will collaborate and dynamically update the dispatched reactive power to each DG agent until the VR reaches its new set point and effectively takes over the feeder voltage support task. Such behavior is shown in the lower graph of Figure 36, where the amount of reactive power output from DG1 and DG2 dynamically decreases with steady increments until they reach zero by the end of this stage.

Stage 4 (76 – 85 sec):

This period shows the new steady state operating point the feeder has reached due to the disconnection of the third DG and the resulting increase in the VR voltage.

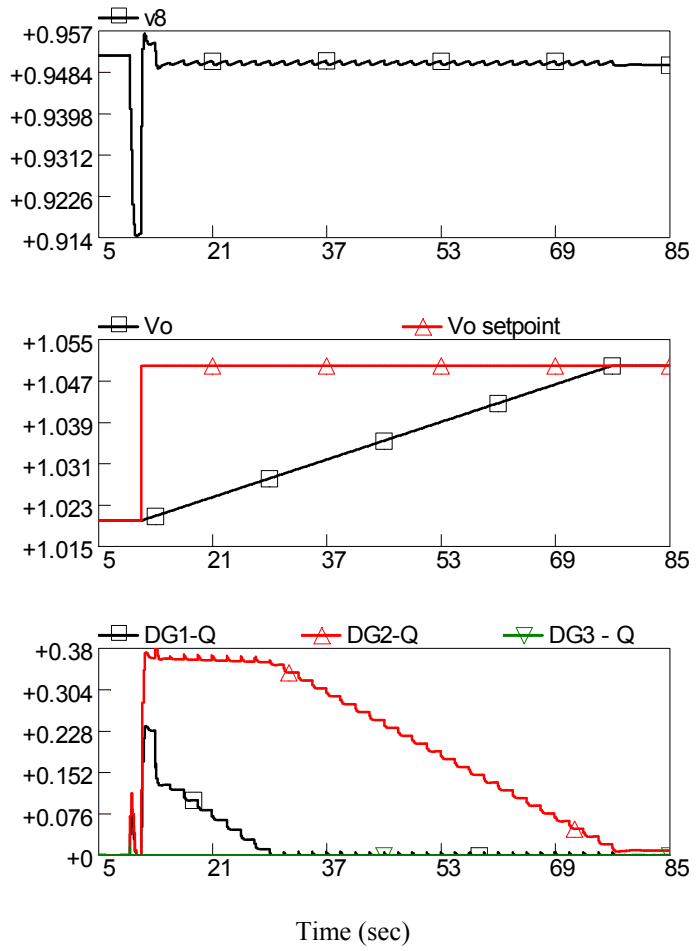

Figure 36: Simulation results for Case A

Comparing the MAS and central controller performance

To evaluate the MAS performance, the same test was repeated with the central controller dispatching the reactive power and setting the VR set point, and the results of both tests were compared. Figure 37 shows the voltage level at the end of the feeder and the reactive power of both DGs with the two control approaches. To see the details better, Figure 38 shows the portion of Figure 37 that corresponds to the 10 - 17 seconds time interval. Similarly, Figure 39 shows a zoomed window of the 50 – 75 seconds time interval.

Figure 38 shows that the MAS overestimates the amount of reactive power needed during the first reactive power dispatch, as it asks DG1 to inject 229 kVAR instead of the 181

kVAR that was assigned by the central controller to that DG. This means that the MAS asked DG1 to inject 48 kVAR more than the optimum solution would be. As seen in the same figure, the amount of reactive power injected by DG1 (the middle graph) for both cases gets closer in value in subsequent dispatch updates, and by the third update, the MAS reaches the optimum solution and continues to evaluate the optimum solution throughout the simulation. As for DG2 (the lower graph), such differences between the MAS and the central controller performance in the first dispatch is not obvious, because in both cases it is asked to inject its maximum available reactive power. Note that the voltage level at the end of the feeder (the upper graph) for the MAS case is higher by 0.004 p.u., this is simply because the amount of reactive power injected by the DGs under the MAS during the first dispatch is higher than that injected by the DGs under the central controller. In the duration presented in Figure 38 the amount of reactive power injected by DG1 under both control strategies has reached zero, and only DG2 is injecting reactive power. The reactive power injected by DG2 under the MAS is higher by 15 kVAR, which is a very small, almost negligible amount that only results in the voltage level at node 8 to be higher by 0.0009 p.u., as shown in the upper graph in the same figure.

This simulation shows that it takes the MAS just three dispatch updates to be able to reach the optimum solution it has been designed to reach. This is because the MAS relies on linearizing the nonlinear problem around the new operating point whenever a new power dispatch is being calculated. The operating points are mainly the node voltages, which only change significantly in the first two intervals and are almost constant for the rest of the intervals. Therefore, for intervals past the first two intervals, the MAS is capable of reaching the optimum solution in one step.

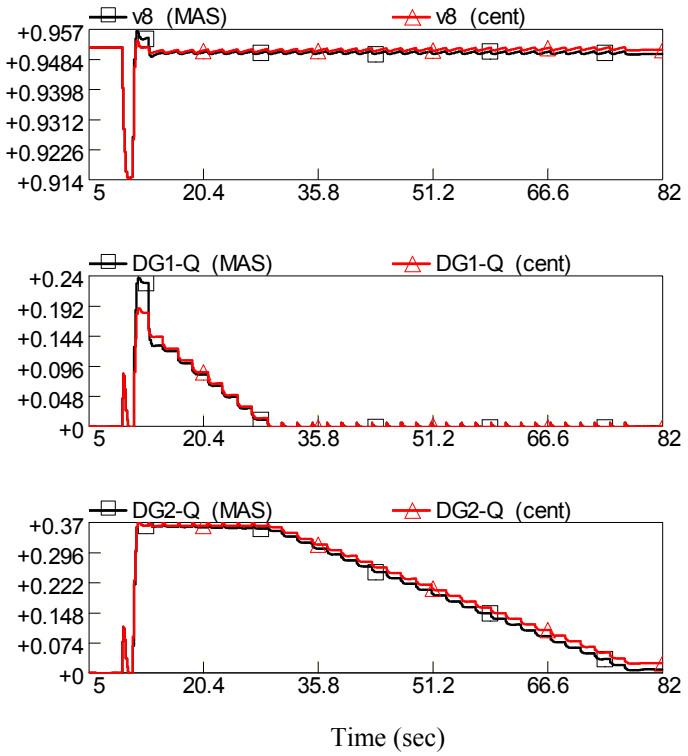

Figure 37: MAS vs. Central controller for Case A

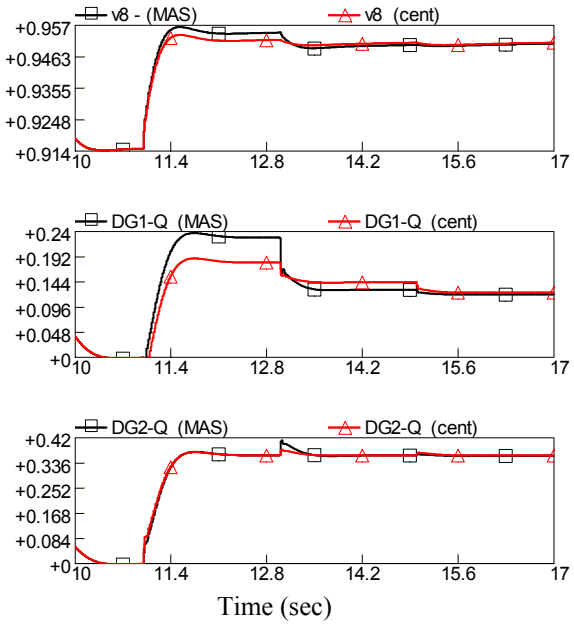

Figure 38: Zoomed window of Figure 37 for duration (10 -17) sec.

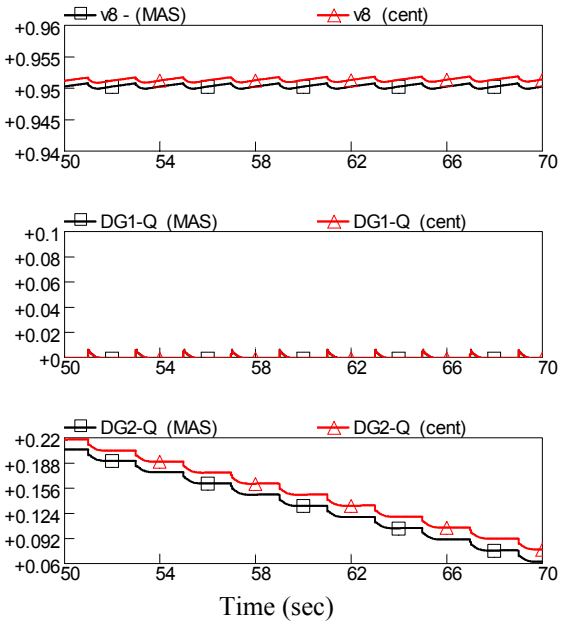

Figure 39: Zoomed window of Figure 37 for duration (50 -70) sec

4.5.2 Test results for case B: *Severe Contingency*

As indicated in Chapter 3, this case simulates a more severe contingency than Case A. This is created by changing the power support from the DGs, in this case the DG1 and DG3 are assumed to provide 500 kW and DG2 to provide 700 KW. As in Case A, contingency corresponds to disconnection of DG3. The simulation results for this case are given in Figure 40, with the four stages of response seen in the figure. The disconnection of DG3 (at 5.2 sec.) causes the voltages to drop, wth the lowest voltage dropping to 0.86 p.u. The MAS starts taking corrective actions 0.8 seconds later (at time equals 6 seconds in the simulation). The VR-agent decides on the new set point for the VR at the maximum level of 1.05 p.u. Similarly, the initial set points for the remaining DG1 and DG2 are set to their maximum limit, operating at 0.85 power factor, and injecting 310 kVAR and 434 kVAR, respectively. This reactive power support from the DGs boosts the minimum voltage level to 0.927 p.u. The DGs maintain their maximum support during the emergency period until the VR raises its output voltage enough so that the minimum voltage reaches the minimum level (at time equals 56 seconds). After that point, the MAS starts relieving the DGs gradually from the voltage support beginning with DG1. The emergency period in this case ends at about

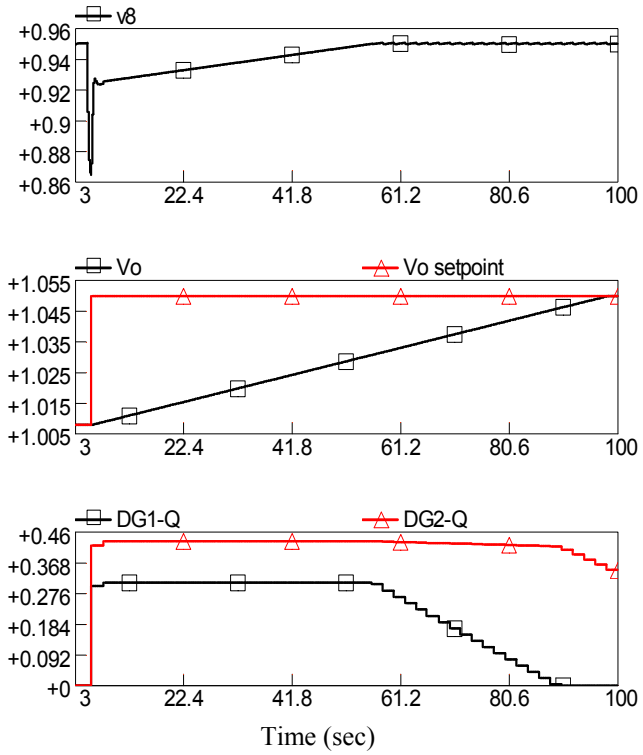

Figure 40: Simulation results for case B

98.4 seconds with the VR reaching its new set point. But in this case, the VR alone cannot raise the minimum voltage above the minimum level. Therefore, the DGs are set to provide reactive power even after this point and DG2 is expected to maintain its output reactive power at 348 kVAR.

Although the DG disconnection does cause severe voltage dip at nodes 6, 7, and 8 making the voltage dip low enough to activate the undervoltage protection of DG2 (0.876 p.u.), the MAS restores the voltage level above the 0.9 p.u. in about 0.8 seconds (as shown in Figure 41), preventing DG2 from tripping due to low voltage.

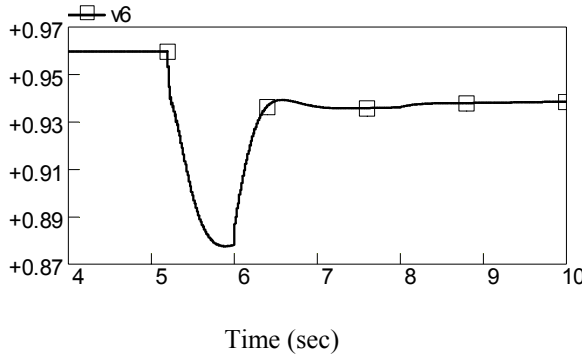

Figure 41: DG2 voltage level during event

Comparing the MAS and central controller performance

To evaluate the MAS performance of this test case, the MAS controller performance is compared with that of the central controller under the same test. Figure 42 presents the voltage level at the end of the feeder together with the output reactive power of both DGs for the two control approaches. Figure 43 shows the duration between time equals 5 and 15 seconds of the simulation, while Figure 44 shows a zoomed window for the duration between 55 and 72 seconds of the simulation. The figures show that during the first 56 seconds of the simulations the two controllers' outputs are identical. This is because during that period, both DGs were asked to inject their maximum reactive power. The difference between the MAS and the central controller can be seen in the duration following time equals 56 seconds. As seen in Figure 44 the reactive power injected by DG2 under the MAS is almost identical to that injected when the central controller is in charge, while the amount of reactive power injected by DG1 under the MAS is higher by

28 kVAR, which is a very small, almost negligible amount that only results in the voltage level at node 8 to be higher by 0.001 p.u.

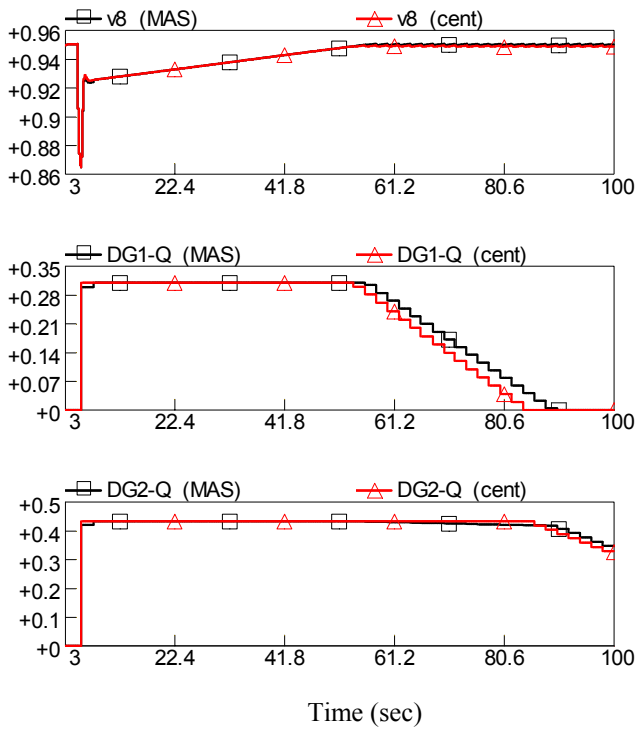

Figure 42: MAS vs. Central controller for case B

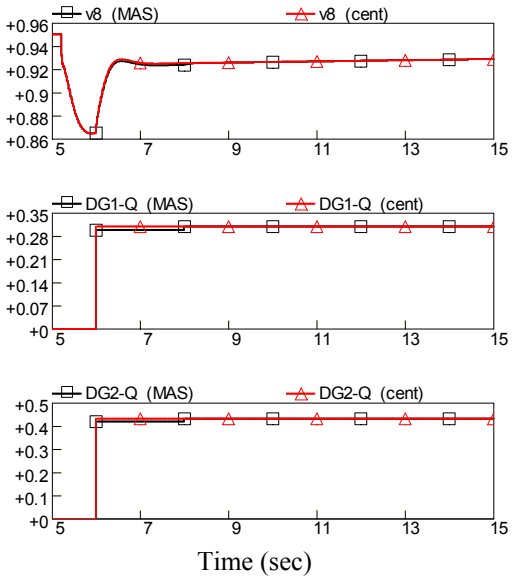

Figure 43: Zoomed window of Figure 42 for duration (5 -15) sec.

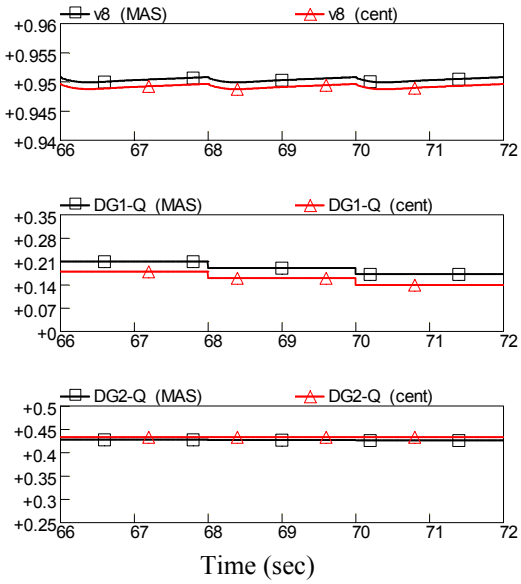

Figure 44: Zoomed window of Figure 42 for duration (66 -72) sec

Unlike the simulation of Case A, this simulation started with both DGs injecting their maximum reactive power. This made the difference in the performance of the MAS and central controller very small, and even through the period where the DGs are being relieved, the difference is still small with a minimal effect on the voltage level at the end of the feeder. This shows that the difference between the two control approaches only occur at the beginning when the operating condition (voltage level) changes abruptly. But when the feeder voltage level is constant, the two proposed approaches perform equally.

4.5.3 Impact of load type on the MAS performance

Feeder loads are usually represented using two models, the PQ model and the RL model. In the PQ model, the amount of active (P) and reactive (Q) power drawn by the load is assumed constant at all operating conditions, and in the impedance model, known as the RL model, the equivalent load resistance (R) and inductance (L) are assumed constant during the control period. Throughout the previous simulations, feeder loads were assumed to be at the constant PQ load. In this section, the impact of having different types of loads on the MAS performance will be studied.

To determine the load type impact on the MAS performance, Case A *(section 4.5.1)* is simulated twice, once with the feeder loads modeled as constant PQ loads and once with the feeder loads modeled as constant RL loads. Figure 45 shows the voltage level at the end of the feeder and the reactive power output of the DGs for both load types, while Figure 46 presents the simulation from time equals 9 seconds till time equals 19 seconds showing the first four intervals in the MAS solution. As previously mentioned in Case A *(section 4.5.1),* the contingency event occurs when DG3 disconnects after 9.5 seconds from the start of the simulation. The voltage drop due to that event will differ depending on the type of load. As shown in the figures below, in the case of a *PQ load,* the voltage level at the end of the feeder will drop to 0.914 p.u., while in the case of the *RL load,* the voltage will drop to only 0.928 p.u. This is because in the case of constant *RL load*, when the voltage drops the amount of active and reactive power drawn by the load decreases, thus the amount of current flowing through the feeder decreases which results in a smaller voltage drop.

At time equals 11 seconds, the MAS starts dispatching reactive power to the DG-agents. In the case of the *RL load,* the MAS will underestimate the amount of reactive power needed, thus the voltage level at the end of the feeder will be equal to 0.944 p.u., which is less than the allowable voltage limit. By the first dispatch update (@ *t=13 s*), the MAS will be able to successfully maintain the voltage at the end of the feeder within acceptable limits (Figure 46, upper graph).

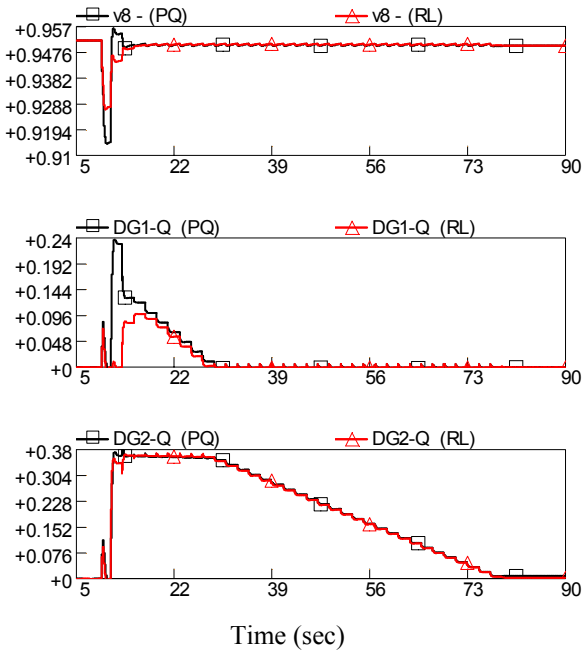

Figure 45: MAS performance for different load types (case A)

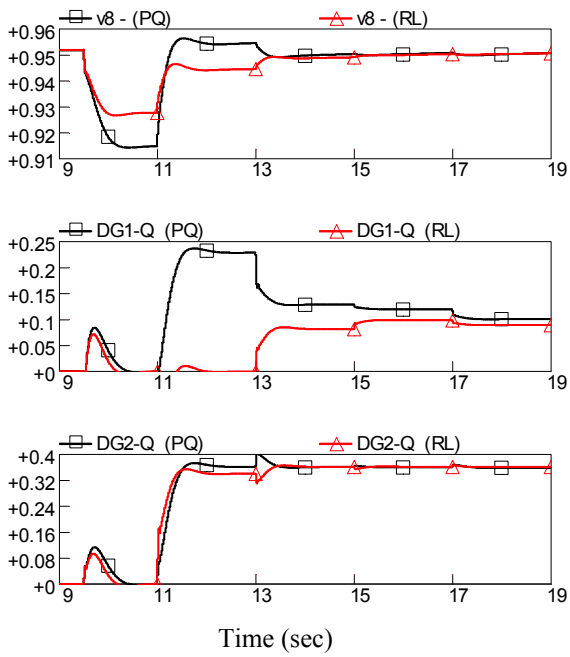

Figure 46: Zoom on first 10 seconds of the simulation (case A)

Figure 47 shows the MAS performance for Case B *(section 4.5.2)* with the two load types. The active power output for both DGs, shown in the middle and lower curves, are identical for the two different load types. During the second and third stages, where the VR hadn't reached its new set point, yet both DGs injected their maximum available reactive power for the two different load types. It is important to mention that v_8 (upper graph in Figure 47) during the second stage, where both DGs are injecting their maximum reactive power, is different for the two load types. This is because the *RL load* will withdraw less P and Q at lower voltages than the *PQ load,* thus the resulting voltage drop is less and the node voltage level is higher. As the voltage of v_8 gradually increases, the amount of P and Q withdrawn by the *RL load* gets closer to that withdrawn by the *PQ load*, until the voltage level reaches

0.95 p.u. (the same value prior to fault), where active and reactive power withdrawn from both load types is identical.

During the fourth stage, where the DGs are being gradually relieved from the voltage support, the dispatched reactive power for each DG is the same for both load types. This is because at that voltage level (0.95 p.u.) the P and Q withdrawn by both load types are equal.

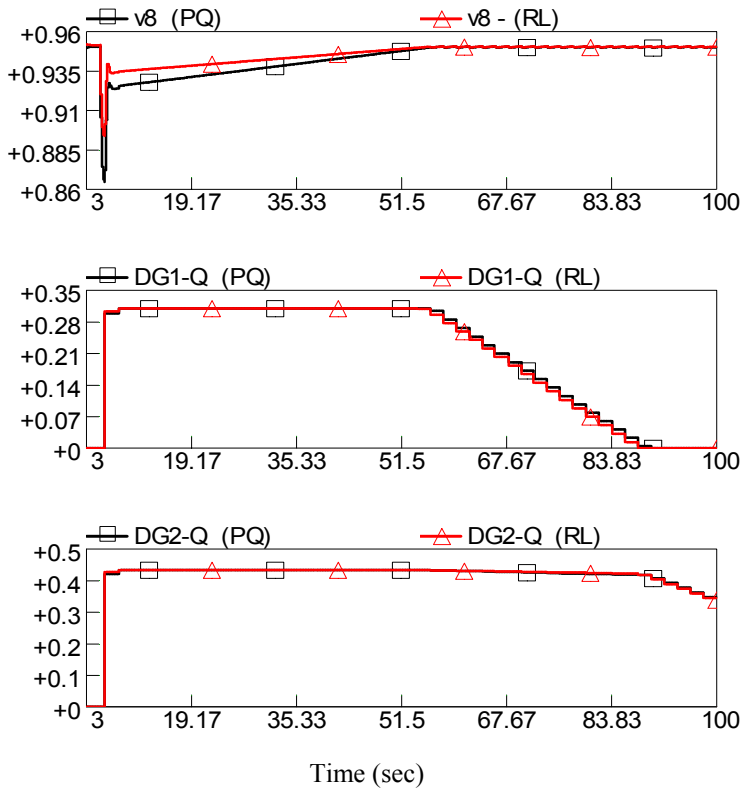

Figure 47: MAS performance for different load types (Case B)

4.6 Summary

This chapter developed a distributed MAS based controller for voltage regulation of feeders with the DGs. The new approach has the advantage of not needing the exact feeder model. Therefore, it facilitates the plug and play feature by which DGs can be connected to a feeder and contribute to the feeder voltage regulation without any changes on the other existing controllers on the feeder. It was shown that the approach is based on decomposing the problem by utilizing special characteristics of the feeder voltage regulation optimization

problem. The decomposed problem then can be solved by agents who only need to sense their local variables and cooperate with other agents in the MAS.

A quick overview of the multi-agent system was also presented. The steps of designing the MAS for feeder voltage regulation were described along with the MAS architecture. It was shown that a CNP-type protocol will enable the MAS to solve the voltage regulation problem.

Simulations were used to evaluate the MAS performance. Two cases were tested and compared with that of the central controller. The results showed that the MAS is effective in reaching the correct global optimum solution in all simulated cases. Finally, the impact of different load types on the performance of the MAS was discussed, and simulations were used to show that the MAS performance was not affected by different load types.

To conclude, a novel approach was presented in this chapter and the approach successfully managed to regulate the feeder voltage at minimum cost. The approach could be easily integrated with current VR and DG control technologies, as the agents are superimposed over current control devices, since it only adjusts and controls the conventional set points of these devices. Moreover, each DG can "*test and measure"* its local data, known as its sensitivity factor, as soon as it is connected to the feeder. Finally, this control approach is extremely flexible and allows any number of DGs to be added to the system without the need to re-adjust or re-tune already existing devices.

CHAPTER FIVE

Fault Analysis for distribution networks with distributed generators

5.1 Introduction

The focus of this chapter is on the development of a fault analysis program that can be used to estimate fault current distribution on a distribution system with distributed generation. The fault analysis is the main tool used to estimate the fault currents on power systems, and the fault current estimates are used to properly select and coordinate the protective devices, such as circuit breakers, reclosers (RC) and fuses [IEEE242]. The goal here is to extend the conventional fault analysis methods so that the new DGs can be included in the analysis, as the conventional analysis methods do not include models for the new inverter interfaced DGs (IIDGs).

In chapter two, section 2.3.2, a literature review was presented indicating that when a DG is connected to a feeder the fault current contribution from the DG will impact the reclosers and the fuses. It was illustrated that the potential impacts on the operation of the recloser are: (i) higher current level during the initial phase of the fault may expose the recloser to mechanical and thermal stresses beyond its rated limits, and (ii) the coordination between the recloser and the downstream fuses may be lost.

In order to address these two problems, we need to take into consideration the contribution the DGs will make to the fault currents that will be seen by the protective devices during fault conditions. To address the first problem, the maximum fault current the RC will see,

which is usually during the first cycle after the fault, needs to be estimated. To address the coordination problem, the fault current level within the first 10 cycles, called the transient period, is needed. Estimating these fault currents constitutes the main part of the fault analysis as defined by IEEE guidelines/standards [IEEE242]. (see Appendix C for details).

Extending the conventional fault analysis to include the inverter interfaced DGs is challenging, because, as it will be shown, it will require more detailed models than the models used to represent conventional turbine driven ac generators [BD00, BJ02, AK02].

In the following section, a quick review on conventional fault analysis techniques will be presented. In Section 5.3, the behavior of the DG during fault conditions will be investigated, and the proposed approach will be presented in Section 5.4. Finally, a case study will be discussed in section 5.5.

5.2 Conventional fault analysis on distribution systems

On conventional distribution systems, the only source for power is the substation. Usually, since the distribution substations are farther away from big generation units, the fault current transients on a distribution circuit/feeder following a fault on the feeder. It does not have the initial high "subtransient component" that one can see in a fault current on the transmission system. An actual fault profile on a feeder is given in Figure 48. As the figure illustrates, the fault current profile is almost flat, therefore, the fault current is usually approximated by its steady-state value.

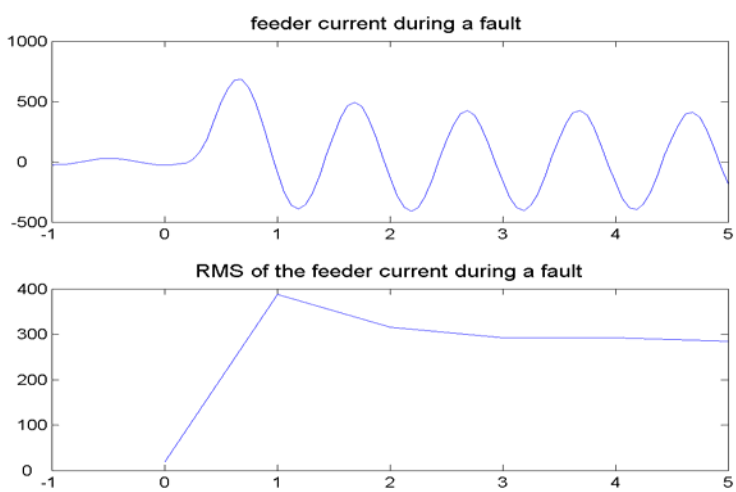

Figure 48: Instantaneous and RMS profile of an actual feeder current during fault

Thus, the feeder can be represented by the steady-state model shown in Figure 49 for fault analysis [Saa99]. As the figure illustrates, the substation is represented by a thevenin equivalent (i.e, a voltage source behind the thevenin impedance, the source impedance), and the loads are represented by equivalent impedances. The faults can similarly be represented by a shunt admittance/ impedance. The equivalent circuit then can be analyzed by using the nodal analysis, which gives a set of equations of the following form, where injected node currents are expressed in terms of node voltages.

$$[Y_f]\ V_f = I_{inj} \qquad \text{---------- (5.1)}$$

where Y_f is the node admittance matrix, V_f is the voltage at each node, and I_{inj} is the current injected at each node.

If there are conventional generators on the feeder, the above feeder model can be extended easily by using the simple equivalent models for the generators. These models use an internal voltage behind a reactance and the value of the reactance is chosen depending on the fault interval being considered, whether it is the subtransient, transient, or steady-state interval. Recently, three-phase fault analysis methods had been extended to incorporate this classical generator models in the analysis [CCI91]. For inverter interfaced DGs, the same technique cannot be applied, since as it will be illustrated below, the inverter interface alters the generator response considerably. Therefore, a new approach is needed in order to incorporate inverter interfaced DGs into the fault analysis.

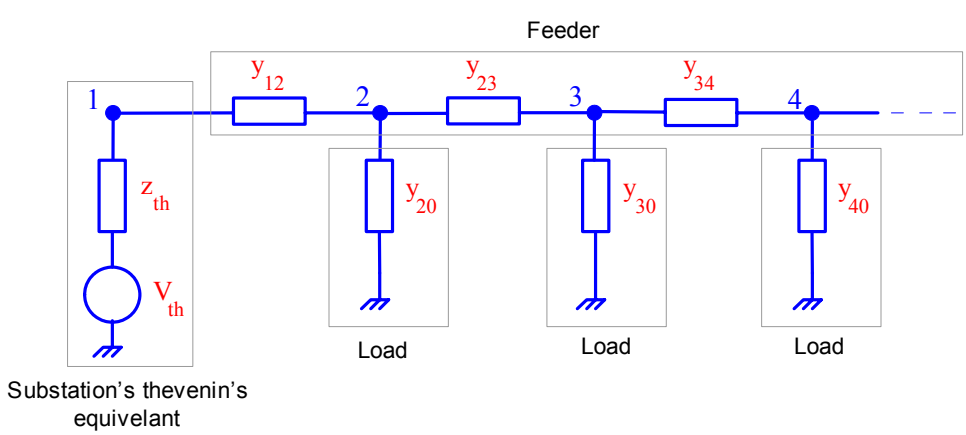

Figure 49: Steady-state feeder model

5.3 DG behavior under fault conditions

To illustrate the response of an IIDG to a fault, we simulated one of the cases mentioned above where contribution of the DG should be considered. This case corresponds to a DG connected upstream of a RC on a feeder, which is illustrated in Figure 9. In this case, we are interested in the contribution of the DG to the fault current the RC will see. The feeder is the 8 node prototype feeder described in section 3.4.1 is used, and the DG is represented by the model introduced in section 3.1.1. The EMTDC program is used to simulate this case. Figure 50 shows the feeder voltage at the DG terminals, and the DG output current and recloser current waveforms when a three phase balanced fault is simulated at t = 1 second at the end of the feeder. The bus voltage drops to 60 percent of its prefault value, the DG responds to the drop in voltage by a corresponding increase in its output current especially during the first cycle, and the current is allowed to reach a value of twice its maximum allowable rated current. Such an increase in the output current causes the DG controller to take corrective actions that brings the current to its new steady-state level. The spike in the DG output current affects the fault current passing through the RC and results in a spike during the first half a cycle that wouldn't have happened if the DG was not connected. The RC fault current with and without a DG is shown in Figure 51.

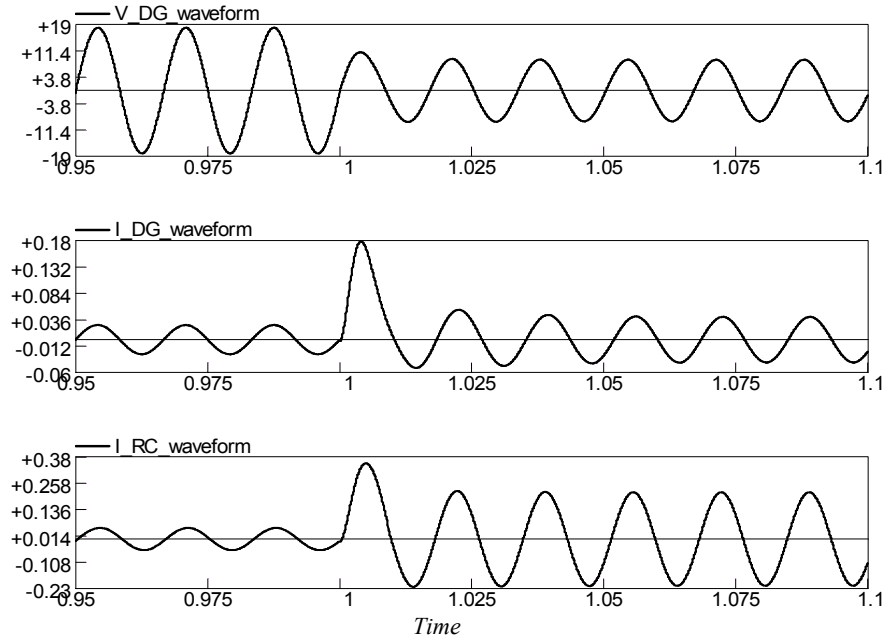

Figure 50: voltage and current waveforms during a fault for the DG and the RC

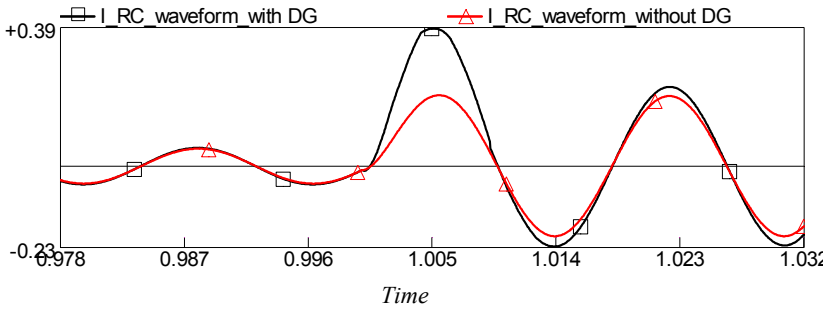

Figure 51: Recloser fault current with and without a DG

To better study the DG behavior under fault, the RMS values of the current and voltage during the first five cycles of the fault are shown in Figure 52 and Figure 53 respectively. The figure indicates that, during the first two cycles (subtransient period), the DG node voltage drops, which leads to an increase in the active and reactive power output from the DG. Therefore, the DG will have a peak current during the subtransient period and the overshoot will depend mainly on the controller's speed of response. The figures also illustrate that the transients end at about the third cycle, and the DG reaches the new steady-state with the controller adjusting the inverter voltage such that the output active and reactive power settles back to the desired set point levels.

This shows that for the transient and steady-state intervals, the DG can be modeled as a current source operating at constant active and reactive power. But for the subtransient interval, where the output current reaches its peak value, the DG needs to be represented in more detail so that the controller's response can be taken into account and the peak current can be captured.

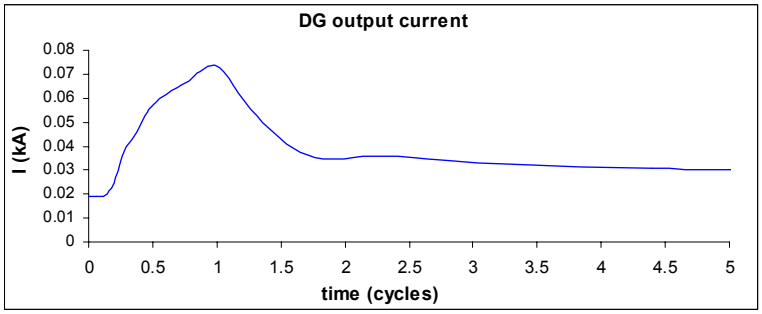

Figure 52: Current RMS during first 5 cycles

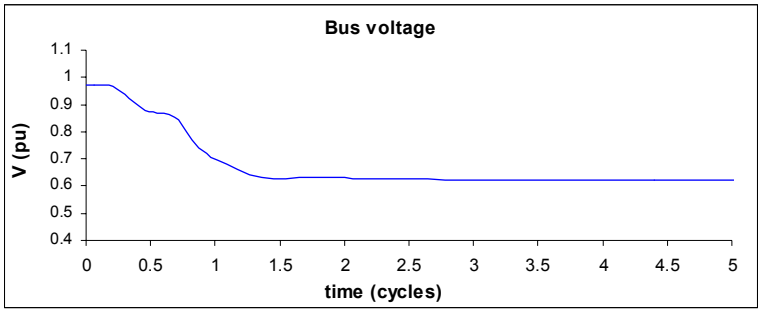

Figure 53: Voltage RMS during first 5 cycles

5.3.1 DG fault protection

Each DG is equipped with a protection scheme to protect the DG against the high fault currents that could damage the DG. The scheme usually detects the fault conditions by monitoring the terminal voltage, as the occurrence of a fault (short-circuit) at a point along the feeder results in a drop of the voltage level of the whole feeder depending on the fault's location and resistance. Therefore, short-circuit conditions on a feeder will be seen by DGs as a drop in the feeder voltage level, and thus, its control and protection schemes will work accordingly. The DG reaction to fault is also clearly stated in the IEEE standard 929-2000 [IEEE929] as follows:

> *"Solid-state inverters do not behave like rotating generators. ... these inverters generally sense a short circuit by an associated voltage drop, rather than by actually sensing short circuit current. Thus, the voltage-trip recommendations are really the equivalent of short circuit protection."*

Therefore, the status of the DG during a fault on the feeder will be determined via the under voltage protection relay. If the location of the fault is close enough to the DG, this will cause the DG bus voltage to drop below the lower acceptable limits, thus triggering the under voltage relay device protecting the DG to trip. The speed of the under voltage relay is stated in the IEEE P1547 standard, where the DG must trip within two seconds, if the bus voltage is $0.5 < V_{DG\text{-}bus} < 0.88$ p.u., and the maximum trip time should not exceed 0.16 seconds, if the DG bus voltage is < 0.5 p.u.

This protection guideline indicates that if the fault is nearby and severe enough, it is possible that the DG will be disconnected before the protection devices on the feeder operate. Therefore, the fault protection scheme on a DG should also be included in the feeder fault analysis. This can be done by checking the postfault DG terminal voltage to be obtained from the fault analysis.

5.3.2 DG representation

Inverter interfaced DGs could be represented as shown in Figure 54. The power generating unit (PGU) produces the DC power and could be a fuel cell, micro turbine or a photovoltaic. A capacitor is used at the DC link between the PGU and the converter. The capacitor decouples the system during fast transient events by supplying/absorbing power during transients. The DC voltage is then converted via an inverter into three-phase as voltage. The inverter's controllers regulate the output voltage's magnitude and angle in order to make the inverter active and reactive power output equal to the desired set point.

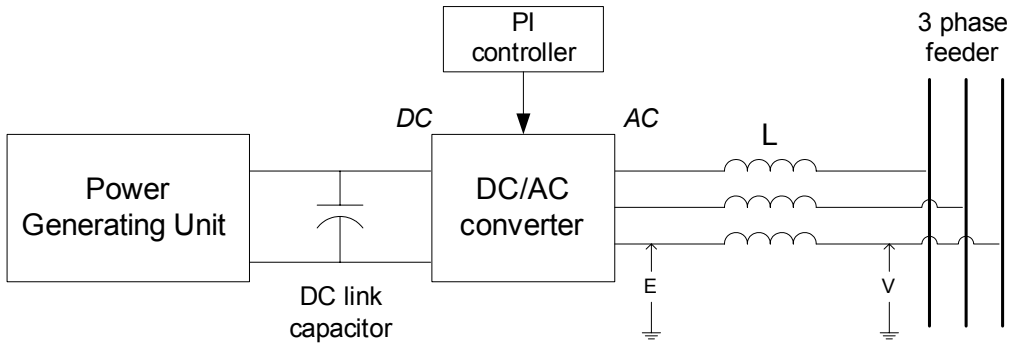

Figure 54: DG representation

Due to the DC link capacitor, the DC output voltage will remain almost constant during short transients. Therefore, we can neglect the dynamics of the PGU and assume that its DC output voltage remains constant. Hence, during a transient the inverter interfaced DG response depends mainly on the dc/ac inverter controller response. The controller on the inverter helps the inverter to synthesize a three-phase balanced ac voltage at the inverter terminals, with some harmonics which can be neglected for control purposes. To regulate the real and reactive power output of the DG, the controller adjusts the amplitude and the

phase of this synthesized inverter voltage (E_f) with respect to the system voltage (V_{bus}) the DG obtains at its terminals. Figure 55 illustrates the voltage controlled equivalent circuit that can be used to represent this response.

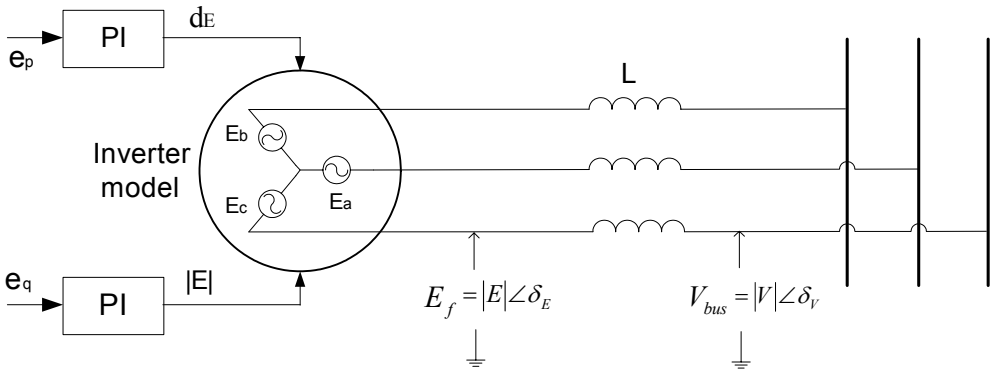

Figure 55: DG representation for fault analysis

The inverter controller adjusts the active and reactive power output using the following relationships that indicate that the inverter output active power depends mainly on the difference between the angles of E_f and V_{bus} and the inverter output reactive power depends mainly on the difference between the magnitudes of E_f and V_{bus}, i.e.,

$$P \ \alpha \ \delta_V - \delta_E \qquad \text{and} \qquad Q \ \alpha \ |V| - |E|$$

In practice, a simple PI type controller is used for power regulation. The input error signals to the controller are the active and reactive power error signals:

$$e_p = P_{actual} - P_{set}, \qquad \text{and} \qquad e_q = Q_{actual} - Q_{set}.$$

The controller adjusts the inverter voltage magnitude and angle such that the input error signals becomes zero, thus regulating the output active and reactive power to their setpoints. For the fault analysis, we need to simulate the response of the controller. Assume that the controller is of the PI type with a transfer function of the following form:

$$H_c = k_p + \frac{k_i}{S} \qquad \text{---------- (5.2)}$$

To choose the typical values for the parameters k_p and k_i. Simon [Sim01] indicates that the controller is usually tuned to have a bandwidth with two orders of the line frequency. With the integral time constant, k_i, of 0.003 seconds, as a typical value, then we can compute the

corresponding proportional gain, k_p, using the following relation $w_{BW}{}^2(1-2k_p{}^2)=k_i{}^2$. For details see appendix C.

Finally, the controller can be discretized using the trapezoidal transformation rule. The discretized controller equation indicating the relation between the controller's input error and output signal is shown below, with the proof in appendix C.

$$y^{k+1} = y^k + e^{k+1}\left[k_P + k_i T/2\right] + e^k\left[-k_P + k_i T/2\right] \qquad \text{---------- } (5.3)$$

Where "T" is the time step length, and "*e*" and "*y*" are the controller's input and output signals respectively.

5.4 Incorporating IIDG model into fault analysis: the proposed approach

As illustrated earlier, in order to capture the peak fault current injected by a DG during the subtransient period, the DG controller response has to be taken into consideration. Therefore we need to integrate the DG model developed above with the feeder model. The challenge here is that, as introduced earlier, conventional fault analysis uses a steady-state model, whereas, ideally we need a time domain model to calculate the peak current.

The first approach we tried involved characterizing the real and reactive power adjustments the DG controller makes in response to a fault. After investigating that approach and actually developing a PQ model for DGs under three-phase balanced faults, we found that generalizing the developed PQ model on all types of faults, balanced and unbalanced, is extremely difficult. The reason for this is because the DG controller monitors and regulates the total three phase active and reactive power, and since single-phase power output during unbalanced faults are also unbalanced, it becomes impossible to make an accurate estimate of the power flowing through each phase during unbalanced faults by knowing only the total three-phase power output.

The alternative approach we developed uses the DG model developed above to do time domain simulation during the subtransient period. The challenge in this approach is the use of the steady-state feeder model to estimate the system response.

For time domain simulations, we can consider the distribution feeder and the DG as two coupled systems as shown in Figure 56. Each system can be represented by its own dynamic set of equations and both systems are interconnected with a set of coupling variables.

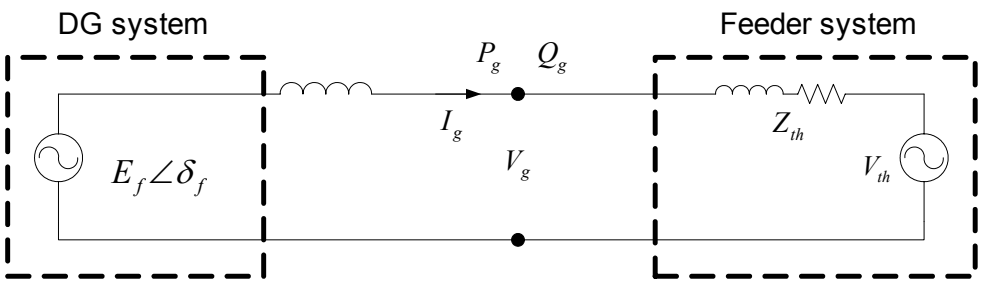

Figure 56: DG and feeder system models

The systems could be represented as follows:

DG: $\dot{X}_g = f_g(X_g, U_g)$ ---------- *(5.4)*

where the *input* U_g is the power (P_g, Q_g), and X_g represents the DG controller state variables.

Feeder: $\dot{X}_S = f_S(X_S, E_f)$ ---------- *(5.5)*

where *input* E_f is the DG internal voltage ($|E_f|$, δ_f), and X_s represents the state variables for the feeder.

Following a fault, these two systems interact as follows. The fault on the feeder causes the main transients on the feeder, which cause the current flow on the feeder to increase and voltage to drop. As indicated before, the DG senses the changes in system conditions mainly through the interface variable, the terminal voltage V_g, and the controller determines the appropriate response. Note that the impact of the DG response on the feeder will be rather small, especially if the DG is of small/medium size (i.e., its contribution to the fault current is a fraction of the feeder fault current). This feature indicates that when solving feeder equations numerically, we can approximate the coupling variable E_f as constant, provided that we choose a simulation step-length small enough so that E_f does not change much. This

approximation is important because it will allow us to solve the two subsystems sequentially, as it will be elaborated later.

To test the validity of this approximation, we repeated the fault simulation on the prototype feeder, but this time kept the inverter voltage of the DG constant at the pre-fault value. Figure 57 shows how the power output of the DG differs in this case from the original case in which the DG inverter voltage varies due to controller action. The figure shows that during the first fraction of a cycle (about quarter of a cycle), the two curves follow each other very closely.

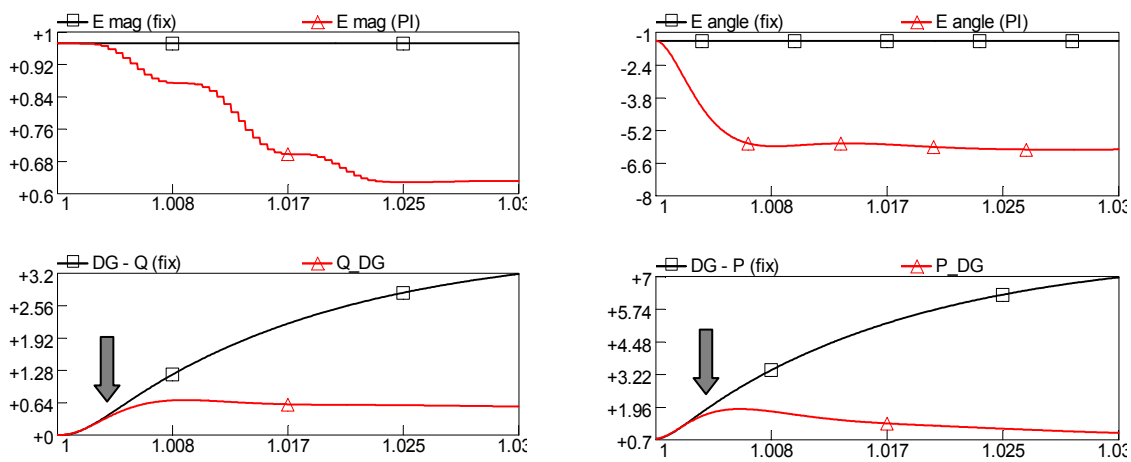

(a) (b)

Figure 57: DG output power during fault, with both fixed and PI controlled DG internal voltage

Now using this approximation, we can do the simulation by solving the two subsystems sequentially, as follows.

For each time step t_k:

<u>A. Feeder response update</u>

- Given the DG internal voltage E_f, and assume $E_f^{\,k}$ is constant during the time-step, update the feeder variables and obtain $X_s^{\,k+1}$.
- From $X_s^{\,k+1}$, get corresponding DG output active and reactive power (P_g, Q_g), which is the input $U_g^{\,k+1}$ for DG.

B. DG response update

- Given values of the DG controller's input variables for the previous and the current time instances, $U_g^{\,k}$ and $U_g^{\,k+1}$, assume that U varies linearly from $U_g^{\,k}$ to $U_g^{\,k+1}$ in time period t_k up to t_{k+1}.
- Use equation (5.3) to determine the new DG state $X_g^{\,k+1}$, which is the DG internal voltage $E_f^{\,k+1}$.

Note that determining the DG response is rather easy in step B using the DG model presented previously, as it involves using the discretized DG controller equation (5.3). Obtaining the feeder response is however challenging, because we do not have the dynamic equations, but rather want to use the steady-state model. Another issue that needs to be addressed is the selection of the time step, as it would impact the constant inverter voltage assumption we have in the feeder update in step A. These issues will be addressed in the following sections.

5.4.1 Feeder response update

In the feeder update step, the inverter voltages of the DGs are given, and we need to estimate the new feeder state $X_s^{\,k+1}$ so that we can determine the corresponding real and reactive power $P_g^{\,k+1}$ *and* $Q_g^{\,k+1}$ the controller will measure at DG terminals. Since we want to extend the classical fault analysis to include DGs, we investigated to see if it is possible to do this update based on the steady-state response determined by the fault analysis.

First, since we assume E_f of the DG remains constant, we can calculate the new steady-state values for the feeder using the feeder fault equations (equation 5.1), and from this we can calculate the steady-state power $P_{g(ss)}^{\,k+1}$ and $Q_{g(ss)}^{\,k+1}$ injected by the DG. The next step is to determine how the P_g, Q_g moves from $P_g^{\,k}$, $Q_g^{\,k}$ to $P_{g(ss)}^{\,k+1}$, $Q_{g(ss)}^{\,k+1}$. For this, we simulated the assumed condition using EMTDC. The lower graph in Figure 58 illustrates how the P_g and Q_g change if we held the DG's inverter voltage constant during a fault. Figure 59 shows how P_g , Q_g changes when we change E_f stepwise. In the simulation, E_f changes in a step manner half a cycle after the fault occurs, as shown in the upper graph of the figure. The P_g ,

Q_g of both simulations are superimposed and plotted together in Figure 60. The figures illustrates that the P_g , Q_g change from the initial state to the new steady-state in a well-defined, exponential fashion with the same time constant "τ". During the first half a cycle after the fault, both simulations are identical, when E_f changes in the second simulation P_g and Q_g reache their new steady-state values with the same exponential behavior as in the first simulation. This observation will prove to be important later in this chapter.

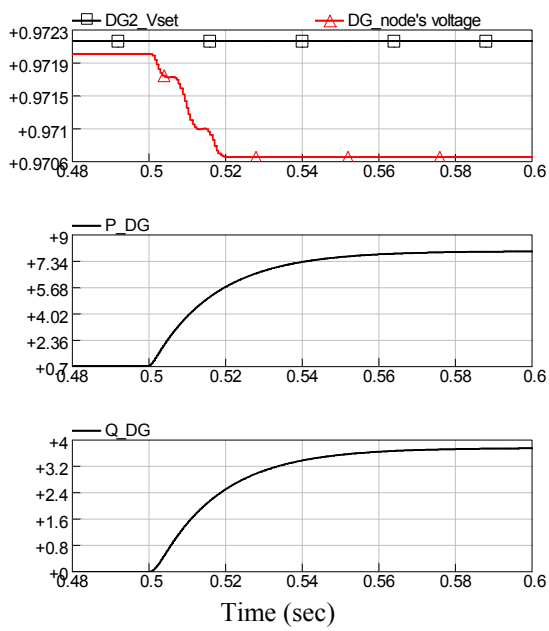

Figure 58: Impact of fault event with constant DG internal voltage

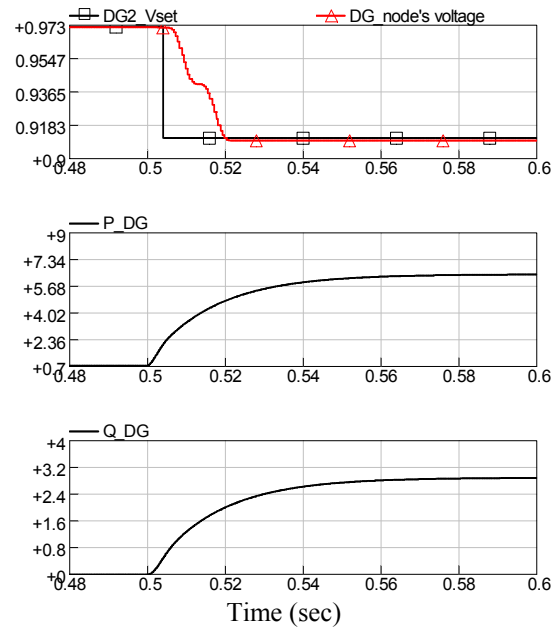

Figure 59: Impact of sudden change in DG internal voltage

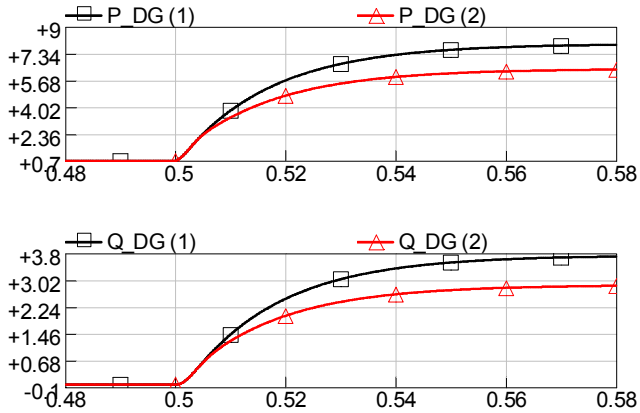

Figure 60: P and Q of simulations shown in Figure 58 and Figure 59

Therefore, the P_g and Q_g variations can be approximated as follows:

$$u(t) = u_0 + \Delta u(1 - e^{-t/\tau}) \qquad \text{---------- (5.6)}$$

where $\Delta u = u_{ss} - u_0$ and $t > 0$

This indicates that the feeder response as seen by the DG controller through P_g and Q_g can be approximated by a first order circuit. Simply stated, the feeder can be approximated at the DG terminals by its thevenin equivalent, as shown in Figure 49. Indeed, when we calculated the thevenin equivalent impedance of the system, which can be calculated using the feeder fault equations 5.1, and obtained the corresponding time constant of the circuit "τ", where

$$\tau = \frac{L_{th}}{R_{th}}$$

We found that it closely matched the time constants of the P_g and Q_g curves in Figure 58 and Figure 59 and equals 0.015 sec. This indicates that the P_g and Q_g variation at each time step can be approximated by an exponential curve, and the time constant parameter can be obtained using the thevenin's impedance. Therefore, by using this approximation, we can then calculate P_g^{k+1} and Q_g^{k+1} from their steady-state values using equation 5.6 with $t = T$.

5.4.2 Time step selection

We want to choose the value of the time step "*T*" such that the DG inverter voltage (E_f) doesn't change substantially, and thus, the approximation in the feeder update step will be acceptable. Note that the DG response is faster than the system (feeder) response, and the DG controller has a bandwidth of 120 Hz. If we select the sampling rate four times that of the bandwidth, then the corresponding time step would be $T = \frac{1}{4 f_{BW}}$, which will give us ⅛ of a cycle for the prototype DG controller. To check that this is a good selection, lets look at the speed of the controller response. The IIDG's PI controller responds to system changes based on the error signal it calculates. Since the error signal will be the largest immediately following the fault, the controller response will change the most in this period. Figure 57 *a & b* shows the DG's voltage magnitude and output power during a fault, for two cases; a fixed and a *PI*-controlled DG voltage. From Figure 57a, we can see that during the first ⅛ of

a cycle (indicated by the solid arrow) the change in the voltage magnitude between the two cases is negligible, and thus, the output reactive power for the two cases is almost identical. This shows that the ⅛ of a cycle time period previously chosen results in very small error. From Figure 57b, we can see that the output active power for the two cases is almost identical during the first ⅛ of a cycle (indicated by the solid arrow), but that is not the case for the internal voltage angle. This means that regulating the voltage magnitude has a stronger and faster impact on the value of both the active and reactive power, thus the reactive power controller is the one that must be considered when choosing the appropriate time step length "T".

5.5 Case study 1: Balanced fault

To test the performance of the proposed fault analysis method, simulations have been performed on the prototype feeder shown in

Figure 61, the prototype data were presented in section 3.4.1. The case study will be conducted as follows; first the feeder's Thevenin's equivalent impedance as seen by the DG will be calculated as part of the initial data needed for the fault analysis. Then the proposed method will be used to estimate the fault current contribution of the DG and also the fault current seen by the Recloser (RC) during the subtransient period of first cycle. From the simulation results, the peak current of DG and RC will be extracted. Finally, these results will be compared with the actual ones, which will be obtained from the EMTDC simulation on the same prototype system.

5.5.1 Feeder settling time

To determine the feeder's time constant, the Thevenin's equivalent impedance for the system as seen by the DG is evaluated, using (5.1) we get $Z_{th} = 28.47\angle 76.8 = R_{th} + jX_{th}$

Therefore, $$\tau = \frac{X}{377R} = \frac{|Z_{th}|\sin\delta}{377|Z_{th}|\cos\delta} = \frac{\sin\delta}{377\cos\delta} = \frac{\sin 76.8}{377\cos 76.8} = \frac{1}{377\times 0.201} = \frac{1}{75.6}$$

Therefore it takes 0.063 seconds to reach steady state value that is 3.82 cycles.

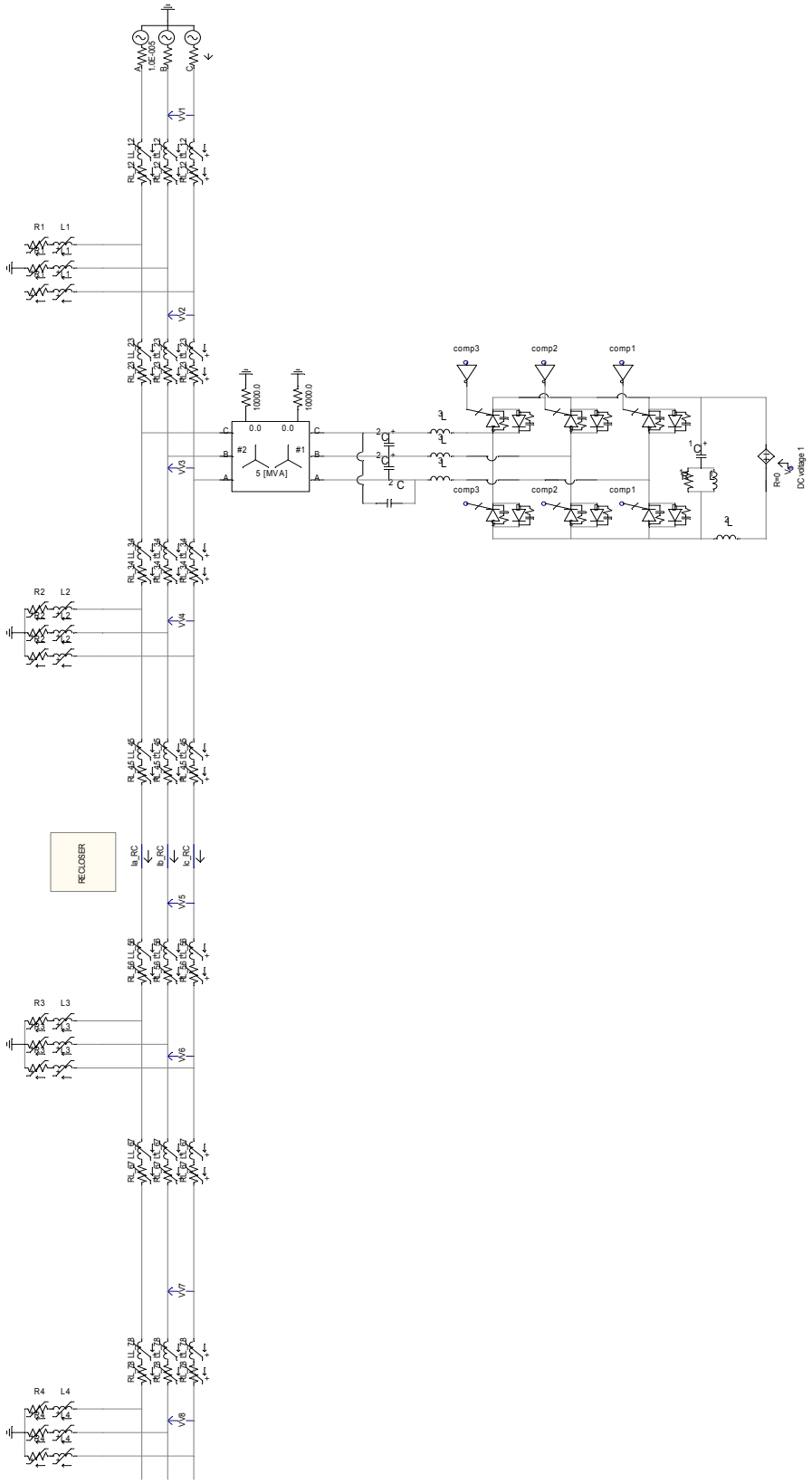

Figure 61: Prototype feeder used on testing the proposed technique

5.5.2 Simulation

A summary of the computation steps of the proposed method are as follows:

Initial (pre-fault) Conditions: (@ t = 0 cycles)

The PI controllers' input error signals are equal to zero

$e_p^0 = 0$ $\qquad$ $e_q^0 = 0$

And the corresponding PI outputs are equal to:

$u_p^0 = -1.353$ **degrees** $\qquad$ $u_q^0 = 0.972181$ **pu**

Update at @ t_1 = ⅛ cycle

Step a) Feeder Response:

- The DG inverter voltage $E_f^0 = 0.972\angle -1.353$
- Solve feeder equations (5.1) to get the steady state V_g, P_g Q_g,

  $P_{g(ss)}^{\ 1} = 7.9624$ $\qquad$ $Q_{g(ss)}^{\ 1} = 3.6135$

- Using the feeder first order model approximation of equation (5.6), estimate the P_g and Q_g at t_1 = T,

  $P_g^{\ 1}(t_1) = 1.2698$ $\qquad$ $Q_g^{\ 1}(t_1) = 0.121$

Step b) DG Controller Response:

- Using $P_g(t_1)$, $Q_g(t_1)$ calculate the error the controller will see at its input:

  $e_{p(t1)} = -0.5198$ $\qquad$ $e_{q(t1)} = -0.121$

- Estimate the controller output E^1_f using the controller model (5.3), and assuming that the error varies linearly between e^0 and e^1, therefore:

$$E_f^1 = 0.911247\angle -2.6839$$

Updates $t_2 - t_8$:

The computations of the first update above are repeated and plotted below, with details in Appendix C.

Figure 62 shows the DG inverter voltage obtained from the simulation together with the actual voltage obtained from the EMTDC simulation. The figure shows that the calculated values closely follow the actual voltage level with a slightly higher value (i.e. conservative). The maximum error between the actual and the approximate ones used in the simulation is about 0.04 p.u for the voltage magnitude and 1.5 degree for the voltage angle.

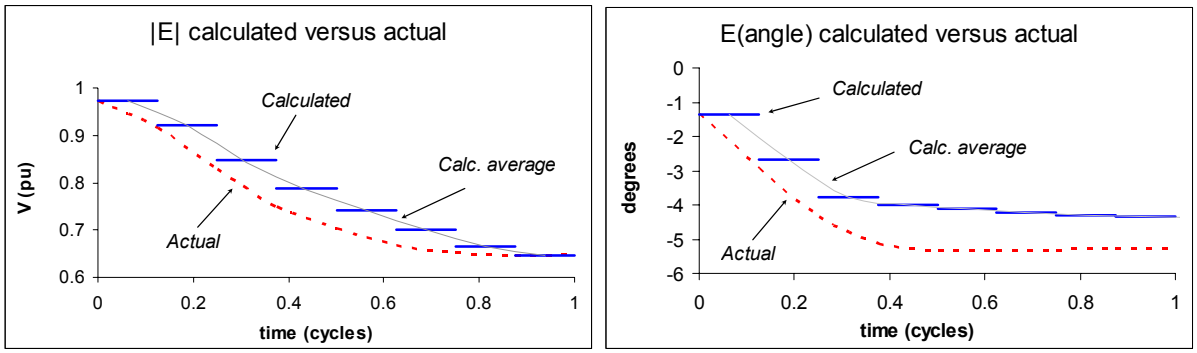

(a) (b)

Figure 62: calculated versus actual internal voltage

Figure 63 presents a comparison between the actual and calculated values of the DG's output active power and reactive power. Since the calculated internal voltage is conservative, the resulting calculated parameters are also conservative in that the calculated P and Q are higher than the actual.

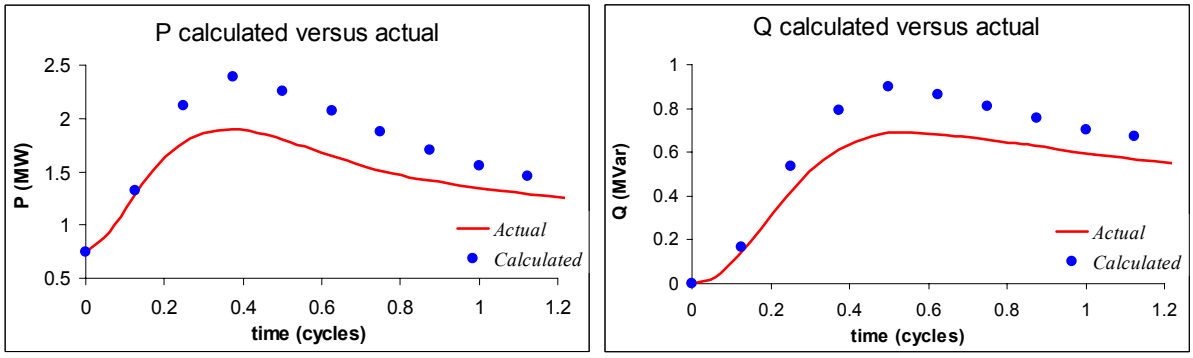

(a) (b)

Figure 63: one cycle window RMS output current, active and reactive power

Figure 64 presents the comparison between the actual and calculated fault currents for the DG and the RC. Again, these results show that the proposed method gives conservative results, which is desirable in fault analysis.

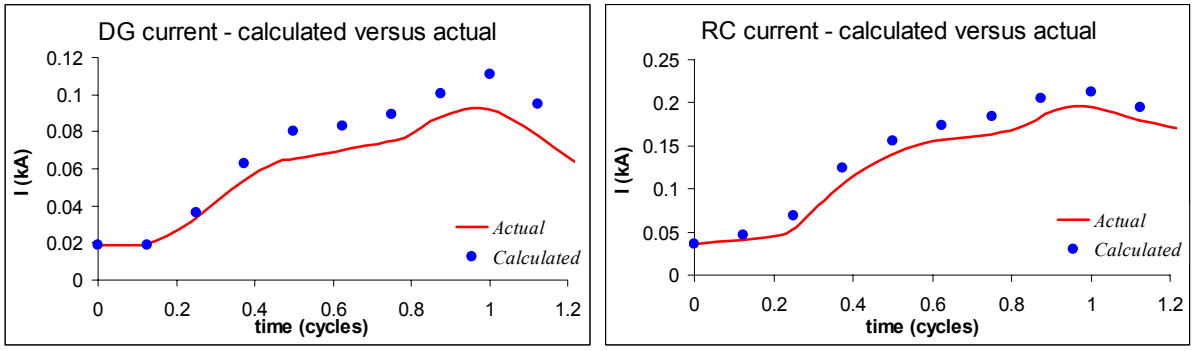

(a) DG current (b) RC current

Figure 64: RMS currents for DG and RC

5.5.3 Determining the peak instantaneous current

The proposed method evaluates the RMS variation at the desired locations (DG and RC). For protection device selection, we also need to estimate the peak amplitude of the current the protection devices like RC will see.

Determining the peak instantaneous current from the RMS value depends on when the fault occurs, the fault will be more severe if it occurs when the voltage is at its peak. The case study simulates this conservative scenario. For the RMS profile shown in Figure 63a, the actual voltage and fault current profiles (obtained from EMTDC) are given in Figure 65. The fault occurs at time equals 0.9858 seconds, which corresponds to the peak voltage at the DG bus, this is shown in the upper graph of the figure. The resulting current waveform is shown in the lower graph with the peak current equal to 217 amps.

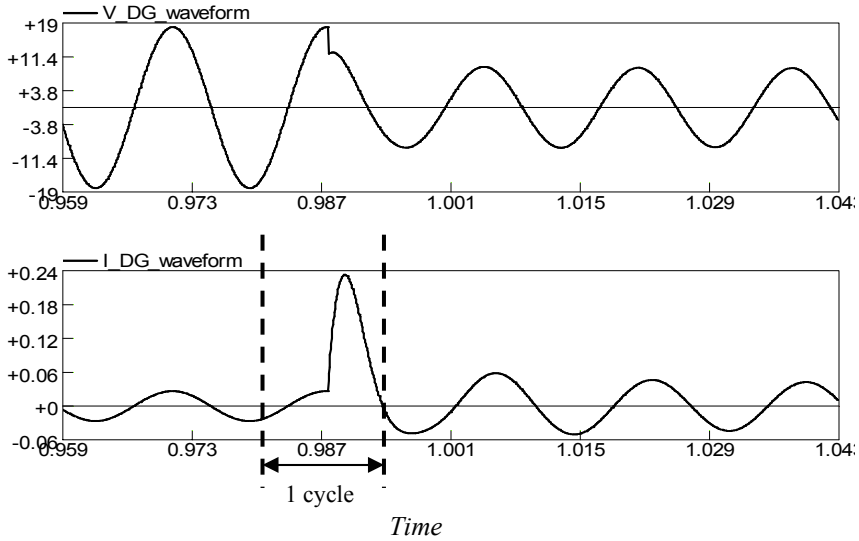

Figure 65: DG voltage and current waveforms with balanced fault at peak voltage crossing

The RMS variations of the currents shown in Figure 64 are calculated by using a moving window of one cycle. To estimate the peak amplitude we use the maximum RMS current, which is at t = 1 cycle Figure 64, as this peak RMS corresponds to the cycle shown with the two dashed lines in Figure 65. The current cycle between the two dashed lines can be approximated as follows; the first half of the waveform is a cosine wave with a peak value of I_a, while the second half is the subtransient current. The Figure indicates that we can approximate this second half cycle with a sine wave that has a dc offset equals to I_a and a peak value of I_c. Note that the overall peak value we are trying to evaluate is I_b, where $I_b = I_a + I_c$.

Therefore, the RMS value of the combined waveform can be calculated by using the two current waveform parameters as follows (see appendix C for proof):

$$I_{RMS} = \sqrt{0.25 I_b^{\ 2} - 0.181 I_a I_b + 0.68 I_a^{\ 2}}$$

For our case study: *The maximum* I_{RMS} = 111 amps (see Figure 64a)

The amplitude before the fault I_a = 25 amps (see Figure 65)

Therefore, from the previous equation I_b = 230 amps

This is close to the actual peak current, 218 amps, and conservative since it is higher than the actual value.

When the same procedure is applied on the RC current in Figure 66,

The maximum I_{RMS} = 229 amps (see Figure 64b)

The amplitude before the fault I_a = 73 amps (see Figure 65)

Therefore, from the previous equation I_b = 471 amps

This is close to the actual peak current, 430 amps, and conservative since it is higher than the actual value.

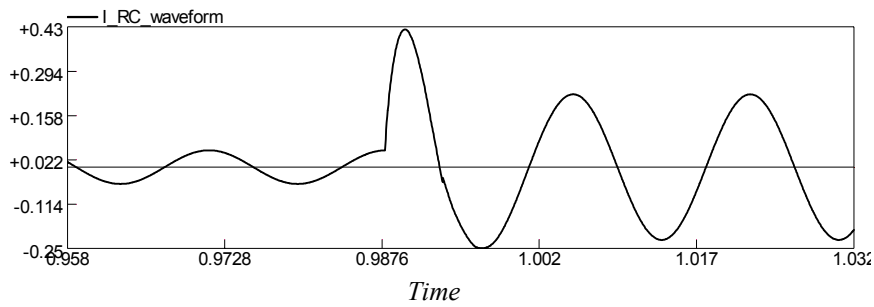

Figure 66: RC current waveform with balanced fault at peak voltage crossing

These results indicate that the proposed method performs as predicted and results are well within the accuracy range for fault analysis.

5.6 Case study 2: Unbalanced fault

The proposed method can be used for both balanced and unbalanced fault analysis. Since an unbalanced fault will mainly affect the feeder response, we investigated this issue in order to determine if the proposed method needs to be changed to handle the unbalanced faults.

As in the previous case, in order to characterize the feeder response, we performed a simulation on the prototype system with three different fault types, a three phase balanced fault, a line to ground (unbalanced fault), and a line to line to ground (unbalanced fault). The inverter voltage in these simulations is kept constant. Figure 67a and b show how the feeder response differs between the two unbalanced faults and the balanced fault. Figure 67a shows the reactive and active power error signals for balanced fault and double line to ground fault, while Figure 67b shows the reactive and active power error signals for balanced fault and line to ground fault. As shown in both figures, the unbalanced fault takes less time to reach steady state than the balanced fault. This means that if we utilize settling time of the balanced fault case, the estimated error at $\frac{1}{8}^{th}$ of a cycle will be less negative than the actual error at that time period. This will make the controller decrease the internal voltage magnitude and angle with a smaller value than what the actual controller would have done. In other words, if we utilize the settling time of balanced faults for unbalanced faults the

calculated output of the controller ($E_{calculated}$) will be slightly higher than that of the *actual* output (E_{actual}), this will result in calculated output current slightly higher than the *actual* output current of the DG during fault, which makes such approximation a conservative one.

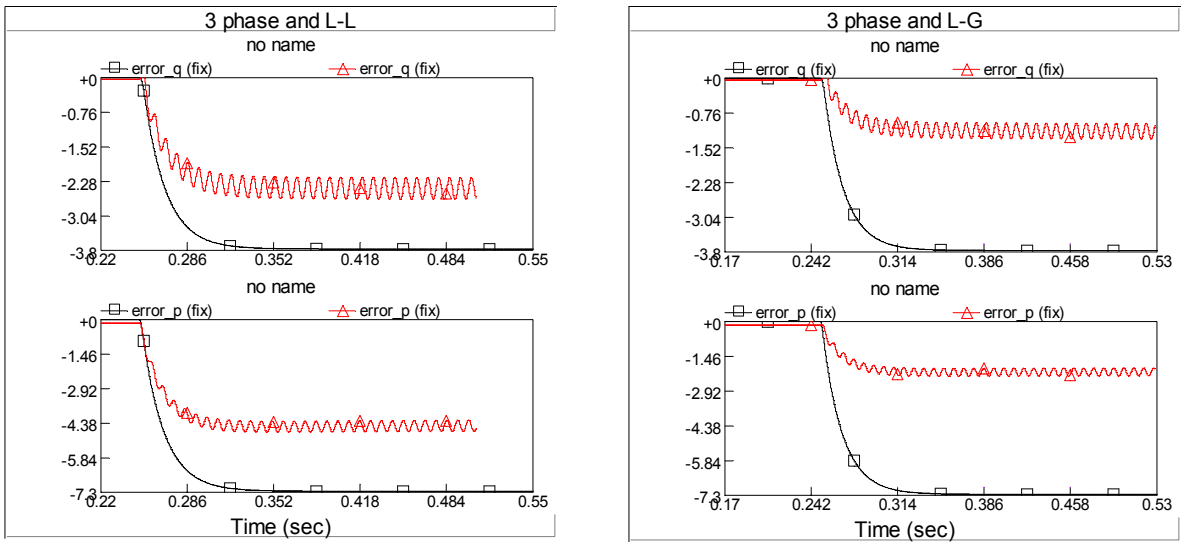

(a) (b)

Figure 67: Unbalanced faults

5.6.1 Simulation of phase to ground fault

The prefault are the same as the three phase fault case study, the summary of the computation steps are as follows:

Update at @ t_1 = ⅛ cycle

Step a) Feeder Response:

- With the DG inverter voltage equal to $E_f^0 = 0.972\angle -1.353$
- Solve feeder equations (5.1) to get the steady state V_g, P_g and Q_g.

$$P_{g(ss)}{}^{1} = 7.636 \qquad Q_{g(ss)}{}^{1} = 3.407$$

- Using the feeder first order model approximation, estimate the P_g and Q_g at t_1 = T,

$$P_g(t_1) = 1.274 \qquad Q_g(t_1) = 0.1009$$

Step b) DG Controller Response:

- Calculate the error the controller will see at its input:

  $e_{p(t1)} = -0.524$ $\qquad$ $e_{q(t1)} = -0.1009$

- Estimate the controller output E_f using the controller model (5.3) therefore:

$$E_f^1 = 0.9212\angle -2.69$$

Updates $t_2 - t_8$:

The computations of the first update above are repeated for $t_2 - t_8$ and plotted below, see Appendix C for details.

Figure 68 shows the DG inverter voltage obtained from the calculations together with the actual voltage obtained from the EMTDC simulation. It is shown that the calculated values closely follow the actual voltage level with a slightly higher margin, showing that the calculated values are conservative.

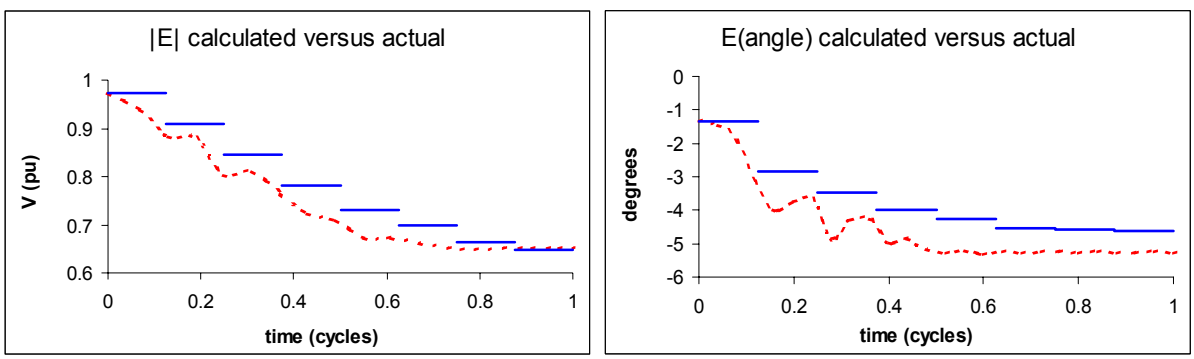

(a) (b)

Figure 68: calculated versus actual internal voltage

Figure 69 presents a comparison between the actual and calculated values of the DG's three phase output active power and reactive power. Since the calculated internal voltage is conservative, the resulting calculated parameters are also conservative in that the calculated P and Q have higher values than the actual.

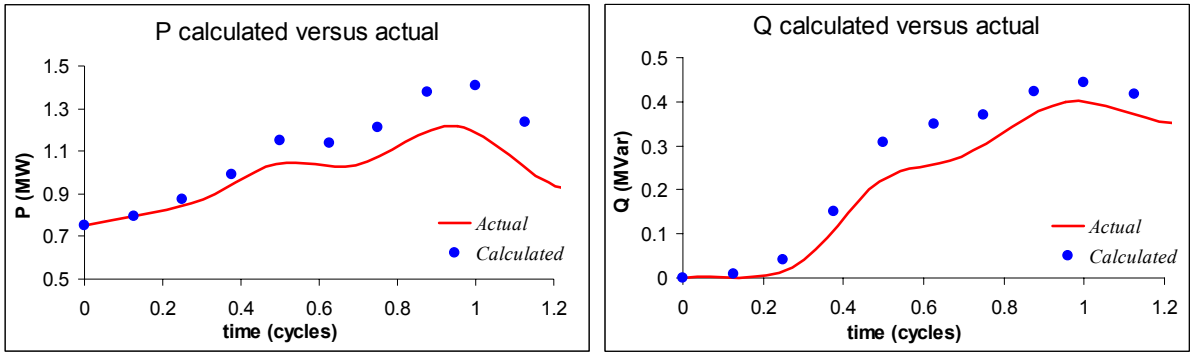

(a) (b)

Figure 69: one cycle window RMS output current, active and reactive power

Figure 70 presents a comparison between the actual and calculated fault current, for the faulted phase, for the DG and the RC. Again, these results show that the proposed method gives conservative results, which is desirable in fault analysis.

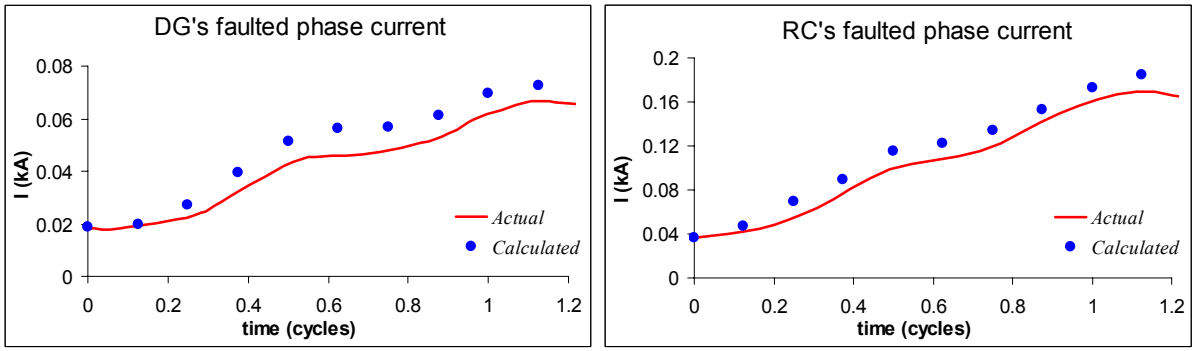

(a) DG current **(b)** RC current

Figure 70: RMS currents for DG and RC

5.6.2 Determining the peak instantaneous current

For protection device selection, we also need to estimate the peak amplitude of the current the protection devices like RC will see. The corresponding peak instantaneous current at the DG and the RC is determined as described in the three phase fault case study, for the DG current at the faulted phase:

The maximum I_{RMS} = 73 amps (see Figure 70a)

The amplitude before the fault I_a = 25 amps (see Figure 65)

Therefore, from the previous equation I_b = 150 amps

This is close to the actual peak current, 128 amps, and conservative since it is higher than the actual value.

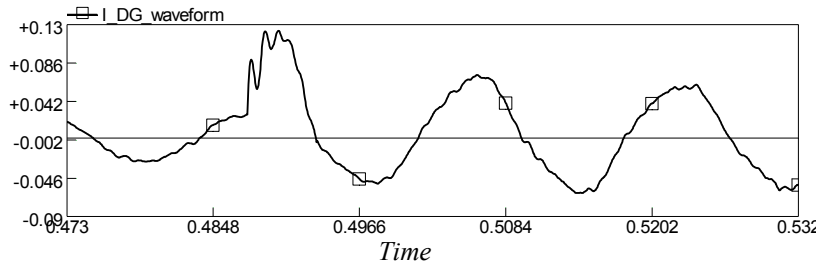

Figure 71: DG current waveform with single phase fault at peak voltage crossing

When the same procedure is applied on the RC current in Figure 72,

The maximum I_{RMS} = 171 amps (see Figure 70b)

The amplitude before the fault I_a = 73 amps

Therefore, from the previous equation I_b = 347 amps

This is close to the actual peak current, 320 amps, and conservative since it is higher than the actual value.

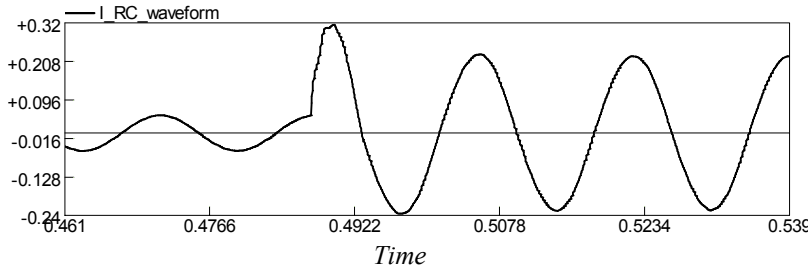

Figure 72: RC current waveform with single phase fault at peak voltage crossing

In conclusion, the two case studies presented shows that the proposed approach for integrating IIDGs in fault analysis is capable of correctly estimating the fault currents at different sections of the feeder under different fault types.

5.7 Summary

This chapter has started with a brief review on conventional fault analysis studies and IIDGs behavior under fault conditions. An approach to extend fault analysis studies to include IIDGs when calculating fault currents in a distribution feeder was presented.

Two case studies were investigated to show that the proposed approach can correctly estimate fault currents on distribution networks with IIDGs under balanced and unbalanced fault conditions.

CHAPTER SIX

Adaptive Over-Current protection for feeders with DGs

6.1 Impact of DG on Over-Current relay performance

Distribution feeders are usually radial with the loads tapped all along the line. The feeder protection strategy aims at optimizing the service continuity to the maximum number of users. This means applying a combination of circuit breakers, automatic reclosers and fuses to clear temporary and permanent faults. The main circuit breaker at the beginning of the feeder is equipped with an over-current (OC) relay to isolate any permanent fault along the feeder. When the feeder current exceeds a certain pickup value the OC relay sends the breaker a trip signal, the speed of tripping the fault is inversely proportional with the fault current magnitude.

This chapter focuses on the impact of DG on the feeder protection, specifically the impact on the OC relay performance. The chapter presents simulation results to show the extent of deterioration a DG can inflict on an OC relay. An approach to solve such problem and restore the OC relay performance is also presented.

6.1.1 Reduced reach

Relays are set to protect a certain part of the feeder; this is sometimes referred to as the "reach". The reach of the relay is determined by its minimum pickup current. The presence of a DG will reduce the reach of the OC relay [Dug02], thus leaving medium impedance

faults at the end of the feeder undetected (Figure 8). To illustrate the effect of DGs on reducing the reach of the feeder's OC relay, the system in Figure 4 is simulated for different fault locations (appendix A). The pickup current of the OC relay protecting this feeder is set to 700 amps (appendix A).

Before connecting any DGs to the feeder, a fault at node 7 with R_f = 10.4 Ω will create a current at the relay = 710 amps, and the relay will trip.

After connecting the DG, the same fault will create a fault current at the relay of 650 amps, thus the relay will not trip.

Figure 73 represents the maximum fault resistance at each node that will create fault current that can still be detected by the relay at each node with the DG connected at node 6. For example for a fault at node 7, the maximum fault the relay can detect is a fault with R_f = 9.4 Ω, any higher fault resistance will go undetected. From the figure we can see that for a fault with R_f = 10.4 Ω to be detected by the relay it has to be located at least at node 6. If the fault is further down stream it will go undetected. For this fault resistance the reach of the relay is reduced from 100% to 83% of the feeder length.

Figure 74 shows the effect of the amount of power injected by a DG on the reduction in the relay reach for three different fault resistances. The reduction in reach is increased with the amount of power injected by the DGs. For a specific R_f as the DG power increase the relay reach decrease, until the whole feeder becomes unprotected against that specific fault resistance. For example for DG total power equal 70% of total feeder load, a fault with R_f equal 10.4 cannot be detected along the whole feeder.

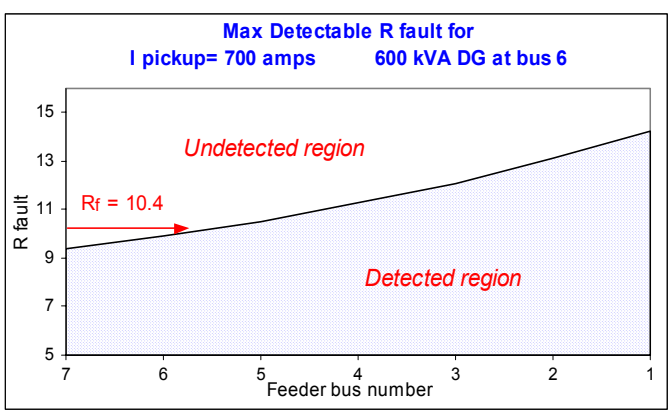

Figure 73: Maximum Rf detected at each node with DG injecting 10% of feeder load

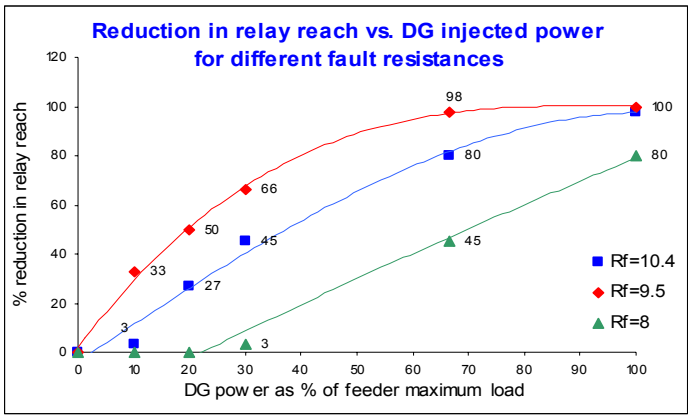

Figure 74: Reduction in reach vs. DG injected real power

6.2.2 Overall relay effectiveness

Connecting DGs to a feeder will affect the overall effectiveness of the OC relay protecting this feeder. The area under the curve labeled (*w/o DG*) in Figure 75 represents all possible values of R_f along the feeder that could be detected by the OC relay, if there wasn't any DGs connected to the feeder. Similarly the area under the curve labeled (*w DG*) represents all possible values of R_f along the whole feeder that could be detected by the relay, in case of a 600 kVA DG connected at node 6. It is obvious that the area between the two curves represents all faults that could have been detected if there weren't any DGs connected, but will be missed when a DG is connected at node 6 carrying 10% of the load. For this network topology the undetected region due to DG represents 7.2% of the total area under *w/o DG* curve, this means that the effectiveness of the relay in detecting faults is reduced by 7.2% due to the presence of the DG.

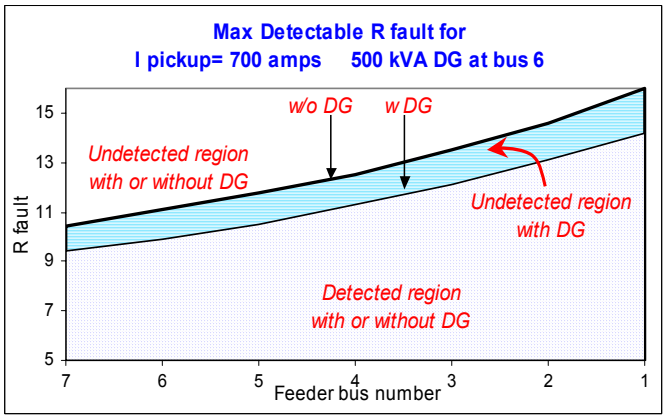

Figure 75: Effect of DG on relay effectiveness

To understand the influence of the DGs on the relay effectiveness, we simulated different topologies and compared the relay effectiveness for each case. (Simulation results in appendix A)

The results indicated that the number of DGs and their location has a minor effect on the relay effectiveness, and the key factor affecting the relay effectiveness is the total power supplied by the DGs. Figure 76 shows the % reduction in relay effectiveness for five cases, when the total power supplied by DGs is 0, 10, 20, 30 and 66% of the total load. It is obvious that the % reduction in relay effectiveness increases as the total power supplied by the DGs increase. This shows that the power injected by all the DGs is the main parameter influencing the reduction in the effectiveness of the OC relay protecting the feeder.

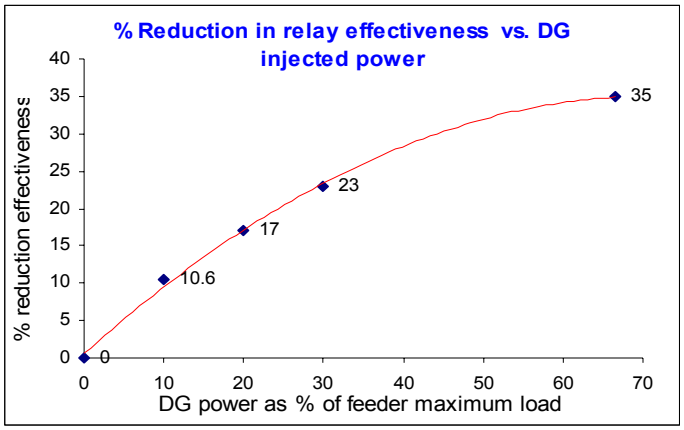

Figure 76: Effect of DG power injected on relay effectiveness

6.2 Adaptive Over-Current relay

As mentioned previously, the presence of a DG will reduce the reach of the over-current relay, thus leaving medium impedance faults [And99] at the end of the feeder undetected. To understand why the presence of DGs will cause such problem we simulated the same prototype feeder, once without any DGs and once with only one DG connected at node 4; and created a fault at node 8. We will then plot the fault current as seen by the relay in the two cases against the relay time-current characteristics.

The over-current relay has an inverse time-current characteristic where the tripping time gets longer as the fault current decreases, and the tripping time is maximum for a fault current equals to the I_{pickup} of the relay. The following equation represents the relationship between the fault current and the tripping time [And99].

$$t_p = \frac{T_1}{\left(I/I_{pick}\right)^{\alpha}} + T_2$$

Where t_p is the time for pickup, T_1 is a time constant depending on relay design parameters, T_2 is a time constant that accounts for saturation in the magnetic circuit, α is changed according to type of relay (inverse, extremely inverse .. etc.), and finally I_{pickup} is the relay set pickup current. We used the values for these constants that represent the ABB inverse time over-current relay type CO-8, where α = 2, T_1 = 13, and T_1 = 0.59 [And99]. Figure 77 shows the relay's current-time characteristics.

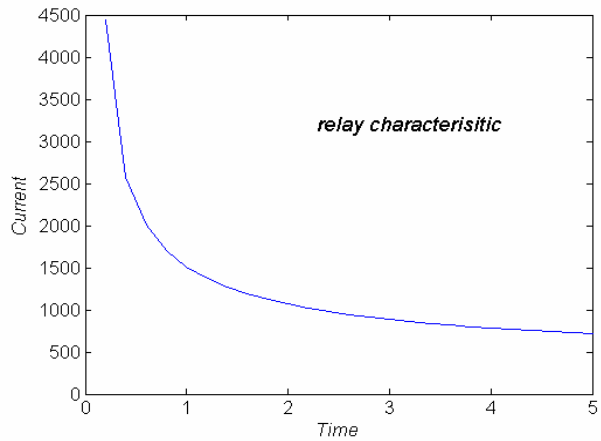

Figure 77: Inverse time relay characteristics

In Figure 78, we superimposed the relay characteristics over the fault current seen by the relay. The figure shows that for the case where there are no DGs connected to the feeder it will take the relay about 4.9 seconds to trip. This, in fact, is the longest trip time because the fault conditions where chosen to yield a fault current almost equal to the relay minimum pickup current. The figure also shows that the relay will not trip for the same fault conditions when a DG is present.

To solve this problem, we are proposing an approach to change the relay pickup current I_{pickup} as seen in Figure 79, such that the I_{pickup} decreases as the total amount of power

injected by all DGs increase. Thus keep protecting the feeder against the same fault conditions it was originally protected against. But how will we get the values of the I_{pickup} along that curve?

To try to answer this question we need to understand how the inverter interfaced DG will react to a fault at the feeder, the effect of that reaction on the fault current seen by the relay, and finally a tool to estimate the fault current at the relay when several DGs are connected to the feeder prior and during a fault.

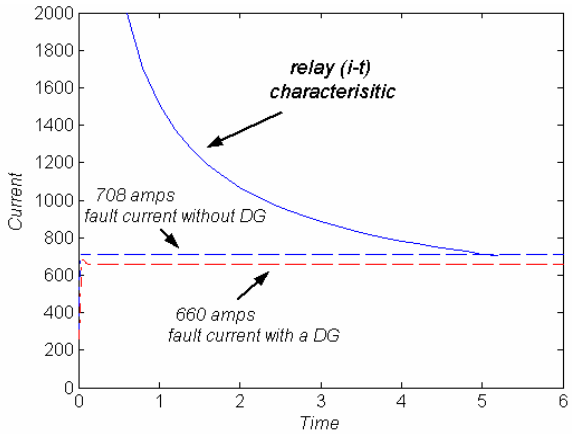

Figure 78: Relay characteristic and I fault

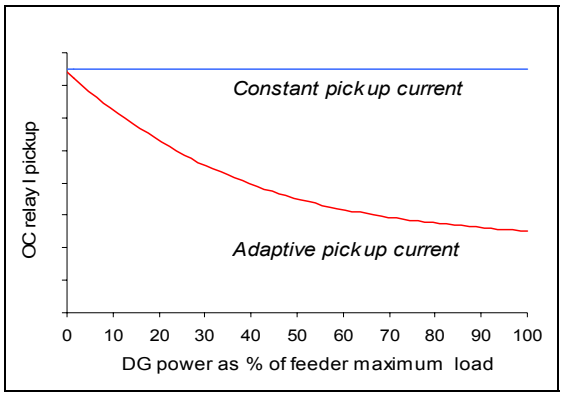

Figure 79: Constant and adaptive I-pickup

As illustrated in the previous chapter, during a fault event the DG's controller is capable of adjusting the DG's output active power and reactive power to their original setpoint values within 5 – 8 cycles, which is less than 150 milliseconds. And since we are focusing on the time the OC relay will take to trip a fault current equal to its pickup current, which is in the order of a few seconds. We can neglect the fault current transient and subtransient intervals studied in the previous chapter. And focus on the steady state interval where the DG continues to supply the same amount of active and reactive power as it was just before the fault.

6.2.1 Solution approach

As mentioned earlier our solution approach depends on estimating the fault current at the relay, while taking into consideration the DG location and output current. Therefore we need first a system model.

To determine our system model, we will make two approximations, the first approximation is to neglect the transients in the DG response, that is neglect the DG response during the first 0.1 seconds of the fault duration. This approximation is acceptable since it is more conservative to account only for the steady state current. This approximation will allow us to model the DG as a current source with constant output power during fault duration.

The other important approximation is considering the fault current at the relay to be constant and equal to the steady state fault current value, as seen in Figure 80. This will introduce an insignificant error that could be neglected. With these two approximations our system model can be represented as shown in Figure 81.

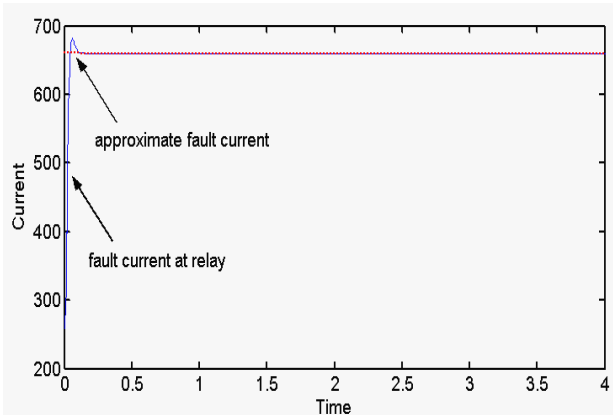

Figure 80: Fault current approximation

We propose to use a power flow technique, where the current and voltage at every node can be evaluated for a given DG output. This will result in a set of nonlinear equations which can be solved using the Gauss-Newton method. Such an approach is tested and its results were compared with the results from simulating the feeder using PSCAD, and the current value at the relay was found to be identical with ± 1 ampere accuracy.

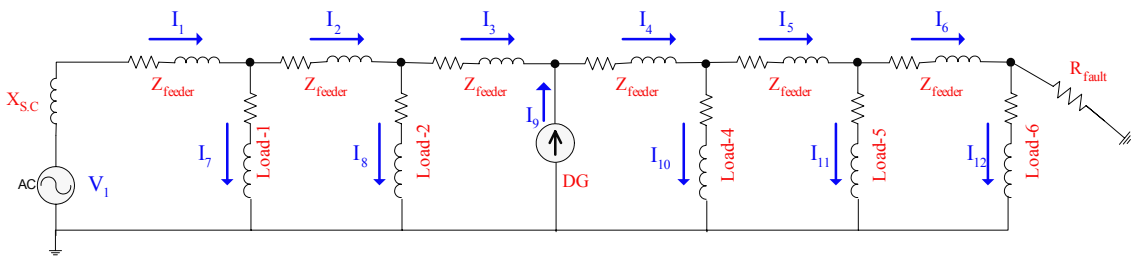

Figure 81: Feeder model

Now that we estimate accurately the value of the fault current at the relay, we can adjust the minimum pickup current of the relay depending on the feeder configuration. As seen in Figure 82, when there are no DGs connected to the feeder in our example, we will set the relay to a minimum pick up current of 700 amps. When a DG is connected we can recalculate the value of the fault current and change the relay minimum fault current setup as seen in the figure. This adaptive technique will ensure that the feeder is always protected from the same range of faults whether DGs are connected to the feeder or not.

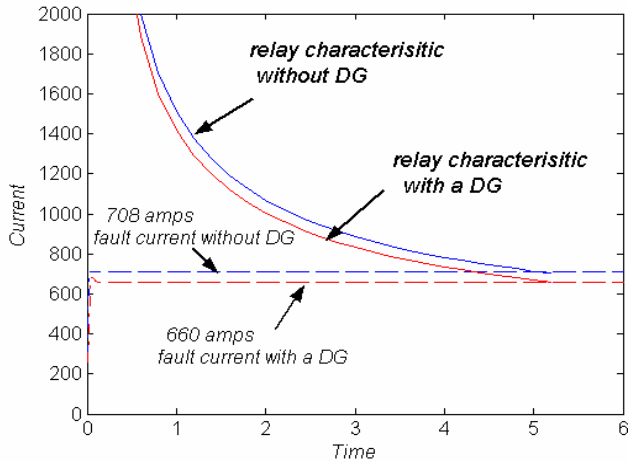

Figure 82: Actual and modified relay characteristic with fault current

One last issue we need to address is the fact that some DGs might trip during a fault for under voltage reasons. To resolve this issue, we adopted a conservative approach, which assumes that all DGs remain online, even if some of them may trip during the fault. This decision is justified due to the fact that fault current seen by the relay will be higher if some

of the DGs drop during fault. Therefore, the relay will trip faster than simulated if indeed some DGs trip. According to Figure 83, if we set the relay pickup current to the fault current when 3 DGs are considered it will take the relay time "t2" to trip. But if only two DGs remain connected, the actual short circuit current will be higher and it will take the relay time "t1" to trip.

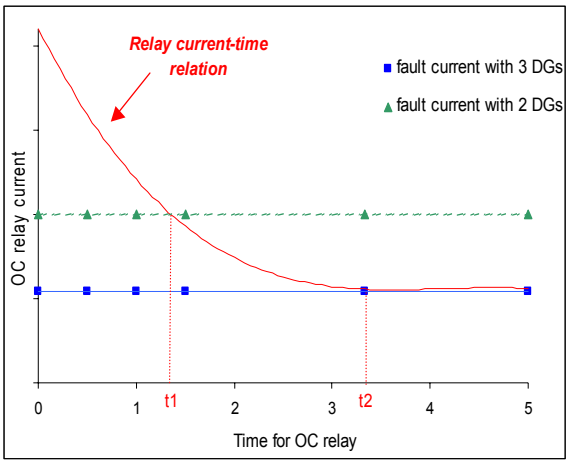

Figure 83: Relay minimum pickup current

6.3 Summary

This chapter focused on the impact of DG on the feeder protection, specifically the impact on the overcurrent relay performance. The chapter started by describing the reduced reach phenomenon and how it affects the protection ability of circuit breakers and reclosers. Simulation results were used to show such impact and how it affected the overall effectiveness of the relay

An approach was then proposed to solve this problem, by adaptively changing the relay pickup current setting according to the total amount of power injected by DGs increase, thus fully restoring the relay protection capabilities.

To determine the value for the appropriate pickup current for each situation, the DG response under fault conditions was examined, resulting in an acceptable approximation that allowed us to model the DG during faults as a current source with constant output power. The proposed solution used the power flow technique that resulted in a set of nonlinear equations, which were then solved using the Gauss-Newton method. A simulation was

shown to prove the effectiveness of this approach in estimating the correct pickup current setting for each case.

CHAPTER SEVEN

Conclusions

The connection of DGs to distribution networks greatly impacts the networks performance and reliability. The dissertation focuses on the DG's impact on the networks control and protection schemes. In the following section, the contributions of this dissertation to the DG and distribution network field is highlighted, followed by a list of possible avenues for future research that have been revealed during the course of this research.

7.1 Contributions

The dissertation studied and proposed solution approaches for problems related to the connection of DGs to distribution networks. The contributions of this dissertation could be summarized in four main points as follows.

A central supervisory controller for feeder voltage regulation with DGs

The dissertation formulates an optimization problem for regulating the distribution feeder's voltage at minimum costs, when DGs are connected to the feeder. A supervisory central controller was designed, and tests presented showed how the controller effectively regulated the feeder's voltage with DGs connected.

A distributed controller – MAS – for feeder voltage regulation with DGs

The dissertation presents a MAS capable of regulating the feeder's voltage level in a distributed manner. The MAS was designed to only utilize each agent's local data without the need for an explicit feeder model, thus fulfilling the plug-and-play feature wanted by DG manufacturers and regulating entities. The different design steps of the MAS were presented along with test results. The test results proved the ability of the MAS to regulate the feeder's voltage as efficient as an omniscient agent that is capable of sensing the whole system. The ability of the MAS to regulate feeders with different load types was also shown.

Fault analysis on distribution systems with DGs

The impact of inverter interfaced DGs on the feeder's protective devices' performance and coordination, during fault events, was studied in this dissertation. An approach was presented to extend the conventional fault analysis studies to include the contribution of inverter interfaced DGs during faults. Two case studies were presented to show that the proposed approach successfully calculated the peak fault current at a recloser (RC), during balanced and unbalanced faults with DGs connected.

An adaptive OC relay for maintaining feeder protection with presence of DGs

The impact of DGs on the effectiveness and the reach of the OC relay protecting the feeder were illustrated through this dissertation. An adaptive OC relay that changes its pickup current according to the feeder topology was proposed. The proposed technique depends on modeling the DG as a current source with constant output power and through power flow analysis, chooses the appropriate pickup current for the relay.

7.2 Recommendations for future research

Through the course of this research, several interesting topics have been revealed that need to be studied. These include:

- Incorporating learning techniques in the MAS where agents can act first depending on their *"experience"* and *"beliefs"* for faster regulation, then use the CNP to ensure a minimum cost regulation. The agents will need to store previous events and actions of other agents in order to estimate each agent's action and thus determine its own.
- Upgrading the MAS to operate in the Micro-grid concept, also known as intentional islanding, is a very interesting topic, where each feeder or group of feeders are seen as a Micro-grid that can operate independently or cooperate with neighboring Micro-grids to form a more reliable, flexible, and maneuverable utility grid.
- More research is required on the implementation of the MAS. The hardware requirements for fast and reliable operation need to be studied. Questions on the appropriate means of communication need to be addressed, such as whether a dedicated LAN is required, or the use of Power Line Carrier (PLC) technology is possible, or even utilizing the Internet.
- There is a need to design a test procedure by which the DG's controller parameters, integral and proportional gain, could be estimated on site.
- Incorporating islanding protection with the proposed approach and utilizing the DG agents for better and reliable islanding protection.

Appendices

Appendix A

A1. Simulated System

Feeder: 11 kV, 7 node feeder.

Load: All node loads are 0.75 MW@0.9 pf. Total feeder load is 6 MVA

DG size: 600 kW fuel cell connected at node 6 and operating at constant 0.9 pf. (DG is about 10% of feeder load)

Utility bus is represented by a large synchronous generator

Relay current: Without DG Ir = 325 A, with 1 DG Ir = 292 A, with 2 DG's Ir = 260 A

For each feeder segment: R= 0.48, X= 0.2859. ΔV between node 1&7=10% (max allowed)

Relay pickup current:

The minimum short circuit current for the system is 2.15 kA, and the maximum load current is 325 A. the relay pickup current is set according to the following relationship

$$2I_{\max-load} < I_{pick-up} < \frac{I_{sc-\min}}{2-3}$$

The pick up current of the over-current relay must be greater than twice the maximum load current (650 A), and I_{sc} min /3 = 720 A. So we will set the relay I_{pickup} = 700 A.

A2. Testing different DG connections in reduction in reach

The max detected fault resistance under different scenarios: different fault & DG location

								area under the curve
I pickup = 700 A			600 kVA DG at bus 6					
Bus number	**7**	**6**	**5**	**4**	**3**	**2**	**1**	
without DG	10.4	11.1	11.8	12.5	13.5	14.6	16	76.7
with DG	9.4	9.9	10.5	11.3	12.1	13.1	14.2	68.7
difference in ohms	*1*	*1.2*	*1.3*	*1.2*	*1.4*	*1.5*	*1.8*	
difference in %	10%	11%	11%	10%	10%	10%	11%	10.4%
I pickup = 700 A			600 kVA DG at bus 4					
Bus number	**7**	**6**	**5**	**4**	**3**	**2**	**1**	
without DG	10.4	11.1	11.8	12.5	13.5	14.6	16	76.7
with DG	9.4	9.9	10.5	11.3	12.1	13.1	14.2	68.7
difference in ohms	*1*	*1.2*	*1.3*	*1.2*	*1.4*	*1.5*	*1.8*	
difference in %	10%	11%	11%	10%	10%	10%	11%	10.4%
I pickup = 700 A			2 X 300 kVA DG at buses 6 & 2					
Bus number	**7**	**6**	**5**	**4**	**3**	**2**	**1**	
without DGs	10.4	11.1	11.8	12.5	13.5	14.6	16	76.7
with DGs	9.3	9.9	10.5	11.3	12.1	13.1	14.2	68.65
difference in ohms	*1.1*	*1.2*	*1.3*	*1.2*	*1.4*	*1.5*	*1.8*	
difference in %	11%	11%	11%	10%	10%	10%	11%	10.5%
I pickup = 700 A			2 x 600 kVA DG at buses 6 & 2					
Bus number	**7**	**6**	**5**	**4**	**3**	**2**	**1**	
without DGs	10.4	11.1	11.8	12.5	13.5	14.6	16	76.7
with DGs	8.6	9.1	9.7	10.5	11.2	12.2	13.3	63.65
difference in ohms	*1.8*	*2*	*2.1*	*2*	*2.3*	*2.4*	*2.7*	
difference in %	17%	18%	18%	16%	17%	16%	17%	17.0%
I pickup = 700 A			3 x 600 kVA DG at buses 6, 4 & 2					
Bus number	**7**	**6**	**5**	**4**	**3**	**2**	**1**	
without DGs	10.4	11.1	11.8	12.5	13.5	14.6	16	76.7
with DGs	7.9	8.4	9	9.7	10.5	11.4	12.4	59.15
difference in ohms	*2.5*	*2.7*	*2.8*	*2.8*	*3*	*3.2*	*3.6*	
difference in %	24%	24%	24%	22%	22%	22%	23%	22.9%
I pickup = 700 A			2 X 2000 kVA DG at buses 6 & 2					
Bus number	**7**	**6**	**5**	**4**	**3**	**2**	**1**	
without DGs	10.4	11.1	11.8	12.5	13.5	14.6	16	76.7
with DGs	6.3	6.9	7.5	8.2	8.9	9.7	10.6	49.65
difference in ohms	*4.1*	*4.2*	*4.3*	*4.3*	*4.6*	*4.9*	*5.4*	
difference in %	39%	38%	36%	34%	34%	34%	34%	35.3%
I pickup = 700 A			2 X 2000 kVA DG at buses 6 & 4					
Bus number	**7**	**6**	**5**	**4**	**3**	**2**	**1**	
without DGs	10.4	11.1	11.8	12.5	13.5	14.6	16	76.7
with DGs	6.5	7.1	7.7	8.3	9	9.8	10.7	50.5
difference in ohms	*3.9*	*4*	*4.1*	*4.2*	*4.5*	*4.8*	*5.3*	
difference in %	38%	36%	35%	34%	33%	33%	33%	34.2%

A3. Different DG models for power generating unit

a) Fuel Cell model

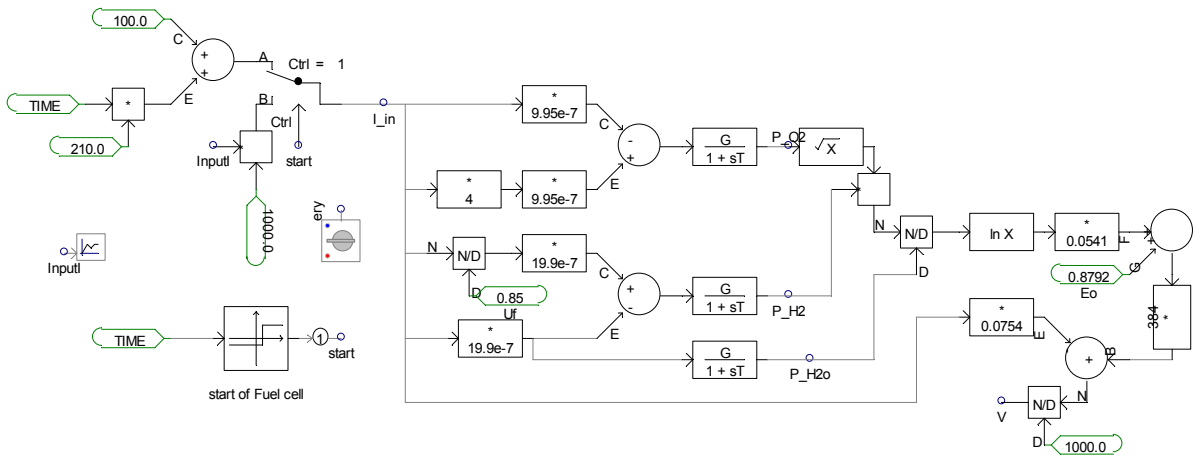

c) Micro-turbine Model

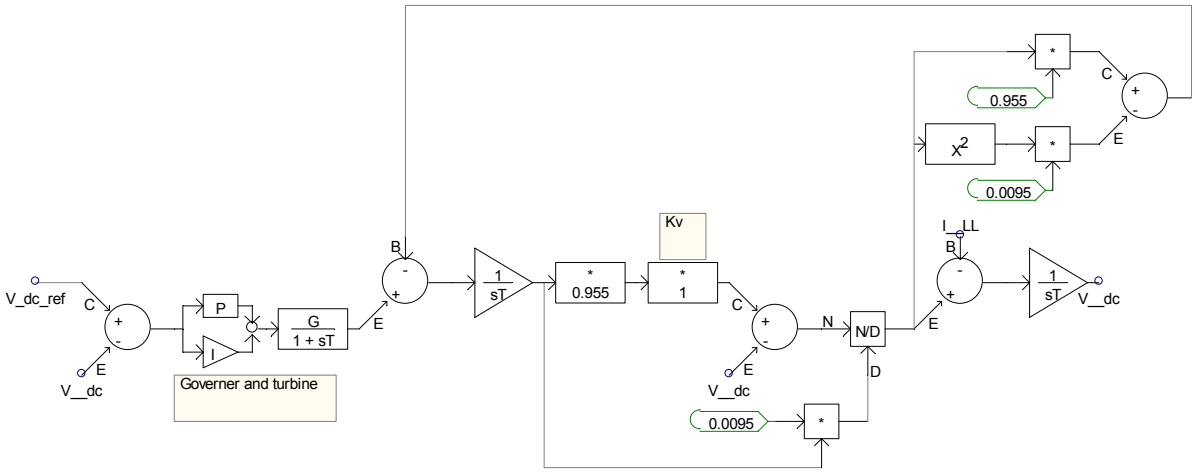

Appendix B

B1. Linearizing the power flow equations

The Taylor series expansion for a function *f(x)* is as follows:

$$f(x+\Delta x) = f(x) + \frac{\partial f(x)}{\partial x}\Delta x + h.o.t$$

where *h.o.t* stands for "higher order terms". In case of the vector Taylor series, instead of one equation we get *n* equations that could be written as follows:

$$f(x+\Delta x) = f(x) + J(x)\cdot\Delta x + h.o.t$$

where *J(x)* is the partial derivative matrix shown below and is called the "Jacobian matrix" of *f* evaluated at *x*.

$$J(x) = t\begin{bmatrix} \frac{\partial f_1(x)}{\partial x_1} & \cdots & \frac{\partial f_1(x)}{\partial x_n} \\ \vdots & & \vdots \\ \frac{\partial f_n(x)}{\partial x_1} & \cdots & \frac{\partial f_n(x)}{\partial x_n} \end{bmatrix}$$

For a *general* case the real and imaginary power flow equations will be as follows:

$$P_i(x) = \sum_{k=1}^{n} |V_i||V_i|\left[g_{ik}\cos(\theta_i-\theta_k) + b_{ik}\sin(\theta_i-\theta_k)\right] \qquad i=1,\ 2,\ldots.n$$

$$Q_i(x) = \sum_{k=1}^{n} |V_i||V_i|\left[g_{ik}\sin(\theta_i-\theta_k) - b_{ik}\cos(\theta_i-\theta_k)\right] \qquad i=1,\ 2,\ldots.n$$

by applying the Taylor series expansion on the equations we get

$$\begin{bmatrix} \Delta P \\ \Delta Q \end{bmatrix} = \begin{bmatrix} J_1 & J_2 \\ J_3 & J_4 \end{bmatrix} \cdot \begin{bmatrix} \Delta\theta \\ \Delta v \end{bmatrix}$$

where $J_1 = \frac{\partial P}{\partial \theta}$, $J_2 = \frac{\partial P}{\partial V}$, $J_3 = \frac{\partial Q}{\partial \theta}$, and $J_1 = \frac{\partial Q}{\partial V}$

$$J_1 = \frac{\partial P_i}{\partial \theta_i} = \sum_{k=1}^{n} |V_i||V_i|\left[g_{ik}\cos(\theta_i-\theta_k) + b_{ik}\sin(\theta_i-\theta_k)\right]$$

The linearization of these equations around the operating point will result in the following set of linear equations (see Appendix B for detailed proof):

B2. Decoupling the linear power flow equations

The linear power flow equations could be decoupled based on the following facts [Ber86]:

- The branches resistance is much smaller than its inductance, $r << x$, therefore g_{ij} is quite small.
- $\theta_i - \theta_k < 10^0$, therefore $\cos(\theta_i - \theta_k) \cong 1.0$ and $\sin(\theta_i - \theta_k) \cong 0.0$
- Voltages are around 1.0 p.u.

And since:

$$\frac{\partial P_i}{\partial V_i} \cong 2|V_i|g_{ij} + \sum_{i \neq j} |V_j| g_{ij} \quad \text{and} \quad \frac{\partial P_i}{\partial V_j} \cong -|V_i| g_{ij}$$

$$\frac{\partial Q_i}{\partial \theta_i} \cong |V_i| \sum_{i \neq j} |V_j| g_{ij} \quad \text{and} \quad \frac{\partial Q_i}{\partial \theta_j} \cong -g_{ij}$$

Therefore

$$\frac{\partial P_i}{\partial V_i} \cong 0, \quad \frac{\partial P_i}{\partial V_j} \cong 0, \quad \frac{\partial Q_i}{\partial \theta_i} \cong 0, \quad \text{and} \quad \frac{\partial Q_i}{\partial \theta_j} \cong 0$$

Therefore:

$$J_2 = \frac{\partial P}{\partial V} = 0$$

and

$$J_3 = \frac{\partial Q}{\partial \theta} = 0$$

B3. Proof that all diagonal elements in matrix M (page 47) has positive values, and all nondiagonal, nonzero elements have negative values

$$M = \begin{bmatrix} -B_{33} + \frac{B_{23}^{\ 2}}{B_{22}} + \frac{B_{34}^{\ 2}}{B_{44}} & \frac{B_{34}B_{45}}{B_{44}} & 0 \\ \frac{B_{34}B_{45}}{B_{44}} & -B_{55} + \frac{B_{45}^{\ 2}}{B_{44}} + \frac{B_{56}^{\ 2}}{B_{66}} & \frac{B_{56}B_{67}}{B_{66}} \\ 0 & \frac{B_{56}B_{67}}{B_{66}} & -B_{77} + \frac{B_{67}^{\ 2}}{B_{66}} + \frac{B_{78}^{\ 2}}{B_{88}} \end{bmatrix} \quad \text{------- (B3.1)}$$

- *For diagonal element (1, 1)*

$$M(1,1) = -B_{33} + \frac{B_{23}^{\ 2}}{B_{22}} + \frac{B_{34}^{\ 2}}{B_{44}}$$

$$M(1,1) = -(b_{23} + b_{34}) + \frac{b_{23}^{\ 2}}{b_{12} + b_{23}} + \frac{b_{34}^{\ 2}}{b_{34} + b_{45}}$$

$$M(1,1) = b_{23}\left(\frac{b_{23}}{b_{12} + b_{23}} - 1\right) + b_{34}\left(\frac{b_{34}}{b_{34} + b_{45}} - 1\right)$$

The terms within the brackets are always negative. And knowing that any b_{ij} has a negative value, then $M(1,1)$ is always positive.
Similarly, all other diagonal elements will have positive values.

- *For Non-diagonal elements*

Since $B_{ii} = \sum_{j=0}^{n} b_{ij}$ & $B_{ij} = -b_{ij}$

Therefore $B_{ii} \rightarrow -ve$ & $B_{ij} \rightarrow +ve$

Then we can conclude that all nonzero elements in the matrix will have a negative value. For example $M(1,2) = \frac{B_{34}B_{45}}{B_{44}} = \frac{d}{-e} = -m$

- *For the last diagonal element (n, n)*

$$M(3,3) = -B_{77} + \frac{B_{67}^{\ 2}}{B_{66}} + \frac{B_{78}^{\ 2}}{B_{88}}$$

$$M(3,3) = -(b_{67} + b_{78}) + \frac{b_{67}^{\ 2}}{b_{56} + b_{67}} + \frac{b_{78}^{\ 2}}{b_{78}}$$

$$M(3,3) = -b_{67} + \frac{b_{67}^{\ 2}}{b_{56} + b_{67}}$$

$$M(3,3) = \frac{-b_{67}(b_{56} + b_{67}) + b_{67}^{\ 2}}{b_{56} + b_{67}} = \frac{-b_{56}b_{67}}{b_{56} + b_{67}}$$

Therefore, $M(3,3) = -M(2,3) = -M(3,2)$
This is because at the last bus, $B_{88} = -B_{78}$, therefore this could be generalized for an n node feeder, $M(n,n) = -M(n-1, n) = -M(n, n-1)$

Finally, matrix M will always have the following form

$$M = \begin{bmatrix} a & -m & 0 \\ -m & b & -c \\ 0 & -c & c \end{bmatrix}$$

Q.E.D

Similarly, for a 10 node feeder with 4 generators nodes, M will have the following structure:

$$M = \begin{bmatrix} a & -m & 0 & 0 \\ -m & b & -n & 0 \\ 0 & -n & c & -d \\ 0 & 0 & -d & d \end{bmatrix}$$

B4. <u>Proof that M^{-1} has the structure mentioned in equation (4.5) page 47</u>

Since matrix M has the following structure

$$M = \begin{bmatrix} a & -m & 0 \\ -m & b & -c \\ 0 & -c & c \end{bmatrix}$$

Then the M^{-1} will have this structure:

$$M^{-1} = \begin{bmatrix} \frac{b-c}{a(b-c)-m^2} & \frac{m}{a(b-c)-m^2} & \frac{m}{a(b-c)-m^2} \\ \frac{m}{a(b-c)-m^2} & \frac{a}{a(b-c)-m^2} & \frac{a}{a(b-c)-m^2} \\ \frac{m}{a(b-c)-m^2} & \frac{a}{a(b-c)-m^2} & \frac{ab-m^2}{c(a(b-c)-m^2)} \end{bmatrix}, \quad M^{-1} = \begin{bmatrix} u & k & k \\ k & n & n \\ k & n & p \end{bmatrix} \quad \text{-------- } \textbf{\textit{(B4.1)}}$$

To prove this claim, we will show that:

$$M \cdot M^{-1} = I$$

i.e.

$$\begin{bmatrix} a & -m & 0 \\ -m & b & -c \\ 0 & -c & c \end{bmatrix} \cdot \begin{bmatrix} \frac{b-c}{a(b-c)-m^2} & \frac{m}{a(b-c)-m^2} & \frac{m}{a(b-c)-m^2} \\ \frac{m}{a(b-c)-m^2} & \frac{a}{a(b-c)-m^2} & \frac{a}{a(b-c)-m^2} \\ \frac{m}{a(b-c)-m^2} & \frac{a}{a(b-c)-m^2} & \frac{ab-m^2}{c(a(b-c)-m^2)} \end{bmatrix} = \begin{bmatrix} 1 & 0 & 0 \\ 0 & 1 & 0 \\ 0 & 0 & 1 \end{bmatrix}$$

Obtaining the first column in R.H.S multiplication matrix

$$a\frac{b-c}{a(b-c)-m^2} - m\frac{m}{a(b-c)-m^2} = \frac{a(b-c)-m^2}{a(b-c)-m^2} = 1$$

$$a\frac{m}{a(b-c)-m^2} - m\frac{a}{a(b-c)-m^2} = 0$$

$$a\frac{m}{a(b-c)-m^2} - m\frac{a}{a(b-c)-m^2} = 0$$

Obtaining the second column in R.H.S multiplication matrix

$$-m\frac{b-c}{a(b-c)-m^2} + b\frac{m}{a(b-c)-m^2} - c\frac{m}{a(b-c)-m^2} = \frac{-m(b-c)+bm-cm}{a(b-c)-m^2} = \frac{-m(b-c)+m(b-c)}{a(b-c)-m^2} = 0$$

$$-m\frac{m}{a(b-c)-m^2} + b\frac{a}{a(b-c)-m^2} - c\frac{a}{a(b-c)-m^2} = \frac{-m^2+ba-ca}{a(b-c)-m^2} = \frac{-m^2+a(b-c)}{a(b-c)-m^2} = 1$$

$$-m\frac{m}{a(b-c)-m^2} + b\frac{a}{a(b-c)-m^2} - c\frac{ab-m^2}{c(a(b-c)-m^2)} = \frac{-m^2+ba-(ab-m^2)}{a(b-c)-m^2} = \frac{(ab-m^2)-(ab-m^2)}{a(b-c)-m^2} = 0$$

Obtaining the third column in R.H.S multiplication matrix

$$-c\frac{m}{a(b-c)-m^2}+c\frac{m}{a(b-c)-m^2}=0$$

$$-c\frac{a}{a(b-c)-m^2}+c\frac{a}{a(b-c)-m^2}=0$$

$$-c\frac{a}{a(b-c)-m^2}+c\frac{ab-m^2}{c(a(b-c)-m^2)}=\frac{-ca+ab-m^2}{a(b-c)-m^2}=\frac{a(b-c)-m^2}{a(b-c)-m^2}=1$$

Therefore, M^{-1} has structure mentioned in equation (B4.1)

<u>The (b = m + c) condition</u>

If $b = m + c$

Therefore, $M^{-1}(1,1) = M^{-1}(1,2) = M^{-1}(2,1) = k$

Then M^{-1} will have the following structure:

$$M^{-1}=\begin{bmatrix} k & k & k \\ k & n & n \\ k & n & p \end{bmatrix}$$

The question is, will the condition $b = m + c$ always be true for any feeder topology?

From equation (B3.1):

$$m=\frac{-B_{34}B_{45}}{B_{44}} \longrightarrow m=\frac{-b_{34}b_{45}}{b_{34}+b_{45}} \qquad \textbf{-----(B4.2)}$$

$$c=\frac{-B_{56}B_{67}}{B_{66}} \longrightarrow c=\frac{-b_{56}b_{67}}{b_{56}+b_{67}} \qquad \textbf{-----(B4.3)}$$

$$b=-B_{55}+\frac{B_{45}^{\ 2}}{B_{44}}+\frac{B_{56}^{\ 2}}{B_{66}} \longrightarrow b=-(b_{45}+b_{56})+\frac{b_{45}^{\ 2}}{b_{43}+b_{45}}+\frac{b_{56}^{\ 2}}{b_{56}+b_{67}}$$

$$b=-b_{45}+\frac{b_{45}^{\ 2}}{b_{43}+b_{45}}-b_{56}+\frac{b_{56}^{\ 2}}{b_{56}+b_{67}}$$

$$b=\frac{-b_{45}(b_{43}+b_{45})+b_{45}^{\ 2}}{b_{43}+b_{45}}+\frac{-b_{56}(b_{56}+b_{67})+b_{56}^{\ 2}}{b_{56}+b_{67}}$$

$$b=\frac{-b_{45}b_{43}}{b_{43}+b_{45}}+\frac{-b_{56}b_{67}}{b_{56}+b_{67}} \qquad \textbf{-----(B4.4)}$$

From *(B4.2), (B4.3) and (B4.4), it is obvious that* $b = m + c$

Therefore, this sufficient condition is always satisfied for any feeder topology, thus the structure of M^{-1} always will be:

$$M^{-1} = \begin{bmatrix} k & k & k \\ k & n & n \\ k & n & p \end{bmatrix}$$

where

$$k = \frac{m}{a(b-c)-m^2}$$

$$n = \frac{a}{a(b-c)-m^2}$$

$$p = \frac{ab-m^2}{c(a(b-c)-m^2)}$$

Q.E.D

Similarly, for a 10 node feeder with 4 generators nodes, M will have the following structure:

$$M^{-1} = \begin{bmatrix} k & k & k & k \\ k & n & n & n \\ k & n & p & p \\ k & n & p & q \end{bmatrix}$$

And for a general case

$$M^{-1} = \begin{bmatrix} k & \cdots & & & k \\ \vdots & n & \cdots & & n \\ & \vdots & \ddots & & \\ & & & r & r \\ k & n & & r & t \end{bmatrix}$$

B5. Program flow in section 4.4.2 on page 59

1) From the $P_{DG\text{-}i}$ evaluate $Q_{DG\text{-}i\text{-}max}$, at power factor 0.9
2) Use v_1 and each node's P_i and Q_i to get all nodes' voltage level prior to any event.

$$V_1\ P_i\ \&\ Q_i \longrightarrow \boxed{\text{Feeder model}} \xrightarrow{V_1 \ldots V_8}$$

3) Get K_3, K_5 and K_7 by injecting 0.5 MVAR by corresponding DG, then measure change in the local node Δv_3, Δv_5 and Δv_7 respectively. Use equations 11-13.

Start of iteration

4) $n = 0$
5) Calculate α_i for each agent, where $\beta_i^{(n)} = K_i\ v_i^{(n)}$
6) Calculate available reactive power for each agent

$$\Delta Q^{(n+1)}{}_{i-\max-available} = Q_{i-\max} - Q^{(n)}{}_{i-set}$$

7) Calculate required amount of voltage $\Delta v_8 = 0.95 - v_8$
8) Program representing the moderator decision making, will assign reactive power to the agent with the higher sensitivity factor. And if we still need more then we utilize the DG with the second highest sensitivity factor, until:

$$\Delta v_8 = \sum \frac{\Delta Q^{(n+1)}{}_{i-set}}{\beta_i^{(n)}}$$

then the output is $\Delta Q^{(n+1)}{}_{i-set}$

9) Update: $Q^{(n+1)}{}_{i-set} = Q^{(n)}{}_{i-set} + \Delta Q^{(n+1)}{}_{i-set}$
10) Check the resulting voltage level, if $v_8 = 0.95$, END
11) Else, $n = n + 1$ and go to step 4

Appendix C

C1. Fault current characterization by IEEE std. 242-86

Fault analysis studies are used to select and size protective devices, such as circuit breakers, reclosers and fuses, at different parts of the network. According to the [IEEE242] some protective device operate after few cycles and others after a time delay, therefore short circuit currents at any point of the network needs to be calculated at three different intervals throughout a fault. Those intervals are known as the subtransient, transient and steady state calculation times, and are respectively discussed below.

Calculation times

1) First cycle consideration (subtransient)

Maximum symmetrical values immediately after fault initiation are always required and are often the only values needed. This fault current is usually the maximum value among all durations, although it is too short, yet it indicates the maximum level of thermal and mechanical stresses the protective devices will be exposed to.

2) After 8 cycles (transient)

Maximum values after a few cycles are required for deciding on the minimum acceptable interrupting ratings.

3) About 30 cycles (steady state)

Minimum values should be calculated to determine whether sufficient current is available to open the protective devices within satisfactory time.

C2. <u>Proof of equation (5.1) for the PI discrete formula (page 81)</u>

The PI controller's transfer function is as follows:

$$G(s) = k_p + \frac{k_i}{S}$$

If we transform from continues to discrete using the trapezoidal transformation rule, then we will replace every $s \rightarrow \frac{2}{T}\frac{z-1}{z+1}$ where T is the time between each discrete value.

$$G(z) = k_p + \frac{k_i}{\left(\frac{2}{T}\frac{z-1}{z+1}\right)}$$

$$G(z) = k_p + \frac{Tk_i(z+1)}{2(z-1)}$$

$$G(z) = k_p + \frac{Tk_i}{2}\frac{(1+z^{-1})}{(1-z^{-1})}$$

$$G(z) = \frac{k_p(1-z^{-1}) + \frac{Tk_i}{2}(1+z^{-1})}{1-z^{-1}} = \frac{Y(z)}{E(z)}$$

Therefore:

$$Y(z) - Y(z)z^{-1} = k_p\left(E(z) - E(z)z^{-1}\right) + \frac{Tk_i}{2}\left(E(z) + E(z)z^{-1}\right)$$

From the z-domain to the time domain

$$y_k - y_{k-1} = k_p\left(e_k - e_{k-1}\right) + \frac{Tk_i}{2}\left(e_k + e_{k-1}\right)$$

$$y_k = y_{k-1} + e_k\left(\frac{Tk_i}{2} + k_p\right) + e_{k-1}\left(\frac{Tk_i}{2} - k_p\right)$$

Therefore:

$$y_k = y_{k-1} + e_k\left(\frac{Tk_i}{2} + k_p\right) + e_{k-1}\left(\frac{Tk_i}{2} - k_p\right)$$

Q.E.D

C3. Data for balanced and unbalanced fault case studies

Case Study 1: Balanced Fault

T	*P*	*Q*	*I (DG)*	*I (RC)*
0	0.75	0	0.0188	0.0365
0.125	1.33	0.167	0.0188	0.047
0.25	2.17	0.534	0.036	0.069
0.375	2.42	0.79	0.0625	0.124
0.5	2.26	0.9	0.08	0.155
0.625	2.03	0.866	0.0831	0.173
0.75	1.87	0.812	0.0895	0.184
0.875	1.67	0.753	0.1008	0.205
1	1.56	0.704	0.1108	0.229
1.125	1.47	0.672	0.0951	0.194
1.25	1.825	0.613	0.0944	0.19

Case Study 2: Unbalanced Fault

T	*P*	*Q*	*I (DG)*	*I (RC)*
0	0.75	0	0.0188	0.0365
0.125	0.796	0.009	0.02	0.047
0.25	0.877	0.04	0.0273	0.069
0.375	0.99	0.152	0.0395	0.09
0.5	1.149	0.309	0.0512	0.115
0.625	1.14	0.349	0.0564	0.122
0.75	1.209	0.371	0.057	0.134
0.875	1.38	0.423	0.061	0.153
1	1.407	0.444	0.0697	0.169
1.125	1.235	0.417	0.0727	0.171
1.25	0.796	0.3	0.07	0.163

C4. **Proof that for signal shown:** $I_{RMS} = \frac{1}{2}\sqrt{I_a^2 + I_b^2}$

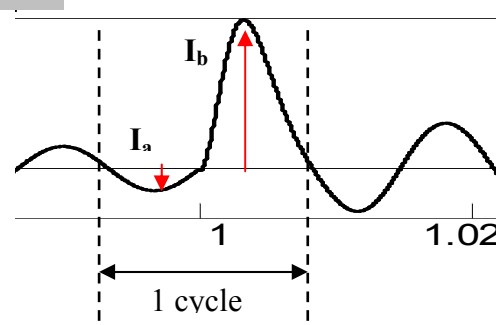

$$\text{RMS} = I_{RMS} = \sqrt{\frac{\left[\int_0^{\pi}(I_a \sin wt)^2\,dt + \int_{\pi}^{2\pi}(I_b \sin wt)^2\,dt\right]}{2\pi}} = \sqrt{\frac{A}{2\pi}} \qquad \text{----------(1)}$$

$$A = \int_0^{\pi}(I_a \sin wt)^2\,dt + \int_{\pi}^{2\pi}(I_b \sin wt)^2\,dt$$

$$A = I_a^{\,2}\int_0^{\pi}(\sin^2 wt)dt + I_b^{\,2}\int_{\pi}^{2\pi}(\sin^2 wt)dt$$

$$A = \frac{I_a^{\,2}}{2}\int_0^{\pi}(1-\cos 2wt)dt + \frac{I_b^{\,2}}{2}\int_{\pi}^{2\pi}(1-\cos 2wt)dt$$

$$A = \frac{I_a^{\,2}}{2}\left[t - \frac{\sin 2wt}{2w}\right]_0^{\pi} + \frac{I_b^{\,2}}{2}\left[t - \frac{\sin 2wt}{2w}\right]_{\pi}^{2\pi}$$

$$A = \frac{I_a^{\,2}}{2}[\pi] + \frac{I_b^{\,2}}{2}[\pi]$$

$$A = \frac{\pi}{2}\left[I_a^{\,2} + I_b^{\,2}\right]$$

Substitute in equation (1)

$$I_{RMS} = \sqrt{\frac{\frac{\pi}{2}\left[I_a^{\,2} + I_b^{\,2}\right]}{2\pi}}$$

$$I_{RMS} = \sqrt{\frac{I_a^{\,2} + I_b^{\,2}}{4}}$$

Therefore: $$I_{RMS} = \frac{1}{2}\sqrt{I_a^{\,2} + I_b^{\,2}}$$

Q.E.D

C5. <u>Proof that for signal shown</u> $I_{RMS} = \sqrt{0.68 I_a^{\,2} + 0.25 I_b^{\,2} - 0.182 I_a I_b}$

The first half of the waveform could be approximated as a cosine wave with a peak value of I_a, while the second half could be approximated as a sine wave with a dc offset equal to I_a with a peak value of I_c.

Note that the overall peak value we are trying to evaluate is I_b, where $I_b = I_a + I_c$

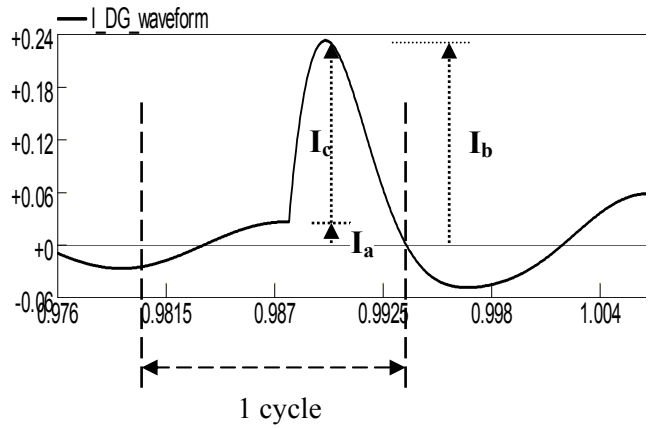

The equation of the first half cycle

$$= -I_a \cos wt$$

The equation of the second half cycle

$$= I_a + I_c \sin wt$$

$$\text{RMS} = I_{RMS} = \sqrt{\frac{\left[\int_0^{\pi} (-I_a \cos wt)^2\, dt + \int_0^{\pi} (I_a + I_c \sin wt)^2\, dt\right]}{2\pi}} = \sqrt{\frac{A}{2\pi}} \qquad \text{----------(1)}$$

$$A = \int_0^{T/2} (-I_a \cos wt)^2\, dt + \int_0^{T/2} (I_a + I_c \sin wt)^2\, dt$$

$$A = I_a^{\,2} \int_0^{T/2} (\cos^2 wt)\, dt + \int_0^{T/2} \left(I_a^{\,2} + I_c^{\,2} \sin^2 wt + I_a I_c \sin wt\right) dt$$

$$A = \frac{I_a^{\,2}}{2} \int_0^{T/2} (1 + \cos 2wt)\, dt + \int_0^{T/2} \left(I_a^{\,2} + I_a I_c \sin wt + I_c^{\,2} \sin^2 wt\right) dt$$

$$A = \frac{I_a^{\,2}}{2} \int_0^{T/2} (1 + \cos 2wt)\, dt + \int_{T/2}^{T/2} \left(I_a^{\,2} + I_a I_c \sin wt + \frac{I_c^{\,2}}{2}(1 - \cos 2wt) \right) dt$$

$$A = \frac{I_a^{\,2}}{2} \left[t - \frac{\sin 2wt}{2w} \right]_0^{T/2} + \left[I_a^{\,2} t + \frac{I_c^{\,2}}{2} t - I_a I_c \frac{\cos wt}{w} - \frac{I_c^{\,2}}{2} \frac{\sin 2wt}{2w} \right]_0^{T/2}$$

$$A = T \frac{I_a^{\,2}}{4} + \left(\left(I_a^{\,2} + \frac{I_c^{\,2}}{2} \right) T - I_a I_c \frac{\cos(wT/2)}{w} - \frac{I_c^{\,2}}{2} \frac{\sin wT}{2w} \right) - \left(\left(I_a^{\,2} + \frac{I_c^{\,2}}{2} \right) \frac{T}{2} - I_a I_c \frac{-1}{w} \right)$$

$$A = T \frac{I_a^{\,2}}{4} + \left(I_a^{\,2} \frac{T}{2} + I_c^{\,2} \frac{T}{4} + \frac{I_a I_c}{w} - \frac{-I_a I_c}{w} \right)$$

$$A = T \frac{I_a^{\,2}}{4} + \left(I_a^{\,2} \frac{T}{2} + I_c^{\,2} \frac{T}{4} + \frac{2 I_a I_c}{w} \right)$$

$$A = T \frac{3 I_a^{\,2}}{4} + T \frac{I_c^{\,2}}{4} + T \frac{I_a I_c}{\pi}$$

Substitute in equation (1)

$$I_{RMS} = \sqrt{\frac{T\frac{3I_a^{\ 2}}{4} + T\frac{I_c^{\ 2}}{4} + T\frac{I_a I_c}{\pi}}{T}}$$

$$I^2{}_{RMS} = \frac{3I_a^{\ 2}}{4} + \frac{I_c^{\ 2}}{4} + \frac{I_a I_c}{\pi}$$

But $I_b = I_a + I_c$

Therefore

$$I_c = I_b - I_a$$

$$I^2{}_{RMS} = \frac{3I_a^{\ 2}}{4} + \frac{(I_b - I_a)^2}{4} + \frac{I_a(I_b - I_a)}{\pi}$$

$$I^2{}_{RMS} = \frac{3I_a^{\ 2}}{4} + \frac{I_b^{\ 2} + I_a^{\ 2} - 2I_a I_b}{4} + \frac{I_a I_b}{\pi} - \frac{I_a^{\ 2}}{\pi}$$

$$I^2{}_{RMS} = I_a^{\ 2}\left(1 - \frac{1}{\pi}\right) + \frac{I_b^{\ 2}}{4} + I_a I_b\left(\frac{1}{\pi} - \frac{1}{2}\right)$$

$$I^2{}_{RMS} = 0.68I_a^{\ 2} + 0.25I_b^{\ 2} - 0.182I_a I_b$$

Therefore:

$$I_{RMS} = \sqrt{0.68I_a^{\ 2} + 0.25I_b^{\ 2} - 0.182I_a I_b}$$

Q.E.D

Bibliography

[ABB] ABB website, Product technical guide 1ZSE 5492-104.

[AK02] Interaction between distributed generation and the distribution network: operation aspect. *2002. Thomas Ackermann and Valery Knyazkin*

[And99] P.M. Anderson, *Power system protection*, published by McGraw Hill, Inc., New Jersey, USA, pages 60-64, 214.

[BD00] P. Barker, R. W. DeMello, "Determining the impact of DG on power systems, radial distribution", IEEE Power Engineering Society Summer Meeting, vol. 3, 2000, pp 1645 -1656.

[BE02] M. Baran, I. El-Markabi, "An EMTP Based Simulator for Distribution Systems with Distributed Generation" Proceedings of the power system conference on Impact of distributed generation, Clemson 2002.

[Ber86] Arthur R. Bergen, *Power system analysis*, Published by Prentice Hall Inc., New Jersey, USA, 1986, pp. 151 – 173.

[BJ02] P.P. Barker, B.K. Johnson. "Power systems modeling requirements for rotating machine interfaced distributed resources". Power Engineering Society Summer Meeting, IEEE, vol. 1, July, 2002

[CCI91] T. Chen, M. Chen, T. Inoue, P. Kotas, E.A. Chebli, **"**Three-phase cogeneration and transformer models for distribution system anaylsis" IEEE Transaction on Power delivery, vol. 6, No. 4, October 1991.

[DM02] R.C. Dugan and T.E. McDermott, "Operating conflicts for distributed generation on distribution systems", Rural Electric Power Conference, April, 2001.

[Doy02] M.T. Doyle, "Reviewing the impact of distributed generation on distribution system protection", Power Engineering Society Summer Meeting, 2002 IEEE, vol. 1 , 21-25 July 2002.

[DS90] N. Deeb, and S. Shahidehpour, "Linear reactive power optimization in a large power network using the decomposition approach", IEEE transaction in power systems, Vol. 5, No. 2, May 1990.

[Dug02] R. Dugan, "Distributed Generation", IEEE Industry Applications Magazine 2002

[GB01] A. Girgis, and S. Brahama, "Effect of distributed generation on protective device coordination in distribution system". Large Engineering Systems Conference on Power Engineering, LESCOPE '01, July 2001

[GM02] J.C. Gomez, M.M. Morcos. "Coordinating overcurrent protection and voltage sag in distributed generation systems". Power Engineering Review, IEEE, vol. 22 , Feb. 2002

[Gro96] B.J. Grosz, "Collaborative Systems," AI magazine, Vol. 17, No. 2, pp. 67-85, 1996

[Hir98] J. H. Hirschenhofer, *Fuel Cell Handbook*, Published by the Federal Energy Technology Center (FETC), U.S. Department of Energy, 1998, pp. 24 – 70.

[IEEE34] IEEE 34 node radial test feeder @ http://ewh.ieee.org/soc/pes/dsacom/testfeeders.html.

[IEEE242] IEEE Recommended Practice for Protection and coordination of industrial and commercial power systems, IEEE std. 242-1986, published by IEEE, 1986.

[IEEE47] IEEE std. P1547, published by IEEE, 2000.

[IEEE929] IEEE Recommended Practice for Utility Interface of Photovoltaic (PV) Systems, IEEE std. 929-2000, published by IEEE, 2000.

[IL01] Mark d'Inverno, Michael Luck, *Understanding agent systems*, Published by Springer, Berlin, Germany, 2001, pp.1 – 7.

[JA00] Nick Jenkins, Ron Allan, *Embedded Generation*, Published by the Institution of Electrical Engineers, London, United Kingdom, 2000, pp.50 – 93.

[Jen96] N. R. Jennings, *Foundation of distributed artificial intelligence*, published by John Wiley & sons, Inc., 1996, pp. 4-46, 187-192, 203-208.

[JH98] Y. Jihoon, R. Havaldar, "Coordination of distributed knowledge networks using contract net protocol", IEEE information technology conference, 1998, pp 71 -74.

[JOG00] G. Joos, B.T. Ooi, F.D. Galiana, "The potential of distributed generation to provide ancillary services" IEEE Power Engineering Society Summer Meeting, vol. 3, 2000, pp 1762 – 1767.

[Lop02] J.P. Lopes, "Integration of distributed generation on distribution network - impact studies". *2002.*

[Man] Manitoba HVDC Research Center, "PSCAD/EMTDC V2 User's Manual", Copyright Manitoba HVDC Research Center.

[PF00] K. Pandiaraj, B. Fox, "Novel voltage control for embedded generators in rural distribution networks," Proceedings of the power conference on power system technology 2000, vol. 1.

[RB99] M Ropp, M. *Begovic,* "Analysis and performance assessment of AFD method islanding detection", IEEE Transactions on Energy Conversion, vol. 14, 1999, pp 810 -816

[Rop00] M. Ropp, "Determining the effectiveness of islanding detection methods using NDZ", Energy Conversion, IEEE Transactions, vol. 15, 2000, pp 290 -296.

[Saa99] Hadi Saadat, *Power System Analysis*, Published by McGrow-Hill, 1999, pp. 189 – 211.

[San93] T. Sandholm, "An Implementation of the Contract Net Protocol Based on Marginal Cost Calculations". Eleventh National Conference on Artificial Intelligence (AAAI-93), Washington DC, 1993, pp. 256-262.

[San96] T. Sandholm, *Negotiation among Self-Interested Computationally Limited Agents.* Ph.D. Dissertation. University of Massachusetts at Amherst, computer science department, 1996.

[Sch01] Michael Schumacher, *Objective coordination in MAS Engineering, Design & implementation*, Published by Springer, Berlin, Germany, 2001, pp.9 – 23.

[Sim01] Simon R. Wall, "Performance of inverter interfaced distributed generation", Transmission and Distribution Conference and Exposition, Vo. 2, Oct, 2001.

[SJR00] S.K. Salman, F. Jiang, W.J.S. Rogers, "Investigation of the operating strategies of remotely connected embedded generators to help regulating local network voltage," Inter. conf. on opportunities and advances in international electric power generation, (conf. pub. no. 419).

[SJR93] S.K. Salman, F. Jiang, W.J.S. Rogers, "The effect of private generators of the voltage control of 11 kV network and on the operation of certain protective relays", Athens international power technology conference, vol. 2, 1993, pp 591 – 595.

[SR01] S.k. Salman, and I.M. Rida, "Investigating the impact of embedded generation on relay setting of utilities' electrical feeders". IEEE Transactions on Power Delivery, vol. 16, Issue: 2 , April 2001.

[Sut01] M. Suter, "Active filter for a microturbine," IEEE, 23rd Telecommunications Energy Conference, INTELEC 2001, pp. 162 – 165.

[SW03] M. Shahidehpour and Y. Wang, *Communication and control in electric power systems, application of parallel and distributed processing*, Published by the John Wiley & Sons, IEEE Press, 2003, pp. 332 – 348.

[Syc98] Katia Sycara, "Multi-agent systems", AI magazine 1998, vol. 19, No. 2, pp. 79-92.

[TC00] S.N. Talkudar, and E. Componogara, "Collaborative Nets", Proceedings of the 33rd Hawaii international conference on system science, January 2001.

[Wal01] Performance of inverter interfaced distributed generation. *2001. Simon R. Wall*

[Wei99] Gerhard Weiss, *Multiagent Systems, a modern approach to DAI*, Published by the MIT press, Cambridge, London, England, 1999, pp. 100 – 104, 233-236.